UNCLASSIFIED

AD 491984

DEFENSE DOCUMENTATION CENTER

FOR

SCIENTIFIC AND TECHNICAL INFORMATION

CAMERON STATION, ALEXANDRIA, VIRGINIA

UNCLASSIFIED

NOTICE: When government or other drawings, specifications or other data are used for any purpose other than in connection with a definitely related government procurement operation, the U. S. Government thereby incurs no responsibility, nor any obligation whatsoever; and the fact that the Government may have formulated, furnished, or in any way supplied the said drawings, specifications, or other data is not to be regarded by implication or otherwise as in any manner licensing the holder or any other person or corporation, or conveying any rights or permission to manufacture, use or sell any patented invention that may in any way be related thereto.

THE PENNSYLVANIA STATE UNIVERSITY
COLLEGE OF ENGINEERING AND ARCHITECTURE

Address reply to:
ORDNANCE RESEARCH LABORATORY
P. O. BOX 30
State College, Pennsylvania

June 21, 1954

AD 491 984

Chief of Naval Research
Office of Naval Research
Department of the Navy
Washington 25, D. C.

Attention: Mechanics Branch, Code 438

Subject: Tip-Vortex Cavitation

Reference: ONR Project NR 062-139

Enclosure: Two copies of a thesis by B. W. McCormick

Dear Sir:

Enclosed please find two copies of the thesis by Mr. Barnes W. McCormick submitted in partial fulfillment of the requirements for the degree of Doctor of Philosophy at The Pennsylvania State University, June 1954. This work is entitled "A Study of the Minimum Pressure in a Trailing Vortex System." It was supported under the reference project in connection with our study of tip-vortex cavitation. These copies of the thesis are being submitted as evidence of our accomplishment.

Very truly yours,

Gilford G. Quarles
Director

J. M. Robertson
By direction

GGQ:JMR:jb

Ordnance Research Laboratory operates under U. S. Navy Contract NOrd 7958

Best
Available
Copy

The Pennsylvania State University

The Graduate School

Department of Aeronautical Engineering

(6) A Study of the Minimum Pressure in a Trailing Vortex System,

Doctoral thesis,

A dissertation
by

(10) Barnes Warnock McCormick, Jr.

Submitted in partial fulfillment
of the requirements
for the degree of

Doctor of Philosophy

(11) June 1954,

(12) 141 p.

(15) NOR - 7458

NR - 062-134

Approved:

Department of Aeronautical Engineering

Head of the Department

Acknowledgments

It is with sincere appreciation that the writer acknowledges the guidance and constructive criticisms of Dr. Henry G. Lew, not only in the preparation of this dissertation but throughout his graduate study.

This work under Project No. NR-062-139 was sponsored by the Office of Naval Research. Appreciation is offered collectively to many members of the Ordnance Research Laboratory and in particular to Mrs. James M. Robertson and Donald Ross for the interest which they have shown in this work; to Messrs. Samuel R. Robinson, George E. Norton and Phillip Vonada for their excellent machining work; to Mr. Robert J. Allinedinst for his help in performing the calculations; and to Mrs. Shirley G. Dann for her help in preparation of the manuscript.

Appreciation is also extended to the other members of the examining committee not previously mentioned for their perusal and criticisms of this thesis; Mrs. David J. Peery, Thomas G. Denton, and Norman Davids.

For her love and encouragement throughout the "school years", as well as for the preparation of the final manuscript, I offer my sincerest thanks to my wife, Emily.

Barnes Carnock McDonald, Jr.

May 14, 1962

Summary

The problem of estimating the minimum pressure in a trailing vortex system of a planar lifting surface is investigated both theoretically and experimentally. A semi-empirical solution is obtained after showing that predictions based on kinetic energy and induced drag considerations are not in accord with experimental results. Assuming the boundary layer developed on the lower surface of the wing to be a measure of the vortex sheet thickness, expressions are developed for this distance for the cases of rectangular and elliptic wings from consideration of the wing geometry and distribution of bound circulation. These expressions for the vortex sheet thickness involve unknown constants which must be determined from the experimental results.

The experimental investigation consisted of measurements of vortex cavitation inception conditions for families of rectangular, delta, and elliptic wings in a large, high speed water tunnel. The majority of the testing was done at a Reynolds number of approximately ~~7×10^5~~ but by varying the temperature of the water and using different sizes of wings, measurements were taken for rectangular wings of aspect ratio four over a range of Reynolds numbers from about 2×10^5 to 2×10^6.

The major conclusions to be drawn from the investigation are that: the magnitude of the minimum pressure coefficient in the trailing vortex system of a wing increases nearly linearly with the angle of attack of the wing; this magnitude is almost independent of aspect ratio for elliptic wings but for rectangular wings is slightly higher, the greater the aspect ratio, for a given angle of attack; at a given angle of attack the magnitude of the minimum pressure coefficient increases with increasing Reynolds number; ~~and~~ the thickness of the tip-vortex core, or the thickness of the edge of the trailing vortex sheet is determined by the thickness of the boundary layer on the lower surface of the wing at the trailing edge of the tip and not be any considerations of induced drag and kinetic energy of the vortex sheet itself.

Notation

a radius of the vortex core

a_1 parameter in c_{cf} distribution

a_2 parameter in c_{cf} distribution

b semi-span of the wing or trailing vortex sheet

c wing chord

C contour of integration

C_D wing induced drag coefficient

c_l section lift coefficient

c_{l_0} section lift coefficient at mid-span

C_L wing lift coefficient

c_0 wing chord at mid-span

c_p pressure coefficient, usually meant to be the minimum

c_{p_0} pressure coefficient at the center of a vortex

D_i induced drag of wing

e base of Naperian logarithms

g acceleration of gravity

K kinetic energy

K_{BL} kinetic energy in the "boundary layer" of the vortex sheet between $-x$ and x

K_i kinetic energy of irrotational motion

K_r kinetic energy of rotational motion

l characteristic length

L lift

p pressure

p_1 pressure at edge of vortex core

p_o pressure at center of vortex core

p_v vapor pressure

p_∞ free stream static pressure

r radial distance in polar coordinates

R free stream Reynolds number = $\frac{VD}{\nu}$

R_o mid-span Reynolds number = $\frac{V c_o}{\nu}$

R_Γ characteristic Reynolds number of vortex sheet = $\frac{\Gamma_o}{\nu}$

S wing area; or area over which integration is performed

t time

u radial component of velocity; or x component of velocity

u_1 velocity outside of boundary layer

v tangential component of velocity; or y component of velocity

v_s velocity component tangent to path of integration

V free stream velocity

V_∞ reference or free stream velocity

w velocity induced normal to and in the plane of the ultimate wake; also specific weight

$\bar{w}_o$ value at w at $\bar{x}_o$

x rectangular coordinate; also distance along unit semi-span

$\bar{x}_o$ outer position of bounding streamline in semi-span lengths

x^* inner position of bounding streamline in semi-span lengths

y rectangular coordinate; also distance along span

y_0 particular position along span

$\bar{y}_0$ outer position of bounding streamline

y^* inner position of bounding streamline

z rectangular coordinate

α geometric angle of attack measured from zero lift line (expressed in radians unless otherwise noted)

κ circulatory strength of rectilinear vortex

Γ bound circulation

Γ_0 mid-span value of the bound circulation

δ semi-thickness of vortex sheet

δ_1 displacement thickness

Δ nozzle pressure drop in inches of mercury

η dimensionless distance in boundary layer

$\eta_e(x)$ energy distribution factor

θ momentum thickness, also polar coordinate

μ dynamic viscosity

ν kinematic viscosity

ρ mass density of fluid medium

σ cavitation index

σ_{cr} critical cavitation index

σ_t tip cavitation index

$\sigma_{t_{cr}}$ critical tip cavitation index

ψ stream function

ω vorticity; also angular velocity

Table of Contents

	Page
Acknowledgment	i
Summary	ii
Notation	iv
Table of Contents	vii
1.000 Introduction to the Problem	1
2.000 Previous Investigations	4
3.000 Theoretical Analysis of the Problem	9
3.100 Case of the Completely Rolled-Up Vortex Sheet	9
3.110 Rankine Vortex	9
3.120 Dimensional Analysis of the Core Size	11
3.130 Lamb's Solution for a Rectilinear Vortex in a Viscous Fluid	13
3.140 Prediction of the Core Radius of the TrailingVortices from Considerations of Induced Drag and Kinetic Energy	18
3.141 Rectangular Planforms	20
3.142 Delta Planforms	26
3.143 Elliptic Planforms	27
3.150 Prediction of Minimum Pressure Coefficients for Rectangular, Delta and Elliptic Wings on the Basis of a Rolled-Up Vortex Sheet	27

3.200 Non-Distorted Vortex Sheet ..... 2[illegible]

3.210 Proposed Model of a Non-Distorted Vortex Sheet 31

3.220 Calculation of Model Dimensions 34

3.230 Modification Due to the Distribution of the Energy in the Vortex Sheet ... [illegible]2

3.240 Prediction of Minimum Pressure Coefficient for the Elliptic Wing on the Basis of the Proposed Model of a Non-Distorted Vortex Sheet ..... [illegible]

3.300 Discussion of Theoretical Postulations . [illegible]3

4.000 Experimental Investigation 7

4.100 Basis of Investigation 7

4.200 Test Equipment ..... [illegible]

4.300 Experimental Procedure ..... [illegible]3

4.400 Experimental Results ..... [illegible]

4.410 Elliptic Planforms 69

4.420 Rectangular Planforms ..... [illegible]

4.430 Delta Planforms ..... 7[illegible]

4.440 General Discussion of Results 71

5.000 Semi-Empirical Analysis ..... 7[illegible]

5.100 Rectangular Planforms 77

5.200 Elliptic Planforms ..... [illegible]3

5.300 Discussion of Semi-Empirical Investigation ..... [illegible]7

6.000 Conclusions 88

7.000 References 90

8.000 Appendix 92

8.100 Evaluation of the Integral $\int_0^\infty \frac{(1-e^{-kx^2})}{x^2}\,dx$ ... 92

8.200 Proof that the Induced Velocity Normal to the Trailing Vortex Sheet is Bounded Except at the Edges of the Sheet 93

Table I Specifications of Wings Tested 95

Table II Sample Raw Data Sheet 97

Table III Water Vapor Pressure and Kinematic Viscosity as a Function of Temperature 98

Table IV Summary of Tests 99

Table V Parameters for Circulation Distribution . 103

Figures 104

1.000 Introduction to the Problem

A system of trailing vortices is associated with any finite lifting surface. This system represents the disturbance to the fluid attributable to the lift produced by the surface. For the hypothetical case of a perfect fluid, the system immediately behind the lifting surface is in the form of a vortex sheet. This sheet defines a surface across which the tangential component of the velocity is discontinuous. This vortex sheet, for the usual case, is unstable and tends to roll up into discrete vortices. Although the sheet only approaches asymptotically the configuration of discrete vortices, the rate of rolling up of the sheet varies considerably with the degree and distribution of loading on the lifting surface.

In an ideal frictionless fluid the pressure along the edge of the vortex sheet and at the center of the rolled-up vortices attains a value of minus infinity. This follows from the simple application of Bernoulli's equation, since as will be discussed later, the velocity becomes infinitely large at these locations. In a real fluid, obviously such discontinuities or singularities in the velocity cannot exist. However, the pressure along the edge of the sheet or in the center of the vortices is considerably reduced, even for the real fluid.

The problem investigated herein, both theoretically and experimentally, is that of predicting the minimum pressure which exists in a trailing vortex system in a real fluid.

This problem is important in connection with the design of marine propellers. In regions of low pressure in the trailing vortex system of the propeller blades, the phenomenon of cavitation will occur whenever the pressure is reduced to the vapor pressure of the liquid. This phenomenon is pictured in figure 1. This cavitation is undesirable since; (1) the efficiency of the propeller may be reduced, and (2) the cavitation produces considerable noise. If the various factors which influence the minimum pressure can be determined, then some control can be exercised in the propeller design over the occurrence of the vortex cavitation, as it is referred to in hydrodynamic terminology.

In order to avoid the analytical difficulties inherent with the helicoidal geometry of a propeller, the present study is restricted to planar lifting surfaces in an incompressible fluid. The results for this case should be indicative of what one might expect for propellers. Further, the extension of the method of approach to the case of a propeller does not appear unreasonable.

The difficulties in predicting the minimum pressure in the trailing vortex system of a wing become apparent if one considers briefly the behavior of the system. It might be well to refer to a typical wing and trailing vortex system as depicted in figure 2. If a prediction of the minimum pressure along the section A of this figure were attempted one would have to consider the distribution of the vorticity over the surface of the wing. At any other section, for example C, the vortex sheet is partially rolled-up. Even the section B is distorted from a plane vortex sheet since as the vortex sheet is forming, the induced effects of the vortex system tend to roll up the sheet at the edges. From these considerations, the following questions arise: (1) Can the trailing vortex system be considered independent of the distribution of the circulation over the surface of the wing, and (2) Should the vortex sheet be treated as non-distorted, partially rolled-up, or completely rolled-up. The ideal solution, of course, would be an exact solution of the Navier-Stokes equations of motion subject to the boundary condition that the velocity be zero on the surface of the wing. Such a solution appears extremely unlikely in view of the non-linear nature of the Navier-Stokes equation. Instead, simplifying hypotheses are considered which make the problem more tenable.

In attempting an analytical solution of the problem the following procedure has been followed. First the case of the completely rolled-up vortex sheet is studied. Rankine's hypothesis of a solid rotating core is presented and calculations of the core size are given for rectangular, delta, and elliptic wings. These calculations are based upon the accepted procedure of equating the induced drag of the wing to the kinetic energy of a unit length of the rolled-up vortex system. Using the calculated core sizes predictions are then made of the variation of the minimum pressure coefficient with angle of attack and wing planform. The agreement between this predicted behavior of the minimum pressure and the experimental results is shown to be so poor as to question severely the generally accepted means of calculating the core size.

With this negative result, consideration is given to the non-distorted vortex sheet. A model of a non-distorted vortex sheet is proposed which, in effect, is merely an extension of Rankine's hypothesis to the non-distorted configuration. Again by equating the induced drag of the wing to the kinetic energy per unit length of the non-distorted vortex sheet, the dimensions of the proposed model are determined. In so doing the estimated distribution of the energy in the sheet is also considered. The minimum pressures predicted on this basis are shown to be closer to the experimental results than the previous predictions based on the completely rolled-up sheet. However,

there are still serious discrepancies to be explained and for this reason, a semi-empirical approach is developed. It is reasoned that the thickness of the boundary layer on the lower surface of the wing at the tip of the trailing edge is a measure of the vortex sheet thickness. Expressions are developed for the variation of this thickness with angle of attack, aspect ratio, and Reynolds number for the rectangular and elliptic wings. These expressions involve unknown constants which are determined from the experimental results.

2.000 Previous Investigations

There has been little work performed in the past on the problem as such. Numerous investigators have considered the spread and decay of a vortex sheet, but these works have been for the vortex sheet which is formed behind blunt bodies in which the lines of vorticity are normal to the direction of the main flow. Figure 3 illustrates this type of sheet. Notable investigators of this problem were Prandtl in 1925 and Tollmien in 1926 whose works are found in references (1) and (2). Experimental confirmation of the theories of Prandtl and Tollmien were reported by Fage and Johansen in reference (3) in 1928. Briefly, the problem of the structure of the vortex sheet was attacked by Prandtl and Tollmien with the methods for analyzing turbulent flow. The spread of the zone of the vorticity was assumed to result from the transport of the vorticity by turbulent fluctuations. Since the nature of the problem is so dissimilar from the one considered here and since the method of attack does not appear applicable, nothing further will be said concerning the work of these experimenters. An extensive bibliography on this subject is given in reference (4).

The first investigation to be performed which appears applicable to the problem, as outlined in the introduction, is presented in reference (5). In the case of an isolated vortex, Rankine hypothesized the so-called "combined" or "Rankine" vortex in order to circumvent the infinite

velocity at the center. This idealization consists of an inner core throughout which the motion is rotational with a constant value of the vorticity, and an outer region in which the flow is irrotational.

Further work with an isolated vortex was performed by Lamb, reference (6), in which an irrotational velocity distribution was assumed to exist initially with the subsequent alteration with time due to the action of viscosity being obtained from the analogy of the diffusion of vorticity to heat conduction.

Also of noteworthiness are the results of a recent article by Spreiter and Sacks, reference (7), in which the rolling-up of the trailing vortex system was investigated. The purpose of this investigation was to determine the proper vortex system to be used for downwash calculations. It was found that the rate at which the vortex sheet rolls up depends upon the magnitude and loading distribution of the wing which is generating the system. Further, it was found, at least for downwash calculations, that the rolling-up of the vortex sheet associated with high-aspect ratio wings is of little consequence but that for low-aspect ratio wings, the sheet may be considered to be completely rolled-up into two rectilinear vortices within a chord length of the wing.

In reference (8) as well as the previous reference (7), a method is outlined for obtaining the configuration of the completely rolled-up vortex system from energy considerations

assuming two trailing Rankine vortices. The present work, in addition to a general discussion of the vortex system, presents and extends the methods of (8) to an assumed hypothetical model of a non-distorted vortex sheet.

Numerous other references were used in the investigation reported herein and these will be listed where used.

3.000 Theoretical Analysis of the Problem

In view of the varying configuration of the trailing vortex sheet in the direction of motion it was decided to treat the limiting conditions of a completely rolled-up vortex sheet and a non-distorted vortex sheet. It would seem reasonable to assume that the actual case lies somewhere between these extremes. Actually the configuration of a non-distorted vortex sheet appears more nearly representative of the physical case since the dissapative action of the viscosity in a real fluid would tend to destroy the strength of the sheet as it rolls up. However, considerable insight into the behavior of the vortex system can be realized through consideration of the rolled-up sheet. In addition, a knowledge of the theory of the rolled-up sheet is necessary to an understanding of the theory which is developed for the non-distorted sheet.

3.100 Case of the Completely Rolled-Up Vortex Sheet

In discussing the case of a completely rolled-up vortex sheet, the problems encountered are those associated with a discrete rectilinear vortex. The properties of such a vortex will therefore be discussed before treating the rolled-up system.

3.110 Rankine Vortex

The velocity distribution for a vortex in two-dimensional irrotational fluid motion is

$$v = \frac{\gamma}{2\pi r} \tag{3.1}$$

where: v = tangential velocity

γ = circulatory strength of the vortex

r = radial distance from the center of the vortex

According to this equation the velocity becomes infinite at the center of the vortex. Obviously, this is impossible in a real fluid. The radial variation of the velocity field of a vortex in a real fluid must thus be altered to remove this singularity.

According to the Rankine hypothesis, it is assumed that the vorticity, ω, is constant over a circular core of radius a. Inside the core the motion is rotational so that a complex potential does not exist in this region. However, a stream function can be defined both inside and outside the core. If it is stipulated that the stream function and the velocity be continuous at the edge of the core then it is shown in reference (5) that Rankine's hypothesis is tantamount to assuming the existence of a solid core rotating at an angular velocity of $\frac{\omega}{2}$. Outside of this core pure irrotational motion exists.

The pressure gradient within the core is

$$\frac{\partial p}{\partial r} = \rho r \left(\frac{\omega}{2}\right)^2 \tag{3.2}$$

Integrating gives

$$p = p_o + \frac{\rho r^2 \omega^2}{8}$$

where p_o is the pressure at the center.

In terms of the pressure at the edge of the core

$$p_o = p_a - \rho \frac{a^2 \omega^2}{8}$$

$$= p_a - \frac{\rho}{2}\left(\frac{\gamma}{2\pi a}\right)^2 \qquad (3.3)$$

where p_a is the pressure at the edge of the core. Since the motion outside of the core is irrotational, p_a can be obtained by applying Bernoulli's equation from a point at infinity to r = a

$$p_\infty = p_a + \frac{\rho}{2}\left(\frac{\gamma}{2\pi a}\right)^2$$

Therefore

$$p_o = p_\infty - \rho\left(\frac{\gamma}{2\pi a}\right)^2 \qquad (3.4)$$

p_∞ is the pressure infinitely far from the vortex.

In coefficient form the pressure at the center of the vortex becomes

$$C_{p_o} = \frac{p_o - p_\infty}{\frac{1}{2}\rho V_\infty^2} \qquad (3.5)$$

with V_∞ is the reference velocity.

Substituting in the above expression the relationship of equation (3.4) gives

$$C_{p_o} = -2\left(\frac{\gamma}{2\pi a V_\infty}\right)^2 \qquad (3.6)$$

It is of interest to note that for the Rankine vortex, the pressure drop through the region of irrotational motion is exactly equal to the drop through the core.

For a given vortex of known strength, the problem of calculating the minimum pressure for the Rankine model is equivalent to that of determining the core size. In an effort to gain some insight into the variation of the core size, the following investigations were conducted.

3.120 Dimensional Analysis of the Core Size

It seems reasonable to assume that the core size of a Rankine vortex would be a function of the following quantities:

γ = circulatory strength of the vortex

ρ = mass-density of the fluid

μ = dynamic viscosity of the fluid

V = velocity of the free stream relative to the generating surface

The simple application of the fundamental π - theorem of dimensional analysis results in the two dimensionless π - variables

$$\pi_1 = \frac{aV}{\gamma}$$

$$\pi_2 = \frac{\gamma\rho}{\mu} \tag{3.7}$$

The size of the core can thus be expressed in the form:

$$a = \frac{\gamma}{V} \cdot f\left(\frac{\gamma\rho}{\mu}\right) \tag{3.8}$$

The important result to observe is the formulation of a Reynolds' number characterizing the vortex motion, namely $\frac{\gamma\rho}{\mu}$.

Before continuing further with this analysis, it would be well to consider a wing with a completely rolled-up vortex system as shown in figure 4. As the vortex sheet behind a wing rolls up, the center of the vortices assume a distance apart which is smaller than the wing span. This distance, denoted on the figure as 2b', is a function of the planform shape and spanwise distribution of the loading as will be shown later.

From the law of vortex continuity, as stated by Helmholtz, the strength of each trailing vortex is clearly equal to the mid-span value of the bound circulation on the wing, Γ_o .

From the Kutta-Joukowski theorem, the bound circulation at any station along the wing is given by:

$$\Gamma = \frac{1}{2} c C_l V \tag{3.9}$$

where: C = chord of the station

C_l = the section lift coefficient

V = local resultant velocity at the section (given closely by the free stream velocity)

Substituting (3.9) in (3.8) gives

$$a = c_o C_{l_o} f\left(\frac{C_{l_o}}{2} \frac{\rho c_o V}{\mu}\right) \tag{3.10}$$

where: C_{l_o} = section lift coefficient at mid-span

c_o = chord of mid-span station

Or if the free stream Reynolds number of the wing is given by:

$$R_o = \frac{V c_o \rho}{\mu} \tag{3.11}$$

then the expression for the core radius becomes finally:

$$a = c_o C_{l_o} f\left(C_{l_o} R_o\right) \qquad (3.12)$$

At this point the function of $C_{l_o} R_o$ would have to be determined from experiment. Although the dimensional analysis does not result in a quantitative answer, it does indicate a basis for the correlation and extension of the data.

3.130 <u>Lamb's Solution for a Rectilinear Vortex in a Viscous Fluid</u>

Rankine's hypothesis is merely an artifice which approximates the action of a rectilinear vortex in a viscous fluid. In a viscous fluid obviously the vorticity will not be confined to a limited region at the center of the vortex as supposed. Instead of the velocity function having a discontinuous derivative it is natural to expect that the radial variation of the velocity will be analytic throughout the entire flow field.

By applying the Navier-Stokes equations to flow concentric about an axis, Lamb shows in reference (6) that, in terms of the vorticity, ω, the equations of motion reduce to

$$\frac{\partial \omega}{\partial t} = \nu\left(\frac{\partial^2 \omega}{\partial r^2} + \frac{1}{r}\frac{\partial \omega}{\partial r}\right) \qquad (3.13)$$

But Lamb observes that the above equation is identical

with the equation of radial flow of heat in two dimensions. By analogy to the heat transfer case, the solution is given as:

$$\omega = \frac{\gamma}{4\pi\nu t} e^{-\frac{r^2}{4\nu t}}$$

The velocity distribution is then found as:

$$v = \frac{\gamma}{2\pi r}\left(1 - e^{-\frac{r^2}{4\nu t}}\right) \qquad (3.14)$$

Observe that for the steady case where $\frac{\partial \omega}{\partial t} = 0$, the solution for ω is:

$$\omega = C_1 \log r + C_2$$

Since the vorticity is to vanish at a distance infinitely far removed from the center of the circular motion, it follows that for the steady case

$$\omega = \text{constant}$$

Rankine's hypothesis is thus, in effect, two distinct solutions of the equations of motion for the two regions inside and outside of the core. In crossing the boundary of the core, the hypothesis violates the equations of motion since ω vanishes discontinuously from some finite value.

Returning to the expression (3.14) which Lamb derives for the velocity distribution of a vortex in a viscous fluid, it is to be noticed that when $t = 0$, the velocity distribution is identical to that for a vortex in irrotational motion. Thus equation (3.14) represents the alteration

to the irrotational motion with time as effected by the diffusion of the vorticity due to viscous action.

The pressure at the center of the rotational motion described by (3.14) can be obtained as

$$P_o = P_\infty - \int_0^\infty \frac{\rho}{r}\left(\frac{\gamma}{2\pi r}\right)^2\left(1 - e^{-\frac{r^2}{4\nu t}}\right)^2 dr$$

or in coefficient form:

$$C_p = -2\left(\frac{\gamma}{2\pi V_\infty}\right)^2 \int_0^\infty \frac{\left(1 - e^{-\frac{r^2}{4\nu t}}\right)^2}{r^3} dr$$

The definite integral in the above equation is evaluated in the appendix where it is shown that:

$$\int_0^\infty \frac{\left(1 - e^{-kx^2}\right)^2}{x^3} dx = k \log 2$$

The expression for the minimum pressure coefficient becomes:

$$C_p = -\frac{\log 2}{2\nu t}\left(\frac{\gamma}{2\pi V_\infty}\right)^2 \qquad (3.15)$$

On the basis of the sparse data which is available, the velocity distribution, as given by (3.14) appears to describe the variation of the induced velocity behind a wing satisfactorily even though the initial conditions at t = o for (3.14) are unreal. Figure 5 is a comparison of equation (3.14) with upwash measurements obtained from reference (9). These measurements were taken two chord lengths behind and outboard of a wing with a rectangular

planform with an aspect ratio of six. For comparison purposes arbitrary values of γ and t were selected to give the best fit to the data. The data was insufficient to choose a value of γ and no rational means of selecting t appears satisfactory due to the uncertainty of the initial conditions.

As a test of the validity of Rankine's hypothesis the minimum pressure coefficient for the exact solution will be compared to that which is obtained from the Rankine vortex taking the radius of the core to equal the radius at which the maximum velocity occurs in (3.14). To find this radius, the derivative of (3.14) with respect to r is set equal to zero.

$$-\frac{\gamma}{2\pi r_{max}^2}\left(1-e^{-\frac{r_{max}^2}{4\nu t}}\right)-\frac{\gamma}{4\pi\nu t}\left(-e^{-\frac{r_{max}^2}{4\nu t}}\right)=0.$$

If $X=\frac{r_{max}^2}{4\nu t}$ then the above equation becomes

$$e^X-2X-1=0$$

The solution of the above equation is X = 1.26 from whence

$$r_{max}^2=1.26\,(4\nu t) \tag{3.16}$$

If the above relationship is substituted in expression (3.15), the minimum pressure coefficient for the exact solution in terms of r_{max} becomes

$$C_p=-1.74\left(\frac{\gamma}{2\pi r_{max} V_\infty}\right)^2 \tag{3.17}$$

The magnitude of this expression is seen to be approximately 13% less than that which was obtained for the Rankine vortex as given by equation (3.6). On this basis therefore, the Rankine hypothesis would appear to be a suitable representation of the rolled-up vortex system.

3.140 Prediction of the Core Radius of the Trailing Vortices From Considerations of Induced Drag and Kinetic Energy

The kinetic energy of the trailing vortex system is a manifestation of the power required to overcome the induced drag of the wing. That the kinetic energy per unit length is equal in magnitude to the induced drag can be shown in the following somewhat intuitive manner. Consider the wing having moved a unit distance during which time conditions were steady. In the absence of any viscous drag, the work required to move the wing this distance can only be that required to overcome the induced drag given by $D_i \times (1)$, D_i being the induced drag. During this time, a length of the trailing vortex system is generated equal to the distance moved by the wing. The kinetic energy of the trailing vortex system is increased by the product of the distance moved and the kinetic energy per unit length of the vortex system. Since no agent is present for the dissipation of the work required to move the wing, it follows that the level of the kinetic

energy of the vortex system must increase by an amount equal to the expended work. Thus it follows that

$$K = D_i \tag{3.18}$$

where K = kinetic energy of the trailing vortex system per unit length

D_i = induced drag of the wing

A more elegant proof of this relationship is given later in the course of a theoretical development.

Consider the wing system as shown in figure 4. Suppose a plane is passed through the trailing vortex system. This plane is located far enough aft so that the vortex sheet has essentially rolled up into two discrete vortices as shown. The two-dimensional flow on this transverse plane will be that due to two vortices a distance of 2b' apart with strengths of opposite sense.

According to Rankine's hypothesis, each vortex will consist of an inner circular region of radius "a" over which the vorticity is concentrated and constant (a solid rotating core) and outside of which the flow is irrotational. The induced transverse flow will appear as in figure 6.

To calculate the kinetic energy of the system shown in figure 6, the kinetic energy of the fluid outside of the rotating cores will be calculated separately from that of the cores. It is a well known theorem of fluid

mechanics that the kinetic energy of the two-dimensional, irrotational motion within the closed curve C is given by

$$K_i = \oint_C \psi \, v_s \, ds \tag{3.19}$$

where v_s is the velocity component tangent to the path of integration s, and ψ is the value of the stream function on s. It will now be shown that, for the system of figure 6, the kinetic energy of the irrotational portion of the flow is given by

$$K_i = \lim_{R \to \infty} \int_C \psi \, v_s \, ds \tag{3.20}$$

For a vortex with a core of radius "a" situated at the origin having a strength γ, the stream function is:

$$\psi = -\frac{\gamma}{2\pi} \log \frac{(x^2 + y^2)^{\frac{1}{2}}}{a}$$

Thus the stream function for the combined flow as pictured in figure 6 is

$$\psi = -\frac{\gamma}{2\pi} \log \frac{\left[(x-b')^2 + y^2\right]^{\frac{1}{2}}}{a} + \frac{\gamma}{2\pi a} \log \frac{\left[(x+b')^2 + y^2\right]^{\frac{1}{2}}}{a}$$

The above equation can be reduced to the following expression:

$$\psi = \frac{\gamma}{4\pi} \log \frac{(x+b')^2 + y^2}{(x-b')^2 + y^2} \tag{3.21}$$

If $\frac{(x+b')^2 + y^2}{(x-b')^2 + y^2}$ is set equal to a constant it will be seen that the streamlines are circles of radius r

centered on the x axis at distances of $\pm\sqrt{b'^2 + r^2}$ from the origin.

Now consider the contribution to the contour integral along the circle of radius R.

$$\int_R \psi\, v_s\, ds = \int_0^{2\pi} R\, \psi\, v_s\, d\theta$$

As R approaches the limit infinity either x and/or y approach the same limit with the result that ψ vanishes at infinity. Further upon examination of the contribution of either vortex it can easily be seen that v_s approaches zero as fast as $\frac{1}{R}$. Thus

$$\lim_{R \to \infty} \int_R \psi\, v_s\, ds = 0$$

with equation (3.20) being proved.

The contour integration is thus reduced to the path as indicated in figure 7. The symmetry of the problem allows us to calculate the total contribution as twice the contribution of the integral about one of the cores. Consider the core on the right as pictured in Figure 8.

Since the surface of the flow is a streamline, the value of ψ is constant along its contour. The expression for the kinetic energy outside of the core then becomes

$$K_i = \frac{1}{2} \rho\, \psi_a \int_C v_s\, ds \qquad (3.22)$$

At the boundary of the core x and y are given by

$$\left(x - \sqrt{b'^2 + a^2}\right)^2 + y^2 = a^2$$

or $$(x+b')^2 + y^2 = 2x\left(\sqrt{b'^2+a^2} + b'\right)$$

$$(x-b')^2 + y^2 = 2x\left(\sqrt{b'^2+a^2} - b'\right)$$

These relationships are inserted into equation (3.21) to obtain the value of ψ_a. The result is a constant given by

$$\psi_a = \frac{\gamma}{4\pi} \log \frac{\sqrt{b'^2+a^2} + b'}{\sqrt{b'^2+a^2} - b'} \tag{3.23}$$

The closed line integral of the tangential velocity about the core of the vortex is, of course, simply the measure of the vortex strength and is equal to γ. Thus the kinetic energy outside of the cores is given by:

$$K_i = \frac{\rho\gamma^2}{4\pi} \log \frac{\sqrt{b'^2+a^2} + b'}{\sqrt{b'^2+a^2} - b'} \tag{3.24}$$

The kinetic energy inside the rotating cores can be expressed as:

$$K_r = 2\left[\frac{1}{2}\rho \int_0^{2\pi}\int_0^{a} (\omega r)^2 r\,dr\,d\theta\right]$$

Since at r = a, $\omega a = \dfrac{\gamma}{2\pi a}$ it follows that

$$K_r = \frac{\rho\gamma^2}{8\pi} \tag{3.25}$$

The kinetic energy per unit length of the vortex is determined finally as

$$K = \frac{\rho\gamma^2}{8\pi}\left[1 + 2\log\frac{\sqrt{b'^2+a^2} + b'}{\sqrt{b'^2+a^2} - b'}\right] \tag{3.26}$$

This expression is equated to the induced drag and the resulting expression solved for "a".

$$\frac{a}{b'} = \left[\left\{\frac{1+\exp\left(\frac{4\pi D_i}{\rho\gamma^2} - \frac{1}{2}\right)}{-1+\exp\left(\frac{4\pi D_i}{\rho\gamma^2} - \frac{1}{2}\right)}\right\}^2 - 1\right]^{\frac{1}{2}} \qquad (3.27)$$

The strength of each vortex, according to the law of vortex continuity, is equal to the bound circulation of the wing at mid-span denoted by Γ_o. (See Figure 4) Further

$$\Gamma_o = \frac{1}{2} c_o C_{l_o} V$$

where c_o = mid-span chord

C_{l_o} = mid-span section lift coefficient

Also:

$$D_i = \frac{1}{2} \rho V^2 S C_{D_i}$$

where: s = wing area

C_{D_i} = induced drag coefficient

Thus:

$$\frac{4\pi D_i}{\rho\gamma^2} = \frac{8\pi S C_{D_i}}{c_o^2 C_{l_o}}$$

The distance between the two rolled-up vortices 2b' is determined from the stipulation that the lift impulse must be preserved throughout the rolling-up process; thus:

$$2b' = \frac{L}{\rho V \Gamma_o} = \frac{C_L S}{C_{l_o} c_o} \qquad (3.28)$$

The aspect ratio of a wing is defined by:

$$AR = \frac{(\kappa b)^2}{S} \tag{3.29}$$

Thus with the aid of the above equations, the expression for the induced drag can be written as,

$$\frac{4\pi D_i}{\rho \gamma^2} = \frac{\kappa \pi AR\, C_{D_i}}{C_L^2}\left(\frac{b'}{b}\right)^2$$

Expression (3.27) becomes finally

$$\frac{a}{b} = \frac{b'}{b}\left[\left\{\frac{1+\exp\left[\left(\frac{\kappa\pi AR\, C_{D_i}}{C_L^2}\right)\left(\frac{b'}{b}\right)^2 - \frac{1}{2}\right]}{-1+\exp\left[\left(\frac{\kappa\pi AR\, C_{D_i}}{C_L^2}\right)\left(\frac{b'}{b}\right)^2 - \frac{1}{2}\right]}\right\}^2 - 1\right]^{\frac{1}{2}} \tag{3.30 (a)}$$

Assuming that

$$\exp\left[\left(\frac{\kappa\pi AR\, C_{D_i}}{C_L^2}\right)\left(\frac{b'}{b}\right)^2 - \frac{1}{2}\right] \gg 1$$

a very close approximation is obtained.

$$\frac{a}{b} = 2\,\frac{b'}{b}\exp\left[\frac{1}{4} - \frac{4\pi AR\, C_{D_i}}{C_L^2}\left(\frac{b'}{b}\right)^2\right] \tag{3.30 (b)}$$

From equations (3.29) and (3.30) the quantity $\frac{b'}{b}$ can be written as:

$$\frac{b'}{b} = \left(\frac{C_L}{C_{L_0}}\right)\left(\frac{C_b}{C_0}\right)\frac{1}{AR}$$

Thus with the above equations it should be possible to determine the core size of the trailing vortex for

any wing for which the lift and induced drag characteristics are calculable.

The preceding developments were outlined briefly by Spreiter and Sacks in reference (7). The procedure followed there however was carried through in terms of the velocity potential instead of the stream function. An expression for the kinetic energy of the vortex system was obtained comparable to the expression (3.24) derived here. The form of the expression involved the core radius in a much more complicated manner than does (3.24) so that it was only after considerable manipulation that the two expressions were shown to be equivalent. Because of the complexity of the expression for the kinetic energy derived by Spreiter and Sacks, it was necessary for them to make the simplifying assumption that $\sqrt{b'^2 + r^2} \cong b'$ in order to solve for the core radius. In the present analysis, no such simplification was necessary with the exact solution (3.30a) being obtained for the core radius. A much closer approximation to the exact solution than that in reference (7) is given by equation (3.30b).

The results of the preceding theory for the rolled-up vortex will now be applied to three families of wings having rectangular, delta, and elliptic planforms. For the rectangular planforms, a comparison of Spreiter and Sacks' approximation is made with the expression (3.30).

3.141 Rectangular Planforms

For a wing having a rectangular planform

$$AR = \frac{b}{c_0}$$

so that

$$\frac{b'}{b} = \frac{C_L}{C_{L_0}}$$

and

$$\frac{a}{b} = \frac{C_L}{C_{L_0}} \left[\frac{1 + \exp\left[\frac{-\pi AR\, C_{L_0}}{C_L} \left(\frac{C_L}{C_{L_0}} - 1 \right) \right]}{1 + \exp\left[\frac{-\pi AR\, C_{L_0}}{C_L} \left(\frac{C_L}{C_{L_0}} - 1 \right) \right]} \right] \qquad (3.31)$$

The variation of $\frac{\pi AR\, C_{L_0}}{C_L}$, $\frac{C_L}{C_{L_0}}$ and $\frac{dC_L}{d\alpha}$ as calculated by Falkner in reference (10) is shown in figure 9. Using these values, the graph of $\frac{a}{b}$ versus AR of figure 10 was obtained. A comparison with the results of reference 6 is also given in this figure where it can be seen that the present values are appreciably greater than those of the reference.

3.142 Delta Planform

The aspect ratio of a delta wing is $AR = 4 \frac{b}{c_0}$

Thus:

$$\frac{b'}{b} = \frac{1}{4} \frac{C_L}{C_{L_0}}$$

The substitution for $\frac{b'}{b}$ into (3.30a) gives:

$$\frac{a}{b} = \frac{1}{4} \frac{C_L}{C_{L_0}} \left[\frac{1 + \exp\left[\frac{-\pi AR\, C_{L_0}}{C_L} \left(\frac{C_L}{C_{L_0}} - 1 \right) \right]}{1 + \exp\left[\frac{-\pi AR\, C_{L_0}}{C_L} \left(\frac{C_L}{C_{L_0}} - 1 \right) \right]} \right] \qquad (3.32)$$

The variation of $\frac{\pi AR\, C_{D_i}}{C_L^2}$, $\frac{C_L}{C_{L_0}}$ and $\frac{dC_L}{d\alpha}$ for delta wings as a function of aspect ratio were estimated from the results of references 10, 11 and 16 and are given in Figure 11. Using these data, the variation of $\frac{\lambda}{b}$ with aspect ratio was obtained and is presented in figure 12.

3.143 <u>Elliptic Planform</u>

The elliptic planform has an aspect ratio given by:

$$AR = \frac{\pi b}{C_0}$$

The characteristics of an elliptic wing are:

$$\frac{\pi AR\, C_{D_i}}{C_L^2} = 1.0$$

$$\frac{C_L}{C_{L_0}} = 1.0$$

$$\frac{dC_L}{d\alpha} = \frac{2\pi}{1 + 2/AR}$$

Thus $\frac{\lambda}{b}$ is a constant for all aspect ratios.

$$\frac{\lambda}{b} = 0.1781 \qquad (3.33)$$

Observe that the core radius increases with increasing aspect ratio for delta wings, is constant for elliptic wings, and decreases with increasing aspect ratio for rectangular wings.

3.150 <u>Prediction of Minimum Pressure Coefficients for Rectangular, Delta and Elliptic Wings on the Basis of a Rolled-Up Vortex Sheet</u>

The expression for the minimum pressure coefficient

at the center of a Rankine vortex has been derived earlier as equation (3.6). In addition, it has been shown that the strength of each vortex is equal to the mid-span value of the bound circulation as determined from equation (3.9). Further, the section lift coefficient at the mid-span can be obtained from

$$c_{l_0} = \frac{c_{l_0}}{\alpha_L} \frac{d\alpha_L}{d\alpha} \alpha \qquad (3.34)$$

where α is the absolute angle of attack of the wing.

If the preceding results are substituted in the equation (3.6) for the minimum pressure coefficient, then the result can be written as

$$-\frac{c_{p_0}}{\alpha^2} = \frac{1}{\pi} \left[\left(\frac{c_{l_0}}{\alpha_L} \frac{d\alpha_L}{d\alpha} \right)^2 \right] \qquad (3.35)$$

The term in the brackets is a function of the aspect ratio and the planform. For the example planforms considered here, this term can be calculated with the aid of the relationships just presented. Observe that the above result predicts that the minimum pressure coefficient should vary directly as the square of the absolute angle of attack. The predicted variation of $-\frac{c_{p_0}}{\alpha^2}$ with aspect ratio for the rectangular, delta, and elliptic planforms is presented in graphical form in figure 13. The elliptical case is shown extrapolated for aspect ratio less than four since lifting line results will not be valid in this region.

Without going into a description of the experimental investigation and its results at this point, let it suffice to say that the results for this case of the completely rolled-up vortex sheet are in considerable disagreement with what is found experimentally. Not only is the measured variation of the minimum pressure coefficient with the angle of attack found to be nearly linear but also, the magnitudes of the minimum pressure coefficients are measured to be much larger than predicted on the basis of the rolled-up sheet. For example, from figure 13 one would predict a rectangular wing with an aspect ratio of four to produce a minimum pressure coefficient of -.0344 at an angle of attack of 6°. This value is considerably smaller in magnitude than the value of -1.2 found experimentally as shown in figure (41). For the rectangular wings in particular, the location of the minimum pressure at the higher angles of attack was several chord lengths downstream of the wing where, according to the results of reference (7), the vortex sheet would be essentially rolled-up. Therefore the fact that the predicted minimum pressure is not in accord with the experimental results indicates a fundamental fault in calculating the vortex core size in this manner.

3.200 <u>Non-Distorted Vortex Sheet</u>

A vortex sheet is in effect a continuous distribution of vortex filaments. The concept of a vortex sheet in

potential motion can be arrived at by consideration of figure 14. Suppose in each division of length δ on a side, a two dimensional vortex of strength γ exists. Now if δ is decreased to the limit zero while the strength and number of the vortices is increased proportional to $\frac{1}{\delta}$, then a vortex sheet is obtained.

The strength of a vortex sheet is measured by the circulation around a unit length of the sheet in the direction normal to the axes of the vortices. If v_1 is the velocity tangent to the sheet at the upper surface and v_2 is the velocity tangent at the lower surface as shown in the figure, then the strength of the sheet would be simply $(v_1 - v_2).(1)$. From the symmetry of the motion it follows that $-v_2 = v_1$ so that $\gamma = 2v_1$. To state the result in a slightly different way, it can be said that the velocity immediately adjacent and tangent to a vortex sheet at a given location is equal in magnitude to one half of the strength of the sheet at that location.

Some observations will now be made concerning the velocity induced normal to the plane of a vortex sheet such as trails from a wing. It will be assumed that the vortex sheet is non-distorted and lies in a plane. In addition the sheet will be considered far enough aft of the wing so that the flow can be treated as two-dimensional.

If $\Gamma(y)$ is the distribution of the bound circulation at the wing, then it follows from vortex continuity that the strength of the trailing vortex sheet is $\frac{d\Gamma}{dy}$. The velocity induced normal to the sheet and in the plane of the sheet at the location y_o is given by the integral expression:

$$w(y_o) = \int_{-b}^{b} \frac{\frac{d\Gamma}{dy}}{2\pi(y_o - y)} dy \qquad (3.36)$$

The very important result is proven in the appendix that $w(y_o)$ is bounded except at $y_o = \pm b$. Therefore, the conclusion follows that not only does the minimum pressure occur at the edge of the sheet but further, that only in this region is the reduction in pressure of any consequence. It should be noted that a special case of the distribution of bound circulation exists which does not produce infinite velocities at the edge. This is for the case where the gradient of the bound circulation vanishes at the tips.

Except for this special case, one would expect the induced velocities at the edge of the trailing vortex sheet to be severely altered by the action of viscosity.

3.210 <u>Proposed Model of a Non-Distorted Vortex Sheet</u>

A hypothetical model of a non-distorted trailing vortex sheet is proposed which avoids the infinite induced velocities associated with the vortex sheet in

purely potential motion. The model is a natural extension of Rankine's hypothesis for a rectilinear vortex. Consider the typical wing with its associated trailing vortex system as shown in figure 2. The vortex sheet which is shed aft of the wing is unstable and tends to roll up into two discrete vortices. The rolling-up process is an asymptotic one but for purposes of calculating the induced velocities at the wing, the sheet can often be considered to be completely rolled up within a chord length or two behind the wing; depending upon the aspect ratio, type of planform, and lift coefficient of the wing. The behavior of the vortex system in the so-called "ultimate wake" has been discussed previously. It should be emphasized that although the existence of a region of rotational motion is supposed, the fluid is assumed perfect for, in calculating the kinetic energy of the system of two rectilinear vortices, the dissipative action of viscosity is ignored. Similarly, a perfect fluid will be assumed in this analysis. Consider the motion in a transverse plane aft of the wing as shown in figure 15 where the vortex sheet is essentially non-distorted.

If the motion were entirely potential, then the vortex sheet represents a surface through which the tangential component of the velocity is discontinuous. The direction of the tangential velocity at the surface of the sheet is as shown in the figure. The magnitude of

the velocity is equal to $\frac{1}{2}\frac{d\Gamma(y)}{dy}$ on the left half of the wing and $-\frac{1}{2}\frac{d\Gamma(y)}{dy}$ on the right half. For the usual wing, the magnitude of $\frac{d\Gamma(y)}{dy}$ is zero at the mid-span, increases slightly outboard and in the near vicinity of the wing tip becomes quite large approaching infinity at the tip. In a real fluid where viscosity is allowed to act, the tangential velocity of course is continuous so that the sheet can be thought of as having a thickness, not dissimilar from the thickness of a boundary layer. The thickness of the region in which viscosity predominately changes the irrotational form of the vortex motion is probably of the order of the boundary layer thickness.

Near the center of the sheet, the tangential velocity is small with the energy of that fluid affected by viscosity being concentrated towards the tips. For the following development it will be assumed initially that the rotational motion with its energy is confined entirely within a region defined by a streamline of the potential flow. This hypothetical model of the vortex sheet is shown as proposed in figure 16. Obviously the vorticity cannot be assumed to have a constant value within this region, as is the case for Rankine's model of a rectilinear vortex, since the strength of the vortex sheet varies in the y direction. In the next section, the distribution of

energy along the width of the vortex sheet will be considered with the subsequent modification of the relationships derived in this section.

3.220 Calculation of Model Dimensions

The method of approach will be the same as was taken in the case of the completely rolled-up vortex sheet. That is, the kinetic energy per unit length of the proposed model system will be equated to the induced drag of the wing in order to find the value of the streamline which bounds the region of rotational motion. Immediately the question arises as to how to calculate the kinetic energy of the rotational motion within the bounding streamline. The energy outside of the streamline can be calculated by the method followed in the case of the completely rolled-up sheet but the distribution of the velocity in the rotational portion is not so easily calculable. Fortunately there is a way around this difficulty. Even though the existence of a region of rotation in the fluid is being allowed it has merely been assumed to exist with no stipulation as to how it originated. Thus if this model is allowed to roll up into the system of the two discrete vortices each having an inner core containing the vorticity, the fluid within the boundaries of the region of vorticity for the model of the vortex sheet will then be within the cores of the trailing rectilinear vortices. Now since it

is assumed that there is no agent present for the dissipation of energy, it follows that the energy of the fluid outside of the vortex cores is equal to the kinetic energy of the fluid outside of the streamlines confining the vorticity in the model of the vortex sheet.

The kinetic energy per unit length of the irrotational portion of the model vortex sheet is evaluated by use of the expression previously derived and repeated here.

$$K_i = -\frac{1}{2}\rho \int_C \psi v_s \, ds \qquad (3.37)$$

The path of integration to be considered is indicated in figure 17. The kinetic energy of the potential flow will equal the limit, as ϵ approaches zero, of expression (3.37) evaluated about the path indicated.

Consider first the integral about the outer paths. These paths are chosen so that ψ is constant along them. From the symetry of the problem it is evident that the stream function and v_s along the left hand path are both the negative of the corresponding quantities on the right hand path. Thus for the outer paths, equation (3.37) becomes

$$K_{i_{outer}} = -\rho \psi \oint_C v_s \, ds$$

where the contour is taken as the outer path on the right side of figure 17. But the closed line integral of v_s about this path is simply the value of the bound circulation

at the location where the path cuts the vortex sheet. This value is never larger than Γ_0 ; therefore, it follows that

$$|K_{i_{outer}}| \leq \int \psi' \Gamma_0$$

Now ψ is taken to be zero along the dividing streamline as shown in the figure. Thus for any other streamline, say at $y = \frac{\epsilon}{2}$ as pictured then

$$\psi' = \int_0^{\frac{\epsilon}{2}} w(y)\, dy$$

where w(y) is the velocity induced normal to the sheet as before. Let $W(\epsilon)$ be the least upper bound of w(y) in the interval ϵ . This exists from the proof given in the appendix that w(y) is finite except at the edges of the sheet. It follows then from an elementary integral theorem that

$$\psi' \leq W(\epsilon) \frac{\epsilon}{2}$$

It can thus be stated that

$$|K_{i_{outer}}| \leq \int \Gamma_0 W(\epsilon) \frac{\epsilon}{2}$$

From this it can be seen that as ϵ approaches zero the contribution to equation (3.37) along the outer paths vanish. Therefore the path of integration reduces to that shown in figure 18.

The problem then is that of evaluating equation (3.37) along the path indicated. As an aid in describing the

procedure, positions in figure 18 along the path of integration have been numbered. Thus

$$I = -\left[\int_{1-2-3} \psi_1 \zeta_3 \, ds + \int_{3-4} \psi \zeta_3 \, ds + \int_{4-5} \psi \zeta_3 \, ds + \int_{5-6-7} \psi \zeta_3 \, ds + \int_{7-8} \psi \zeta_3 \, ds + \int_{8-1} \psi \zeta_3 \, ds\right]$$

$$= -\left[I_1 + I_2 + I_3 + I_4 + I_5 + I_6 \right]$$

Along the path 1-2-3 the stream function is a constant. Let the value of this stream function be denoted by $\psi(-y^*)$. Then the first integral becomes

$$I_1 = \psi(-y^*) \int_{1-2-3} \zeta_3 \, ds$$

but $\int_{1-2-3} \zeta_3 \, ds$ is the value of the bound circulation at the position 1 (or 3). If this value is denoted as $\Gamma(-y^*)$ then the first integral becomes finally:

$$I_1 = \psi(-y^*) \Gamma(-y^*)$$

The tangential velocity from 3 to 4 is $\frac{1}{2} \frac{d\Gamma(y)}{dy}$. Thus since ds = dy the second integral can be written as:

$$I_2 = \frac{1}{2} \int_{-y^*}^{0} \psi(y) \frac{d\Gamma(y)}{dy} \, dy$$

The tangential velocity from 4 to 5 in the direction indicated is also $\frac{1}{2} \frac{d\Gamma(y)}{dy}$. The third integral is thus:

$$I_3 = \frac{1}{2} \int_{0}^{y^*} \psi(y) \frac{d\Gamma(y)}{dy} \, dy$$

Along the path 5-6-7 the stream function is constant. If this is denoted by $\psi(y^*)$ then the fourth integral is:

$$I_4 = \psi(y^*) \int_{5-6-7} \zeta \, ds$$

But in the direction indicated on the figure $\int_{5-6-7} \zeta \, ds$ is the negative of the value of bound circulation at y^*, say $\Gamma(y^*)$.

The fourth integral is then:

$$I_4 = -\psi(y^*)\Gamma(y^*)$$

In like manner the fifth integral is; since $ds = -dy$:

$$I_5 = -\frac{1}{2}\int_{y^*}^{0} \psi(y) \frac{d\Gamma(y)}{dy} dy$$

and the last integral is:

$$I_6 = -\frac{1}{2}\int_{0}^{-y^*} \psi(y) \frac{d\Gamma(y)}{dy} dy$$

But $I_2 = -I_6$ and $I_3 = -I_5$. Thus

$$I = -\psi(-y^*)\Gamma(-y^*) + \psi(y^*)\Gamma(y^*)$$
$$-\int_{-y^*}^{0} \psi(y) \frac{d\Gamma(y)}{dy} dy - \int_{0}^{y^*} \psi(y) \frac{d\Gamma(y)}{dy} dy$$

From the symmetry of the problem

$$\Gamma(-y) = \Gamma(y)$$
$$\frac{d\Gamma(-y)}{dy} = -\frac{d\Gamma(y)}{dy}$$
$$\psi(-y) = -\psi(y)$$

The expression for I can then be written as

$$I = 2\left[\psi(y^*)\Gamma(y^*) - \int_0^{y^*} \psi(y)\frac{d\Gamma(y)}{dy}dy\right]$$

Consider the integral in the above expression:

$$\int_0^{y^*} \psi(y)\frac{d\Gamma(y)}{dy}dy = \left[\psi(y)\Gamma(y)\right]_0^{y^*} - \int_0^{y^*} \Gamma(y)\frac{d\psi(y)}{dy}dy$$

$$= \psi(y^*)\Gamma(y^*) - \int_0^{y^*} \Gamma(y)\frac{d\psi}{dy}dy$$

The expression for I then becomes

$$I = 2\int_0^{y^*} \Gamma(y)\frac{d\psi(y)}{dy}dy$$

Now if w(y) denotes the induced velocity in the -z direction at any point on the y-axis, then from the definition of the stream function

$$\frac{d\psi(y)}{dy} = w(y)$$

The final expression for the kinetic energy for the irrotational motion outside of the streamline which intersects the y-axis at y^* is simply

$$K_i = \rho\int_0^{y^*} \Gamma(y)\,w(y)\,dy \qquad (3.38)$$

This expression allows of a simple physical interpretation. Since w(y) is the downwash in the ultimate wake, the downwash at the plane of the wing will be $\frac{w(y)}{2}$. The Kutta-Joukowski Law states that

$$\bar{F} = \rho\,\bar{V}_\infty\,\bar{\Gamma}$$

where: F = force vector

V = velocity vector

Γ = circulation vector

Applying the Kutta-Joukowski Law, the induced drag on a differential length of wing, dy, is given by

$$dD_i = \int_{-y^*}^{y^*} \frac{w_i(y)}{2} \Gamma(y)\, dy$$

Thus expression (3.38) can be seen to be equal to the induced drag contributed by that portion of the wing between $-y^*$ and y^*. If y^* is allowed to approach b, then this constitutes a proof that the kinetic energy per unit length of the vortex system is equal to the induced drag.

Now the kinetic energy of the irrotational motion outside the cores of the model of the completely rolled-up vortex sheet can be expressed as the difference between the induced drag and the kinetic energy within the cores. This circumvents the necessity of calculating the core radius since the kinetic energy in the cores was shown to depend only upon the strength of the vortices. This energy was developed earlier as:

$$K_r = \frac{\rho \Gamma_0^2}{8\pi}$$

Thus:

$$K_i = D_i - K_r = D_i - \frac{\rho \Gamma_0^2}{8\pi}$$

Equating (3.38) to the above gives finally the integral relationship for y^*:

$$\rho \int_0^{y^*} \Gamma(y)\, w(y)\, dy = L_i - \frac{\rho \Gamma_0^2}{\pi} \tag{3.39}$$

The above equation could also be written as

$$\int_{y^*}^{b} \Gamma(y)\, w(y)\, dy = \frac{\Gamma_0^2}{\pi} \tag{3.40}$$

For a given distribution of bound circulation, it is now possible to determine the region in which the rotational flow is assumed to be confined. The expression for the downwash was given previously as

$$w(y_0) = \int_{-b}^{b} \frac{\frac{d\Gamma}{dy}\, dy}{2\pi (y_0 - y)} \tag{3.41}$$

The stream function for a vortex in irrotational motion at the origin is:

$$\psi = \frac{\kappa}{2\pi} \log (z^2 + y^2)^{\frac{1}{2}}$$

For the vortex centered at y the stream function at y_0 along the line z = 0 where $y_0 > b$ is:

$$\psi(y_0) = \frac{\kappa}{2\pi} \log (y_0 - y)$$

The stream function outside of the vortex sheet is found from

$$\psi(y_0) = \frac{1}{2\pi} \int_{-b}^{b} \frac{d\Gamma}{dy} \log (y_0 - y)\, dy \tag{3.42}$$

The procedure then is to calculate w(y) given $\Gamma(y)$. Then by application of (3.39) or (3.40) the value of y^* can be found. The value of $\psi'(y^*)$ is then calculated from

$$\psi'(y^*) = \int_0^{y^*} \Gamma(y)\,dy \tag{3.43}$$

But this streamline for which the stream function has the value $\psi(y^*)$ is also the streamline defining the outer extremity of the rotational flow. $\psi'(y^*)$ is thus equated to (3.42) in order to find $\bar{y}_0$, the location of the edge of the region of the rotational flow. The velocity at this point is then determined from (3.51).

3.230 Modification Due to the Distribution of the Energy in the Vortex Sheet

Since the growth of the region in the vortex sheet in which viscous forces predominate does not necessarily follow the streamlines of the potential flow pattern, the artifice of assuming the rotational motion to be confined within a streamline must be modified in order to be applicable. Conjecture must be made as to the shape of the actual sheet. Allowing for the action of viscosity throughout its breadth, the streamline pattern of a typical trailing vortex sheet will appear as shown in figure 19. The dashed lines running horizontally indicate the region close to the plane of the sheet in which the viscous forces

predominate. For the sake of description, this region is shown considerably thicker than it actually is. Also indicated by dashed lines are the positions of the streamlines of the irrotational motion before acted upon by viscosity.

Now of course what is actually desired in figure 19 is the value of the streamline ψ_1, which outlines approximately the rotational flow around the edge of the sheet. However, since the energy of the core of the rolled-up vortex includes the energy of rotational motion both inside and outside of ψ_1, it follows that by the procedure as outlined, a value of the streamline will be obtained which encloses the streamline ψ_1. In order to obtain the value of ψ_1, the energy of the irrotational motion must be taken as equal to the sum of the energy of the actual irrotational motion as obtained from the rolled-up sheet and the energy of the rotational motion outside of ψ_1. Thus it is to be expected that lower values of the minimum pressures will be obtained in practice than are predicted here. On the other hand it would seem reasonable to expect that predictions based on the bounding streamline would be qualitatively indicative of the results obtained from ψ_1. The experimental results to be discussed later, indicate however that the energy of the inner region cannot be neglected if quantitative predictions are to be made.

For an insight into the behavior of the inner region of this sheet application will be made of the Kármán momentum integral equation, given in reference (13), for the boundary layer. It is realized, in view of the turbulent nature of the flow behind a wing, that the results of such analysis will only be qualitatively indicative of the actual case.

Consider a portion of the vortex sheet as shown in figure 20. Along the outer edge of the "boundary layer," the velocity will be denoted as u_1. For a vortex sheet of constant strength and infinite extent, the velocity induced tangent to the sheet is constant away from the sheet and is equal to one half the strength of the sheet. Thus, if the thickness of the sheet pictured in figure 19 is small as compared to its breadth and if the spanwise gradient of the strength of the sheet is not too great, then in view of the infinite sheet the approximation appears justifiable that the velocity u_1 is equal to one half the strength of the sheet. Such an approximation should hold except in the region of the edge of the sheet. The thickness of the layer will be denoted by δ as indicated on the figure. The general velocity distribution through the layer will be denoted as u. If x is the direction along the sheet in the direction of the velocity and y is

the outward direction normal to the sheet, then the momentum equation states

$$\frac{\mu}{\rho}\left(\frac{\partial u}{\partial y}\right)_{y=0} = u_1 \frac{\partial \theta}{\partial x} + (2\theta + \delta_1)\, u_1 \frac{\partial u_1}{\partial x} \qquad (3.44)$$

where:

$$\theta = \int_0^{\delta} \frac{u}{u_1}\left(1 - \frac{u}{u_1}\right) dy \quad = \text{momentum thickness}$$

$$\delta_1 = \int_0^{\delta} \left(1 - \frac{u}{u_1}\right) dy \quad = \text{displacement thickness}$$

If all distances in the above expressions are made dimensionless with respect to the semi-breadth of the sheet, b, and all velocities with respect to the reference velocity, $\frac{\Gamma_0}{b}$, and if further it is assumed that the form of the velocity distribution, $\frac{u}{u_1}$, is independent of x, the equation (3.44) can be written as

$$I_\theta u_1 \frac{\partial (k_p \delta)}{\partial x} + (I_\delta + 2 I_\theta)(k_p \delta) \frac{\partial u_1}{\partial x} = f'(0) \qquad (3.45)$$

where:

$$f(\eta) = \frac{u}{u_1}$$

$$f'(0) = \left(\frac{df}{d\eta}\right)_{\eta=0}$$

$$\eta = \frac{y}{\delta}$$

$$I_\theta = \int_0^1 f(\eta)\left(1 - f(\eta)\right) d\eta$$

$$I_\delta = \int_0^1 \left(1 - f(\eta)\right) d\eta$$

and all lengths and the velocity u_1 are dimensionless as previously prescribed. Since the strength of the sheet, and thus u_1, is known, the equation (3.45) is of the form

$$\frac{d\delta}{dx} + P(x)\,\delta = Q(x) \qquad (3.46)$$

This is a common linear differential equation, the solution of which is given in closed form as

$$\delta = e^{-\int P\,dx}\int Q\,e^{\int P\,dx}\,dx + K\,e^{-\int P\,dx} \qquad (3.47)$$

K being the constant of integration. The functions P and Q can be seen to be

$$P(x) = \frac{(I_\delta + \alpha I_\theta)\,\delta\,\frac{u_1}{x}}{I_\theta\,u_1}$$

$$Q(x) = \frac{f'(\eta)}{I_\theta\,u_1}$$

The function $f(\eta)$ should be chosen so that $f(1) = 1$ and its derivative at the edge of the layer is equal to that of the irrotational flow. Since this derivative varies along the sheet, for purposes of qualitative analysis, the function will be selected on the same basis as for uniform flow over a flat plate. This discrepancy in the derivative should not seriously alter the results of the analysis since for an infinite vortex sheet of constant

strength this would be exactly the case. If $f(\eta)$ is then chosen of the form $f(\eta) = A\eta + B\eta^2$ to satisfy $f(0) = 0$, $f(1) = 1$, $f'(1) = 1$ then the final function becomes:

$$f(\eta) = 2\eta - \eta^2 \tag{3.48}$$

For this distribution $I_\theta = \frac{2}{15}$

$$I_\delta = \frac{1}{3}$$

$$f'(0) = 2$$

Thus equation (3.55) can be written as

$$\frac{\partial (R_p \delta)}{\partial x} + \frac{9}{2} \frac{\frac{\partial u_1}{\partial x}}{u_1} (R_p \delta) = \frac{15}{u_1} \tag{3.49}$$

or

$$R_p \delta = e^{-\frac{9}{2}\int \frac{\frac{\partial u_1}{\partial x}}{u_1} dx} \int \frac{15}{u_1} e^{\frac{9}{2}\int \frac{\frac{\partial u_1}{\partial x}}{u_1} dx} dx + K e^{-\frac{9}{2}\int \frac{\frac{\partial u_1}{\partial x}}{u_1} dx}$$

The total kinetic energy per unit length of the vortex sheet in the boundary layer of the sheet between -x and x can be found as

$$K_{BL} = 4\left[\frac{\rho}{2}\int_0^x \int_0^\delta u^2 dy\, dx\right] \tag{3.50}$$

In terms of the dimensionless quantities previously employed, this can be rewritten as

$$K_{BL} = \frac{2\rho \Gamma_0^2}{R_p}\left[\int_0^1 f'^2(\eta)\, d\eta\right] \int_0^x u_1^2 (R_p \delta)\, dx \tag{3.51}$$

Some of the uncertainties involved in this development will be circumvented now by, in effect, normalizing the problem. That is, the expression (3.51) will be used only to estimate the distribution of the energy in the rotational motion of the vortex system. For this purpose a factor $\eta_e(x)$ is defined by

$$\eta_e(x) = \frac{\int_0^x u_1^2(R_\Gamma \delta)\, dx}{\int_0^1 u_1^2(R_\Gamma \delta)\, dx} \tag{3.52}$$

where $R_\Gamma \delta$ is obtained from equation (3.49).

To find the energy of the rotational motion between x and -x, the energy between x = 1 and -1 is multiplied by $\eta_e(x)$. Thus equations (3.39) and (3.40) will give more closely the inner location of the streamline ψ_1, in figure 19 if they are modified to read

$$\rho \int_0^{y^*} \Gamma(y) u(y)\, dy = D_i - \frac{\rho \Gamma_0^2}{8\pi}(1-\eta_e) \tag{3.53}$$

$$\int_{y^*}^{b} \Gamma(y) u(y)\, dy = \frac{\Gamma_0^2}{8\pi}(1-\eta_e) \tag{3.54}$$

The question now arises as to how to determine the pressure drop through the region of rotational flow. In order to determine this drop, the distribution of the velocity in the region of rotation must be known. Since

the steady model of the vortex sheet, as in the case of Rankine's model of a vortex is a violation of the equations of viscous motion (in a viscous fluid, the vorticity was shown to be a function of time) a continuous solution of the equation of motion cannot be expected. However, the equations of motion can be considered for the region of rotation distinct from the irrotational flow with conditions at the boundary being ignored. If the streamlines for $|y| > b$ in the rotational motion of the sheet are assumed to lie on circles concentric about the edge of the sheet, then, as in the case of the vortex core, the v component of the velocity would be given closely by ωr. From consideration of the equations of motion, this assumption appears valid, at least for small values of r. At the boundary of the region the velocity is to be continuous and equal to the velocity of the irrotational motion at that point.

Under these conditions the pressure drop through the region of vorticity will equal the drop through the region of irrotational flow. Thus is $\bar{\omega}_0$ equals the velocity at $(0, \bar{y}_0)$ then the minimum pressure coefficient for the model of the vortex sheet will be given by

$$C_p = \frac{p - p_\infty}{\frac{1}{2}\rho V_\infty^2} = -2\left(\frac{\bar{\omega}_0}{V_\infty}\right)^2 \qquad (3.55)$$

3.240 Prediction of Minimum Pressure Coefficient for the Elliptic Wing on the Basis of the Proposed Model of a Non-Distorted Vortex Sheet

To the approximation of a lifting line, the elliptic distribution is readily applicable to the theory just developed for the non-distorted sheet. For an elliptic wing the distribution of bound circulation is

$$\Gamma = \Gamma_0 \sqrt{1 - \left(\frac{y}{b}\right)^2} \tag{3.56}$$

If this distribution of circulation is substituted into equation (3.41) for the downwash velocity, then it will be found that

$$w(y) = \frac{\Gamma_0}{b} \qquad y < b \tag{a}$$

$$w(y) = \frac{\Gamma_0}{2b}\left(\frac{\frac{y}{b}}{\sqrt{\left(\frac{y}{b}\right)^2 - 1}} - 1\right) \qquad y > b \tag{b}$$

(3.57)

The induced drag for this case is calculated as:

$$D_i = \frac{1}{2}\rho V^2 \frac{C_L^2}{\pi AR} \tag{3.58}$$

while the mid-span value of the circulation is related to the wing lift coefficient by

$$\Gamma_0 = \frac{1}{2} c_0 C_L V \tag{3.59}$$

since

$$c_{L_0} = C_L$$

For this particular case, it is somewhat easier to use expression (3.54) for determining y^*. If (3.59) is substituted into expression (3.54) then the result reduces to

$$\int_{x^*}^{1} \sqrt{1-x^2}\, dx = \frac{1}{4\pi}\left[1-\eta_c(x)\right] \tag{3.60}$$

where

$$x^* = \frac{y^*}{b}.$$

or

$$x^*\sqrt{1-x^{*2}} + \sin^{-1}x^* = \frac{\pi^2-1+\eta_c(x)}{2\pi} \tag{3.61}$$

The function $\eta_c(x)$ can be found by integrating equation (3.49) with u_1 given by

$$u_1 = \frac{1}{2}\frac{x}{\sqrt{1-x^2}} =$$

and subject to the condition that $R_r\lambda$ is bounded.

The solution to equation (3.61) will then be found as

$$y^* = .951\, b$$

The stream function at y^* can be found easily by integrating the constant value of the downwash from 0 to y^*

$$\psi(y^*) = \frac{\Gamma_0}{2}\frac{y^*}{b} = 0.476\,\Gamma_0 \tag{3.62}$$

If the Γ' distribution given by (3.56) is substituted into expression (3.42) for the stream function for $y > b$, then upon integrating the resulting equation

it will be found that

$$\psi = \frac{\Gamma_0}{2}\left(\frac{y}{b} - \sqrt{\left(\frac{y}{b}\right)^2 - 1}\right) \tag{3.63}$$

Equating the above to $\psi(y^*)$ gives

$$\bar{y}_0 = 1.00126\, b \tag{3.64}$$

This then is the outer limit of the region of rotational motion for an elliptic wing. The downwash velocity at this location can be found from (3.57b) as

$$w(\bar{y}_0) = 9.47\,\frac{\Gamma_0}{b} \tag{3.65}$$

The minimum pressure coefficient for this case by virtue of expressions (3.55) and (3.65) is

$$\begin{aligned} C_p &= -171.5\left(\frac{\Gamma_0}{bV}\right)^2 \\ &= -171.5\left(\frac{x}{\pi AR}\frac{dC_L}{dx}\right)^2 x^2 \end{aligned} \tag{3.66}$$

This expression has been evaluated for the elliptic wings of aspect ratios 4, 7, and 10.2 with the results given in figure (21). For comparison purposes, the experimental data obtained for these wings are also included. Although the agreement is considerably better than for the case of the rolled-up vortex sheet, there are still appreciable differences between the predicted and experimental results as is obvious from the figure.

3.200 Discussion of Theoretical Postulations

The limiting cases of a completely rolled-up vortex sheet and a non-distorted vortex sheet have been considered from a strictly theoretical sense. Rankine's hypothesis that the vorticity is contained within a streamline of the irrotational motion has been extended to the treatment of the non-distorted sheet.

A major question in these theoretical developments concerns the form of the velocity distribution in the region of rotational motion. Obviously the treatment of either limiting case as a steady two dimensional flow in itself violates the laws of motion of a viscous fluid. However, once the model is established, determination of its geometry to satisfy the energy considerations should produce results in agreement with the physical case. To illustrate this point further for the present case, consider the rolled-up vortex sheet once again. Although there is some argument for assuming a constant value of the vorticity in the core in view of the fact that at least the equations of motion are satisfied locally, it would appeal more to physical intuition to use a velocity profile for which not only is the velocity itself but also its first derivative continuous at the edge of the core.

To see what effect the selection of the velocity profile in the core has upon the prediction of the limiting

pressure the following calculations were performed. Assume the velocity in the core to be given by

$$v_1 = C_1 r + C_2 r^3 \tag{3.67}$$

This is the form of the velocity which is indicated by the first two terms in the expansion of Lamb's solution for small values of the radius. C_1 and C_2 are constants to be determined from the continuity of the velocity and its derivative at the edge of the core with the velocity of the irrotational motion outside of the core.

Without going into the details of these calculations, the expression for the velocity becomes

$$v_1 = \frac{\Gamma}{\pi a}\left[\frac{r}{a} - \frac{1}{2}\left(\frac{r}{a}\right)^3\right] \tag{3.68}$$

The pressure drop through the core for this velocity distribution can be calculated as

$$P_a - P_o = \frac{7\rho\Gamma^2}{24\pi^2 a^2} \tag{3.69}$$

The kinetic energy per unit length of the fluid motion within the core would be

$$K_r = \frac{\rho\Gamma^2}{2.96\pi} \tag{3.70}$$

If this expression for the kinetic energy of the core is used in place of expression (3.25) then the expression for the core radius (3.30a) will read

$$\frac{a}{b} = \frac{b'}{b}\left[\frac{\left(1+\exp\left[\frac{8\pi A C_{D_1}}{C_L^2}\left(\frac{b'}{b}\right)^2 - 1.55\right]\right)^2}{\left(-1+\exp\left[\frac{8\pi A C_{D_1}}{C_L^2}\left(\frac{b'}{b}\right)^2 - 1.55\right]\right)} - 1\right]^{\frac{1}{2}}$$

If the elliptic wing is considered, the core radius is found to be a = .2695 b. The minimum pressure coefficient is predicted to be:

$$\frac{C_p}{\alpha^2} = -.477\left[\frac{C_o}{b}\,\frac{C_{l_o}}{C_L}\,\frac{dC_L}{d\alpha}\right]^2 \qquad (3.71)$$

The minimum pressure coefficient for the elliptic wing assuming a linear variation of the velocity in the core is:

$$\frac{C_p}{\alpha^2} = -.423\left[\frac{C_o}{b}\,\frac{C_{l_o}}{C_L}\,\frac{dC_L}{d\alpha}\right]^2$$

Thus it can be seen that even though two extremely different forms of the velocity distribution in the core were assumed, the considerations of kinetic energy determined a value of the core radius in each case so as to produce predicted minimum pressures which vary only slightly from one another.

Attempts to improve upon the results of the theory of the non-distorted vortex sheet have not proven fruitful. Although the treatment based mainly on the relationship between the induced drag of the wing and the kinetic energy of the vortex sheet neglects any effect on the vortex sheet of the boundary layer developed on the wing or the effect of the turbulence generated by the wing, it is difficult to see how these can be accounted for theoretically. It was mentioned earlier that a solution of the Navier-Stokes equations satisfying the boundary conditions

which the wing imposes would be desirable but even here, the results would be questionable due to the turbulent flow. Because of these reasons it was decided to develop a semi-empirical approach which would furnish engineering answers to the problem. Before presenting this development however it would be well to discuss the experimental investigation and its results.

4.000 Experimental Investigation

4.100 Basis of Investigation

It was mentioned earlier that the problem of the minimum pressure in a trailing vortex system is important in connection with vortex cavitation of marine propellers. It is this same phenomenon of cavitation which was used in the experimental investigation to determine the minimum pressure in the vortex system. It might be well, before getting into a description of the actual experiment, to discuss briefly the phenomenon of cavitation.

Cavitation will occur at a given point in a flow of liquid whenever the local static pressure at that point is reduced to a pressure equal closely to the vapor pressure. The exact pressure for the inception of cavitation, sometimes referred to as the critical pressure, although close to the vapor pressure depends somewhat upon the state of the liquid. This is apparently due to the surface tension which prevents the growth of cavitation bubbles unless nuclei are present about which the bubbles can form. Unless a special effort has been made to reduce the air content, however, the critical pressure and vapor pressure are nearly identical. It will be assumed that such is the case for this experimental investigation.

The series of photographs of figure (22) illustrate the manner in which cavitation is used to determine the minimum pressure. In these photographs water is flowing

past a hemispherical nose. In the first photograph, either the velocity is great enough or the free stream static pressure is sufficiently low so that the local static pressure at the juncture of the hemisphere with the cylindrical afterbody has decreased to the value of the vapor pressure. In this instance vapor pressure exists over a considerable region of the nose with the resulting cavitation occuring over quite a broad band. In the second picture, the velocity has been decreased or the free stream static pressure increased so that the ensuing cavitation is not as pronounced. In the third photograph the free stream conditions are such that only the smallest amount of cavitation remains. If the free stream velocity were decreased slightly or the free stream static pressure increased a small amount then this cavitation would disappear altogether.

Now suppose that p_∞ and V_∞ are the free stream pressure and velocity respectively at which the cavitation just disappears. For these particular values then it is known that the minimum pressure along the body is located at the point where the cavitation had been present, and further it is known that this minimum pressure is equal to the vapor pressure. The minimum pressure coefficient can then be calculated as

$$C_p = \frac{p_v - p_\infty}{\frac{1}{2}\rho V_\infty^2}$$

Thus the minimum pressure coefficient can be determined for the body from observation only with no recourse to direct measurement.

On a body such as that just considered the direct measurement of the minimum pressure is not too difficult. For a trailing vortex however whose location is rather unstable, the advantage of determining the minimum pressure by observing the cavitation at the center of the vortex is apparent. Actually, it is difficult to see how the minimum pressure would be measured directly in a vortex in view of the velocity distribution about the vortex.

It is standard practice in hydrodynamics to define the state of a given flow with regards to cavitation in terms of a parameter known as a cavitation index. This parameter, denoted by σ, is defined as

$$\sigma = \frac{p - p_v}{\frac{1}{2}\rho V^2} \tag{4.1}$$

The particular value of this index at which cavitation just begins is known as the critical cavitation index, denoted by σ_{cr}. Observe that the minimum pressure coefficient is the negative of σ_{cr}. If the operating index, σ, is greater than σ_{cr} then cavitation will not be present while if σ is less than σ_{cr} then the minimum pressure will be less than the vapor pressure and cavitation will occur.

4.200 Test Equipment

The purpose of the experimental investigation was to determine the variation of the minimum pressure in the trailing vortex systems of elliptic, rectangular and delta wings as a function of aspect ratio, angle of attack, and Reynolds number. These results could then be used to compare with any theoretical predictions or, as is done later, be used as the basis for a semi-empirical development. Determination of these minimum pressures was accomplished by observing the cavitation in the trailing vortex systems of families of elliptic, rectangular, and delta semi-wings mounted in the Garfield Thomas Water Tunnel. This tunnel is a facility of the Ordnance Research Laboratory, operated by the College of Engineering and Architecture of The Pennsylvania State University under contract from the U.S. Navy Bureau of Ordnance.

A sketch of the Garfield Thomas Water Tunnel is given in figure (23). This tunnel, with a capacity of 100,000 gallons, has a four foot diameter circular test section with a length of 14 feet. The test section velocity is continuously variable up to a maximum velocity of eighty feet per second. The static pressure at the centerline of the tunnel is variable from three to sixty pounds per square inch absolute.

A diagram of the test equipment mounted in the tunnel test section can be seen in figure (24). A four-by-four foot false floor divides the test section along the horizontal diameter. This false floor is supported in the center by a large strut and at the middle of the leading and trailing edges by smaller struts fabricated from elliptical tubing. At the sides, the floor is attached to the tunnel walls with lengths of angle iron. The large center strut is hollow with a shaft running up through it to a turntable. Mounted on this turntable projecting vertically into the flow is the semi-wing shape to be tested. Since the false floor lies on the dividing streamline of the flow about the wing, except for the boundary layer of the plate the flow about the semi-wing will be unaffected by the presence of the floor.

Figure (25) is a sketch showing the arrangement for turning the wings. A worm-wheel is fastened to the end of the shaft from the turntable. This wheel is driven by a worm gear such that ten turns of the gear produces about 30 degrees travel of the wing. Attached to the shaft which drives the wing is a potentiometer. This potentiometer is connected in an active leg of a bridge circuit. A diagram of this circuit is given in figure (26). This is a null circuit which was used to determine the angular position of the wing. Angular calibrations of the circuit were performed frequently during the tests.

These calibrations are performed as follows. The assumed zero lift line is marked on the base of each wing. A protractor is lined up with a scribe line defining the direction of the undisturbed flow in the tunnel. Then the wing is set to the limit of its angular travel. With the potentiometer A set to a fixed reading, the potentiometer B is adjusted so that the milliammeter reading is zero. The angle of the wing is then changed about two degrees. The setting of the potentiometer B is then recorded which is necessary to once again zero the ammeter. This procedure is performed over the angular travel used in the tests. The result of the calibration is a graph of the angular position of the wing as a function of the setting of the potentiometer B for a fixed setting of potentiometer A. Such a calibration is given in figure (27). The method of attaching the wings to the turntable was relatively simple. A flange at the base of the wing shapes fits into a milled recess in the turntable. A cover plate then slips down over the flange and is bolted down flush with the surface of the false floor.

There were nineteen wings tested altogether. For ease of notation these wings were given an identifying number. The numbers and descriptions of wings are listed in table (I).

Wing number 1 was manufactured to extremely close tolerances by the Technical Services Corporation of

Newport News, Virginia. The cost involved in doing this for all of the wings was prohibitive however, so that it was decided to machine and hand-finish the rest in the Water Tunnel Machine Shops. In order that the effect of manufacturing differences might be determined, at least in part, wing number 10 was selected to have the same planform shape as the first wing. During the course of the experiment however, a special profiler was installed in the Water Tunnel Machine Shops so that it was possible to machine some additional wings accurately using particular stations of wing number 1 as the templates. A photograph representative of the wings which were tested is shown in figure (28).

4.300 Experimental Procedure

The wing to be tested is first mounted on the turntable. A calibration for determining the angular position, as previously described, is then performed. Following this the hatch cover is placed on the test section and the tunnel filled. After filling, the Heise precision type pressure gages which read the test section pressure and a mercury manometer which reads the pressure drop across the nozzle must both be bled to remove any air entrapped in the lines. Also a mercury barometer reading is taken and the Heise gage adjusted to read the correct absolute pressure. With these preliminary arrangements, the testing is ready to begin.

The tunnel is started and the test section velocity and pressure are set to the desired values. Next the wing angle is increased until cavitation in the tip-vortex becomes prominent. The angle is then gradually decreased to the point where the last trace of cavitation just disappears. At this condition readings are taken of the manometer drop across the nozzle, the test section pressure, the water temperature and the wing angle.

With the velocity held constant, the pressure is changed and the procedure is repeated. There is a definite reason for measuring the angle at which the cavitation just disappears rather than that at which it begins. The data obtained is much more consistent. In general, the angle at which cavitation begins is somewhat greater than the angle at which it disappears and is not as repeatable as the latter angle. This is apparently due to the fact that the cavitation itself supplies the necessary nuclei in the form of minute air bubbles about which the cavitation bubbles form; whereas, with no cavitation present, the inception of cavitation is somewhat of a statistical process depending upon the presence of random nuclei. This behavior is characteristic of most cavitation phenomena.

As noted previously, each angular position of the wing is measured relative to an assumed zero lift direction. If this were the correct direction for zero lift then, since the airfoil sections are all symetrical, one would expect the same results for positive and negative angles of attack.

However, because of errors in the manufacture of the wings, errors in the alignment of the wings, or a slight angularity in the test section flow, this is not the case. This uncertainty in the direction of zero lift is easily accounted for however by taking measurements to both sides of the assumed zero lift line and then correcting the measured angles by a constant amount to assure that the results are the same for equal absolute values of the angle of attack. Such a procedure certainly seems legitimate and beyond question. The correction amounted on the average to about four-tenths of a degree and was consistent with the wings.

Tests were conducted at velocities up to about 40 feet per second. Although the tunnel is capable of higher speeds, structural limitations of the false floor prohibited higher speeds. Even at the velocity of 40 feet per second a failure occurred during the course of experimentation. The false floor, although in line with the direction of the flow, experiences a considerable lift force which is probably attributable to the interference of the large central support strut. During the course of a test with wing number (5), the leading edge support tore loose from the relatively soft bronze of the test section allowing the plate to deflect upward producing an even greater lift force. The process being a diverging one occurred in a brief instant when it appeared to the observerer as if everything had simply disappeared before his

eyes. The tunnel was stopped with the emergency stop button but by this time the equipment was badly beaten. The wing was torn loose and carried downstream ending up in the lower leg of the tunnel. Surprisingly enough, however, after having gone through two corner guide vanes and the tunnel impeller, the only damage to the wing was a slightly bent tip which was easily corrected. The false floor however did not fair as well. The force of the water pressed the plate to the top of the test section bending this ½-inch thick aluminum plate to the contour of the tunnel. The tunnel itself suffered some damage with gashes in the bronze walls and a cracked viewing port. Fortunately, this damage could be repaired satisfactorily. After this structural failure, the apparatus was rebuilt with additional strengthening employed.

In addition to the usual tests, measurements were taken over a range of tunnel water temperatures in order to extend the range of Reynolds numbers. It is possible in this manner alone to change the Reynolds number by a factor of two. It is a convenient feature of the tunnel that the temperature can be varied from about 4°C up to 45°C.

A typical raw data sheet is included as table (II). As mentioned previously readings were taken of the test section static pressure and the nozzle drop, as measured by a mercury manometer. The mercury manometer across the nozzle has had the name "Long John" attached to it,

presumably because of its height, hence the headings on the data sheet "Long" and "John" signify the levels of mercury in the two legs. The tunnel has been calibrated and if Δ denotes the pressure drop in inches of mercury across the nozzle, then the average test section velocity is given by

$$V = 8.2\sqrt{\Delta} \quad \text{feet per second} \tag{4.2}$$

The static pressure upon which to base the critical cavitation index cannot be taken simply as the pressure measured by the Meise gage. The Meise gage records the absolute pressure at the start of the test section along the centerline. This pressure must therefore be corrected for the pressure gradient along the test section and also for the height of the wing tip above the centerline of the tunnel.

Let b be the height of the wing above the centerline. Since the surface of the false floor is on the tunnel centerline, this height is also the semi-span of the wing. In addition let p_∞ be the static pressure in the test section at the wing location and p the test section pressure as measured by the Meise gage. If v_∞ is the uniform test section velocity at the location of the wing, then the cavitation index at the wing tip will be given by

$$\sigma_t = \frac{p_\infty - p_v - bw}{\frac{1}{2}\rho V_\infty^2} \tag{4.3}$$

$$= \frac{p - p_v}{\frac{1}{2}\rho V^2}\left(\frac{V}{V_\infty}\right)^2 + \frac{p_\infty - p}{\frac{1}{2}\rho V^2}\left(\frac{V}{V_\infty}\right)^2 - \frac{bw}{\frac{1}{2}\rho V^2}\left(\frac{V}{V_\infty}\right)^2$$

where w is the specific weight of the water. By Bernoulli's equation $p + \frac{1}{2}\rho V^2 = p_\infty + \frac{1}{2}\rho V_\infty^2$

$$\text{or} \quad \frac{p_\infty - p}{\frac{1}{2}\rho V^2} = 1 - \left(\frac{V_\infty}{V}\right)^2 = C_{p_\infty} \qquad (4.4)$$

$$\text{so that} \quad \left(\frac{V}{V_\infty}\right)^2 = \frac{1}{1 - C_{p_\infty}}$$

The expression for the tip cavitation index then becomes

$$\sigma_t = \frac{1}{1 - C_{p_\infty}}\left[\sigma + C_{p_\infty} - \frac{2gb}{V^2}\right] \qquad (4.5)$$

σ is the cavitation index based on the measured pressure and the velocity as given by equation (4.2). The pressure coefficient, C_{p_∞}, is known from calibration tests of the tunnel. It is a slight function of Reynolds number but since it enters as only a small correction to σ, this variation can safely be ignored and an average value of $C_{p_\infty} = -(0.023)$ used.

For ease of computation, the expression for σ_t can be put in the form

$$\sigma_t = 0.977\left[\frac{2.210(p - p_v)}{\Delta} - .023 - .080\frac{b}{\Delta}\right] \qquad (4.6)$$

where: p = test section pressure in psia as read on Heise gage

Δ = nozzle drop in inches of mercury

b = wing semi-span in inches

p_v = vapor pressure in psi

The vapor pressure as a function of temperature is given in table III.

4.400 Experimental Results

The tests which were performed are summarized in table IV. The test numbers correspond to the numbering system used at the Garfield Thomas Water Tunnel. Most of the tests were conducted at a test section velocity of 40 fps with the test section pressure being varied from about 5 or 6 psia up to 20 or 30 psia. The water temperature for the majority of the tests was constant at about 24° C. Some of the later tests were run at extreme ranges of temperatures and different velocities to study the effect of Reynolds number. Before discussing the detailed results of the experiment it might be well to first discuss the general performance of the different types of wings.

4.410 Elliptic Planforms

The behavior of the tip-vortex cavitation was very similar for all of the elliptic wings, irrespective of the aspect ratio. At the higher angles, the location of the minimum pressure was some distance aft of the wings with cavitation disappearing at a distance of about a semi-span downstream. At the lower angles the vortex cavitation appeared to start down a little on the leading edge, curve up around the end and trail from the very

edge of the wing tip. As the vortex cavitation was suppressed it would disappear simultaneously on a small region of the blade and immediately aft of the blade. Figure (29) is a photograph typical of the vortex cavitation from an elliptic wing.

4.420 Rectangular Planforms

As in the case of the elliptic wings, there was little difference in the general behavior of the vortex cavitation from one aspect ratio to the next. Unlike the elliptic wings, at the lower angles of attack the cavitation occurred uniformly along a considerable extent aft of the wing, never appearing initially attached to the wing. The inception of the cavitation was quite definite at the lower angles but at the higher angles it was very sporadic. Two states of vortex cavitation from a rectangular wing with an aspect ratio of four are shown in figures (30) and (31). Figure (30) shows the cavitating vortex leaving the blade and trailing downstream while the second photograph illustrates a state of cavitation where a region exists just aft of the wing in which there is no cavitation.

4.430 Delta Planforms

The cavitating vortex from wing number 5 which is a delta wing with an aspect ratio of 2.55 was considerably different from the other wings tested. The photographs of figurer (32) to (35) inclusive illustrate this cavitation. In these series of photographs the angle of the

wing and test section velocity were held constant while the pressure was varied. There are several points to be observed on these photographs. First it should be noted that a type of vortex cavitation occurs along a considerable extent of the leading edge of the wing. Also notice that the trailing portion is shed from a location inboard of the tip unlike the elliptic and rectangular wings. Finally observe that as the pressure is increased, the cavitation remains the longest on the wing itself.

For the two delta wings of higher aspect ratio it was impossible to obtain vortex cavitation in the trailing vortex system of either of these delta wings. Cavitation occurred along the leading edge as with the small delta wing but a definite cavitating vortex aft of the wings could not be obtained. The effect is shown in the photograph of figure (36) where, instead of the trailing cavitating vortex, only a murky region appears as caused by the air bubbles released from solution by the cavitation on the blade.

4.440 General Discussion of Results

The Garfield Thomas Water Tunnel is a relatively new facility and these tests were the first of this type to be performed in the tunnel. The false floor installation and wing pitching mechanism were designed with little or no previous experience from which to draw. It was only natural therefore that many "bugs" had to be eliminated before

consistent, dependable results could be obtained. The first of these as mentioned previously, was the overall strength of the false floor installation which proved insufficient and failed during a test. The failure was attributable to a large extent to excessive vibration produced by cavitation on the false floor structure itself. Prior to the failure of the apparatus, it was very difficult to turn the wings so that in redesigning the apparatus, the mechanical advantage between the wing shaft and the driving shaft was increased.

The scatter of the data obtained before the failure of the apparatus was rather large. From later experience, this was blamed on two causes. The first was the test procedure in which the velocity and wing angle were held fixed and the pressure varied. The decay of the cavitation was very gradual and offered considerable latitude in the choice of the pressure at which the cavitation was to have disappeared. The second factor to which the scatter was attributed was difficulty in measuring the angle of the wing. Initially a ten-turn helipot potentiometer was connected to the driving shaft since a potentiometer of sufficient accuracy to be attached directly to the wing shaft could not be found. This necessitated two calibration curves for the wing angle in order to account for the backlash in the worm wheel-worm gear drive. Because of sticking in the bearings and "O" ring seals and the nature of the loading

there was always some uncertainty as to which of the calibration curves should be used.

The rebuilt apparatus was strengthened considerably but the location of the active potentiometer was not changed. The testing procedure was changed with the wing angle being varied as described earlier. This proved to be much more satisfactory. All of the earlier tests were repeated in a second series. Unfortunately, in strengthening the equipment a sealing gasket was relocated and did not function properly. This allowed an excessive amount of air to leak into the tunnel at the lower pressures making it difficult to determine whether the investigator was seeing cavitation or a collection of undissolved air in the region of the vortex. The data from the second series of tests, although apparently repeatable within the scatter of the data, displayed inconsistencies which made it advisable to perform additional tests.

The two major faults with the rebuilt apparatus were cured in that a potentiometer was obtained which could be fastened directly to the wing shaft and the sealing gasket was redesigned to function properly.

A third, and by far the most complete, series of tests was performed. Not only were the tests of the first two completely redone but additional wings were made and the tunnel water temperature varied to study the effects of Reynolds number. The apparatus performed entirely satisfactory for the last series of tests with the data obtained

being much more consistent and with less scatter than that obtained in the earlier tests.

The experimental data are summarized in figures (37) to (44), inclusive. Included on the figures are the predicted results based upon the semi-empirical development presented later. The curves of $\sigma_{t_{cr}}$ versus α for each wing were all taken at a velocity of 40 fps. The Reynolds numbers based on the mid-span chords are given on the figures. Figure (44) presents the variation of $\sigma_{t_{cr}}$ with Reynolds number as measured for a series of rectangular wings all of aspect ratio four. The lower Reynolds numbers were obtained at reduced water temperatures of about 10° C and velocities of 25 or 30 fps while the higher Reynolds numbers were obtained with elevated temperatures of about 40° C and a speed of 40 fps. The experimental points given on the figures for the two angles of 4° and 8° represent points on the curves which best fit the data obtained of $\sigma_{t_{cr}}$ versus α at each Reynolds number.

The experimental variation of $\sigma_{t_{cr}}$ with α for the elliptic wings is seen to be nearly linear up to an angle of 6° or 7°. It is also interesting to note that the experimental results are nearly identical for the three aspect ratios considered. This is demonstrated more clearly in figure (45). The data obtained for the rectangular wings do not exhibit the linear variation of the elliptic wings

but tend more towards a parabolic shape. Also, the variation with aspect ratio is more pronounced than that obtained with the elliptic wings. The rectangular wings are compared in figure (46).

5.000 Semi-Empirical Analysis

The experimental results do not agree very well with the earlier predictions based upon considerations of induced drag. The magnitudes of the predicted minimum pressure coefficients based on the completely rolled-up vortex sheet are considerably lower than the critical cavitation indices measured experimentally. The variation with planform, aspect ratio and angle of attack predicted on the basis of the non-distorted vortex sheet, though closer in magnitude than that predicted on the basis of the rolled-up sheet, still deviates appreciably from the measured values. The effect of aspect ratio is not nearly as pronounced as predicted and the variation of $C_{p_{min}}$ with the angle of attack is more linear rather than parabolic as predicted.

The principal fault of the previous approaches appears to be in their neglect of the boundary layer on the upper and lower surfaces of the wing. It does not appear feasible with the present state of the art to attempt a detailed analysis of the turbulent boundary layer near the tip of the wing in consideration of the complicated velocity and pressure fields. Nevertheless, a simplified and approximate analysis can be made which appears to explain to a large extent the observed results. The development will be performed only for the rectangular and elliptic planforms since the delta wings of higher aspect ratio did not exhibit distinct vortex cavitation

behind the wings and the flow over the low aspect ratio delta wing appeared to separate near the tip.

5.100 Rectangular Planform

Immediately adjacent to the trailing edge of the wing the thickness of the trailing vortex sheet is determined by the thickness of the boundary layer at this location. Since the minimum pressure occurs at the edge of the sheet, the boundary layer at the outer end of the trailing edge of the wing would appear to be the governing factor in determining the minimum pressure.

In order to gain some insight into the factors governing this thickness, consider the diagram of figure (47). As shown, the flow approaching the wing is diverted inward over the upper surface and outward over the lower surface. At the tip therefore, the boundary layer can only grow as a result of the flow over the lower surface. Thus the thickness of the boundary layer on the lower surface of the wing at the tip of the trailing edge should be a good measure of the thickness of the edge of the vortex sheet. In order to estimate this thickness, some simplifying assumptions will be made which will be introduced where needed.

Consider the streamline on the lower surface which passes through the trailing edge at the tip as shown in the diagram of figure (48). It will be assumed that approximately this streamline is deflected by a constant angle over the wing. In addition it is assumed that the thickness of the boundary

layer along this streamline is proportional to the distance from the leading edge along the streamline divided by some power of the Reynolds number based on this distance; that is, the thickness of the boundary layer at the trailing edge of this streamline will be given by

$$\delta = k \frac{\ell}{R_\ell^{r}} \tag{5.1}$$

where $R_\ell = \frac{V_r \ell}{\nu}$

V_r = "average" resultant velocity along streamline

k = constant of proportionality

This can be rewritten as

$$\frac{\delta}{b} = \frac{1}{R^{r}} \left[\frac{k \frac{\ell}{b}}{\left(\frac{V_r}{V} \frac{\ell}{b} \right)^{r}} \right]$$

Now the term in the brackets is a function purely of the loading and aspect ratio so that to the approximations which were made:

$$\frac{\delta}{b} = \frac{f(x, AR)}{R^{r}} \tag{5.2}$$

At this point a slight digression must be made. The calculated circulation distributions of most wings do not vary greatly from the elliptic distribution and as such can be approximated very closely by

$$\Gamma = \Gamma_0 \sqrt{1 - x^2} \left(1 + x_1 x^2 + x_2 x^4 + \cdots \right) \tag{5.3}$$

For most purposes it is sufficient to consider only the a_1 and a_2 terms. The calculated distributions of reference (10) for the rectangular and delta planforms were approximated to within an error of less than one per cent all along the span in this manner. The values of a_1 and a_2 which were determined for the rectangular and the delta wings are given in table (V). Now if equation (5.3) is substituted into the expression (3.41) for the downwash velocity than it will be found that for $x_0 > 1$

$$\frac{4\pi b w(x_0)}{c_0 C_L V} = \frac{\pi}{\sqrt{x_0^2-1}} \frac{C_{L_0}}{C_L}\left[\left(1+\frac{a_1}{4}+\frac{a_2}{8}\right)\left(x_0-\sqrt{x_0^2-1}\right) + \left(\frac{3a_1}{4}+\frac{9a_2}{16}\right)\left(x_0-\sqrt{x_0^2-1}\right)^3 + \frac{5a_2}{16}\left(x_0-\sqrt{x_0^2-1}\right)^5\right] \tag{5.4}$$

If the values of w as determined from (5.4) are substituted into equation (3.55), then the variation of σ_{cr}/x^2 with x_0 can be calculated. These curves are given for the three rectangular wings in figure (49).

Now consider equation (5.2) for $\frac{\delta}{b}$. If x_0 is taken to be $1 + \frac{\delta}{b}$ then the variation of $\frac{\delta}{b}$ with Reynolds number can be determined from the data given in figure (44) and the curves of figure (49). The exponent of R in expression (5.1) is then given by the slope of this data plotted on log log paper as presented in figure (50) for angles of 4 and 8 degrees. From these plots the value of r was determined to be 0.35. This value of r is very reasonable in view of the values of 0.2 for a turbulent

layer and 0.5 for a laminar layer on a flat plate.

There is a point to be considered here. It is possible that the expression (5.1) for δ in terms of ℓ and R_ℓ should also contain some factor dependent upon α. As far as the exponent Γ is concerned, it does not appear to vary to any extent with α as is evident from figure (50). Consideration of the loading distribution near the tip will also show that the factor k will vary only slightly with α. This follows from the fact that the product cC_l must always vanish at the tip regardless of the angle of attack. Since c is constant, C_l must vanish at the tip which means that the absolute angle of attack of the tip section must always be zero regardless of the geometric angle of attack.

The variation of $\frac{\delta}{b}$ with aspect ratio and angle of attack will now be determined from the geometry of figure (48). The length ℓ and the resultant velocity are given by

$$\ell = \frac{c}{\cos\Phi}$$

$$V_r = \frac{V}{\cos\Phi}$$

so that

$$\frac{\delta}{b} = \frac{\alpha k}{A R^{.35}} \frac{1}{(\cos\Phi)^{\Gamma}}$$

But $\cos\Phi = \left[1 + \left(\frac{\alpha}{A}\right)^2\right]^{-\frac{1}{2}}$

Thus

$$\frac{\delta}{b} = \frac{2k}{AR\,R^{.35}}\left[1 + \left(\frac{w_r}{V}\right)^{-}\right]^{.15} \tag{5.5}$$

The average velocity ratio $\frac{w_r}{V}$ will be assumed proportional to the circulation distribution at some location near the tip raised to some power

$$\frac{w_r}{V} = \left[K\,\frac{\Gamma_0\left(1 + \alpha_1 + \alpha_2\right)}{c_0 V}\right]^{\frac{n}{2}}$$

$$= \left[\frac{K}{\Sigma}\,\frac{c_{l_0}}{C_L}\,\frac{dc_L}{dx}\left(1 + \alpha_1 + \alpha_2\right)x\right]^{\frac{n}{2}} \tag{5.6}$$

where K = constant of proportionality to be determined

n = unknown exponent to be determined

The use of c_0 instead of b in equation (86) is tantamount to assuming that it is the tip shape and not the aspect ratio which primarily governs the $\frac{w_r}{V}$.

The expression for $\frac{\delta}{b}$ becomes finally

$$\frac{\delta}{b} = \frac{2k}{AR\,R^{.35}}\left(1 + \left[\frac{K}{\Sigma}\,\frac{c_{l_0}}{C_L}\,\frac{dc_L}{dx}\left(1 + \alpha_1 + \alpha_2\right)x\right]^{\frac{n}{2}}\right)^{.15} \tag{5.7}$$

The constants k, K, and n must be determined from experiment. The procedure for doing this is as follows. From the experimental data of figures (41) to (43) and the curves of figure (49) the variation of $\frac{\delta}{b}$ with x can be obtained for the three rectangular wings at a constant Reynolds number. These curves are given as figure (51). The question now arises as to whether suitable

values of k, K, and n can be found to satisfy simultaneously the curves of figure (51).

The constant k can be determined immediately from the extrapolated values of $\frac{\delta}{b}$ for $\alpha = 0$.

$$k = AR\left(\frac{\delta_0}{b}\right)K^{.55} \tag{5.8}$$

where: $\delta_0 = \delta$ for $\alpha = 0$

The constant n is most readily obtained by comparing $\frac{\delta}{b}$ values at α_1 and α_2 for a given wing.

$$\frac{\left(\delta_1/\delta_0\right)^{0.6n6} - 1}{\left(\delta_2/\delta_0\right)^{0.6n6} - 1} = \left(\frac{\alpha_1}{\alpha_2}\right)^{n} \tag{5.9}$$

With n determined, the constant K is found from:

$$K = \frac{\left[\left(\delta/\delta_0\right)^{0.6n6} - 1\right]^{\frac{1}{n}}}{\frac{1}{2}\frac{C_{L_0}}{C_L}\frac{AR}{1\times}\left(1 + \alpha_1 + \alpha_2\right)\alpha} \tag{5.10}$$

For the rectangular wings, the constants were determined as

$$k = .1544$$

$$K = 53.7$$

$$n = 3.37$$

The agreement between the calculated values of $\tau_{t.c}$ using the above values of k, K, and n are included with the experimental values in figures (41), (42), (43) and (44). As is evident, the values of $\tau_{t.c}$ as calculated using equation (5.7) and figure (49), are in quite good

agreement with the experimental measurements. The fact that such agreement was obtained for the different aspect ratios and angles of attack lends considerable support to this semi-empirical approach and to the supposition that the boundary layer on the lower surface of the wing is the factor governing the thickness of the edge of the vortex sheet.

5.200 <u>Elliptic Planforms</u>

The same procedure will now be followed for the elliptic wings taking into account the geometry of the wing tip. This region of an elliptic planform is shown in figure (52).

As in the previous case of the rectangular wings, the thickness of the sheet leaving the wing at the tip will be assumed to be described by

$$\delta = k \frac{\ell}{R_\ell^{.35}}$$

which can be rewritten as

$$\delta = \frac{k\, c_o}{(R_o)^{.35}} \frac{\left(\frac{\ell}{c_o}\right)}{\left(\frac{V c_o}{\nu} \frac{\ell}{c_o}\right)^{.35}} \qquad (5.11)$$

where: $R_o = \frac{V c_o}{\nu}$

c_o = mid-span chord

The chord at any dimensionless x location is given by $c = c_o\sqrt{1-x^2}$. x will be close to unity so if it is assumed that $x = 1 - \varepsilon$ where ε is small compared to

unity, then approximately $1 - x^2 = 2\varepsilon$.

From the geometry of the picture

$$l = \frac{\varepsilon b}{\sin \phi}$$

Also:

$$l^2 = \left(\frac{c_0}{2}\right)^2 + (\varepsilon b)^2$$

But:

$$c^2 = 2 c' c_0^2$$

So that:

$$l^2 = \left(\frac{c_0}{2}\right)^2 2\varepsilon + \varepsilon^2 b^2$$

Equating this to the previous expression for l gives:

$$\varepsilon = \frac{1}{2} \frac{(c_0/b)^2 \sin^2 \phi}{\cos^2 \phi}$$

The ratio $\frac{l}{c_0}$ is then given by

$$\frac{l}{c_0} = \frac{\left(\frac{c_0}{2b}\right) \sin \phi}{\cos^2 \phi}$$

From the geometry of figure (52)

$$\frac{V_r}{V} = \frac{1}{\cos \phi}$$

$$\frac{V_t}{V} = \frac{\sin \phi}{\cos \phi}$$

$$\left(\frac{V_r}{V}\right)^2 = 1 + \left(\frac{V_t}{V}\right)^2$$

Thus the quantity $\frac{l}{c_0} \frac{V_r}{V}$ can be found from

$$\frac{l}{c_0} \frac{V_r}{V} = \left(\frac{c_0}{2b}\right) \frac{V_t}{V} \left[1 + \left(\frac{V_t}{V}\right)^2\right]$$

with $\frac{l}{c_o}$ given by

$$\frac{l}{c_o} = \frac{c_o}{2b}\frac{u_c}{V}\left[1+\left(\frac{u_c}{V}\right)^2\right]^{0.5}$$

Therefore in terms of $\frac{u_c}{V}$, the expression for $\frac{\delta}{b}$ becomes

$$\frac{\delta}{b} = \frac{2k}{R_o^{.35}}\left(\frac{c_o}{2b}\right)^{1.65}\left(\frac{u_c}{V}\right)^{1.65}\left[1+\left(\frac{u_c}{V}\right)^2\right]^{0.15} \qquad (5.12)$$

As in the case of the rectangular wings $\frac{u_c}{V}$ will be expressed by

$$\frac{u_c}{V} = \left[\frac{k}{\pi}\frac{c_{l_o}}{c_L}\frac{dc_L}{d\alpha}\left(1+\alpha_1+\alpha_2\right)\right]^{1/2}$$

$$= \left[\frac{k}{\pi}\frac{dc_L}{d\alpha}\right]^{1/2}$$

Since for an elliptic lift distribution

$$\alpha_1 = \alpha_2 = 0$$

$$\frac{c_{l_o}}{c_L} = 1.0$$

Since for the elliptic wings $\pi A = \frac{4b}{\pi c_o}$, the expression for $\frac{\delta}{b}$ comparable to equation (5.7) for the rectangular wings becomes

$$\frac{\delta}{b} = \frac{2k}{R_o^{.35}}\left(\frac{4}{\pi A}\right)^{1.65}\left[\frac{k}{\pi}\frac{dc_L}{d\alpha}\right]^{1.65/2}\left[1+\left(\frac{k}{\pi}\frac{dc_L}{d\alpha}\right)^2\right]^{0.15} \qquad (5.13)$$

As in the case of the rectangular wings, $\frac{dc_L}{d\alpha}$ can be calculated as a function of x_o. This variation is given in figure (53) for the three aspect ratios of 4, 7, and 10.2. From these curves and the experimental results given in figures (37), (38), and (39), the curves of $\frac{\delta}{b}$ versus x given in figure (51) for the elliptic wings were determined.

Again the question arises as to whether a k, K, and n can be found such that an expression of the form (5.13) can be made to fit the curves of $\frac{\delta}{b}$ versus x. Observe that the form of the expression for the elliptic wings is considerably different than that for the rectangular wings due mainly to the difference in the geometry of the tip. Unlike the rectangular wings, $\frac{\delta}{b}$ for the elliptic wings goes to zero as x goes to zero.

The ideal situation would be of course to have the values of k, K, and n found for the rectangular wings hold for the elliptic wings. There is the question however, as to whether the k or the power of the Reynolds number of 0.35 will remain the same since at the tip of the elliptic wings the boundary layer buildup occurs over a very small length of chord which is increasing in thickness. The K and n are questionable in view of the fact that the edge of the vortex sheet is shed from the very tip of the wing which is ahead of the rest of the trailing edge.

If the values of k, K, and n are inserted into equation (5.13) the calculated values of $\frac{\delta}{b}$ will be found to be too large. By varying n it is possible to obtain values of $\frac{\delta}{b}$ in agreement with the experimental values of figure (51). In fact, with the power of the Reynolds number fixed at .35, the values of k and K must remain the same as for the rectangular wing in order to

obtain suitable agreement with the experimental values. For the elliptic wings therefore, the following values were determined.

$$k = .1544$$

$$K = 53.7$$

$$n = 1.6$$

The agreement between the calculated values of $\sigma_{t_{cr}}$ using the above values of k, K, and n are included with the experimental values in figures (37), (38) and (39). Again the calculated variation of $\frac{\hat{}}{\tau}$ with x and aspect ratio produces values of $\sigma_{t_{cr}}$ in good agreement with experiment.

5.300 Discussion of Semi-Empirical Investigation

The agreement between the experimental results and the calculations based on the semi-empirical investigation supports the basic approach to the analysis. The variation both with angles of attack and aspect ratio for a given planform shape is predicted accurately by consideration of the effect of the geometry of the wing tip and the leading distribution on the growth of the boundary layer on the lower surface of the wing. The necessity of varying the exponent n with planform is not too desirable but this is offset somewhat by the fact that the coefficients k and K remain unchanged. Attempts to predict the variation of n have not proven fruitful to date.

6.000 Conclusions

Theoretical, experimental, and semi-empirical investigations of the minimum pressure in trailing vortex systems of elliptic, rectangular, and delta wings have been presented. The conclusions of these investigations, some of them in the negative sense, are summarized below.

1. The magnitude of the minimum pressure coefficient increases with increasing Reynolds number.
2. The magnitude of the minimum pressure coefficient increases nearly linearly with the angle of attack.
3. The minimum pressure coefficient is almost independent of aspect ratio for elliptic wings.
4. The magnitude of the minimum pressure coefficient increases with increasing aspect ratio for rectangular wings.
5. Because of separation near the tip, only the delta wings of low aspect ratio produces discrete vortex cavitation in the trailing vortex system.
6. The thickness of the tip vortex core, or the thickness of the edge of the trailing vortex sheet is governed by the thickness of the boundary layer on the lower surface of the wing and not by any consideration of induced drag and kinetic energy of the vortex sheet itself.
7. The thicker the boundary layer on the lower surface at the wing tip, the smaller the magnitude of the minimum pressure coefficient.

8. Reduction of the wing loading near the tip does not necessarily reduce the magnitude of the minimum pressure coefficient since the thickness of the boundary layer will be reduced.

7.000 References

1. Prandtl, L., "Uber die ausgebildete Turbulenz", Zeitschrift fur angewandte Mathematik und Mechanik, Vol V, p. 136 (1925).
2. Tollmien, W., "Berechnung turbulenter Ausbreitungsvorgange", Zeitschrift fur angewandte Mathematik und Mechanik, Vol VI, p. 468, (1926).
3. Fage, H. and Johansen, F. C., "The Structure of Vortex Sheets", Phil. Mag. 5, 28 (1928).
4. Krzywoblocki, M. Z., "Vortex Streets in Incompressible Media", Applied Mechanics Reviews, 6, 393 (1953).
5. Milne-Thomson, L. M., "Theoretical Hydrodynamics", London, Macmillan and Company, Lt'd. (1938).
6. Lamb, H., "Hydrodynamics", London, New York, Cambridge University Press (1932).
7. Spreiter, J. R. and Sacks, A. H., "The Rolling Up of the Trailing Vortex Sheet and Its Effect on the Downwash Behind Wings", Jour. Aero. Sci., 18, 21 (1951).
8. Durand, W. F., Editor-in-Chief, "Aerodynamic Theory", Vol II, p. 328, Durand Reprinting Committee (1943).
9. Piercy, N. A. V., "Aerodynamics", London, The English Universities Press Lt'd., (1947).
10. Falkner, V. M., "Calculated Loadings Due to Incidence of a Number of Straight and Swept-Back Wings", ARC, R & M No. 2596, (1952).

11. Jones, R. T., "Properties of Low-Aspect-Ratio Pointed Wings at Speeds Below and Above the Speed of Sound", NACA Tech. Rpt. 835 (1946).

12. Durand, W. F., Editor-in-Chief, "Aerodynamic Theory", Vol II, p.125, Durand Reprinting Committee, (1943).

13. Goldstein, S., "Modern Developments in Fluid Dynamics", Vol II, Oxford, Clarendon Press, (1938).

14. Betz, A., "Applied Airfoil Theory", in "Aerodynamic Theory", Vol IV, Division J., Chpt. III, Durand Reprinting Committee (1943).

15. Isaacs, R., "Airfoil Theory for Flows of Variable Velocity", Jour. Aero. Sci., 12, 113, (1945).

16. Falkner, V. M., "The Effect of Pointed Tips on Wing Loading Calculations", ARC, R & M No. 2483, (1952).

17. Prandtl, L. and Betz, A., "Vier Abhandlungen zur Hydrodynamik und Aerodynamik", Gottingen (1927).

18. Miller, F. H., "Partial Differential Equations", New York, John Wiley and Sons, Inc. (1949).

8.000 Appendix

8.100 Evaluation of the Integral: $\int_0^\infty \frac{(1-e^{-kx^2})^2}{x^3}\,dx$

This integral is first reduced by integrating by parts to the form below:

$$\left[\left(1-e^{-kx^2}\right)^2\left(-\frac{1}{2x^2}\right)\right]_0^\infty + \int_0^\infty \frac{4kxe^{-kx^2}(1-e^{-kx^2})}{x^2}\,dx$$

The first quantity is seen to vanish at both limits. Now if the transformation $t = kx^2$ is applied to the integral, it reduces to:

$$k\int_0^\infty \frac{e^{-t}(1-e^{-t})}{t}\,dt$$

The integrand of this integral can itself be expressed in integral form.

$$\frac{e^{-t}(1-e^{-t})}{t}\,dt = \left[\int_1^2 e^{-tu}\,du\right]dt$$

so that the original integral can be transformed to the double integral

$$k\int_0^\infty\int_1^2 e^{-tu}\,du\,dt$$

Reversing the order of integration and integrating with respect to t gives

$$k\int_1^2 \frac{du}{u}$$

which becomes finally

$$\int_0^\infty \frac{(1-e^{-kx^2})^2}{x^3}\,dx = k \log 2$$

8.200 <u>Proof That the Induced Velocity Normal to the Trailing Vortex Sheet is Bounded Except at the Edges of the Sheet</u>

The velocity induced normal to and in the plane of the sheet is given by

$$w(y_0) = \int_{-b}^{b} \frac{\frac{d\Gamma}{dy}\,dy}{2\pi(y_0 - y)}$$

If $-b < y_0 < b$, this integral cannot be integrated directly by parts from -b to b because of the discontinuity in the integrand at $y = y_0$. In this case it is broken into three integrals

$$w(y_0) = \int_{-b}^{y_1} \frac{\frac{d\Gamma}{dy}\,dy}{2\pi(y_0 - y)} + \int_{y_1}^{y_2} \frac{\frac{d\Gamma}{dy}\,dy}{2\pi(y_0 - y)} + \int_{y_2}^{b} \frac{\frac{d\Gamma}{dy}\,dy}{2\pi(y_0 - y)}$$

where $y_1 < y_0 < y_2$

The first and last integrals can be integrated by parts and since $\Gamma(\pm b) = 0$ the result can be written as

$$2\pi\, w(y_0) = \frac{\Gamma(y_1)}{y_0 - y_1} - \frac{\Gamma(y_2)}{y_2 - y_0} + \int_{-b}^{y_1} \frac{\Gamma\,dy}{(y_0 - y)^2} + \int_{y_2}^{b} \frac{\Gamma\,dy}{(y_0 - y)^2} + \int_{y_1}^{y_2} \frac{\frac{d\Gamma}{dy}\,dy}{y_0 - y}$$

There are no singularities in the range of integration for the first two integrals so that the only question concerns the last integral. For the usual wing the function

$\frac{d\Gamma}{dy}$ is well behaved except at $y = \pm b$. This function is therefore bounded between $y_1 \leq y \leq y_2$. Let the value of the least upper bound be denoted by M. Then

$$\int_{y_1}^{y_2} \frac{\frac{d\Gamma}{dy}\,dy}{y_0 - y} \leq M \int_{y_1}^{y_2} \frac{dy}{y_0 - y}$$

$$\leq M \lim_{\delta \to 0} \left[\int_{y_1}^{y_0 - \delta} \frac{dy}{y_0 - y} - \int_{y_0 + \delta}^{y_2} \frac{dy}{y_0 - y} \right]$$

$$\leq M \log \frac{y_0 - y_1}{y_2 - y_0}$$

If $y_0 = b$ the integral for the downwash can be integrated by parts immediately to give

$$2\pi w(b) = \left[\frac{\Gamma}{b - y} \right]_{-b}^{b} - \int_{-b}^{b} \frac{\Gamma' \, dy}{(b - y)^2}$$

Since $\Gamma(b)$ is zero the first part in brackets will be finite at b providing $\Gamma'(b)$ is finite. In the integral however, the integrand can be seen to have a second order pole at $y = b$ unless $\Gamma'(b)$ is zero and $\Gamma''(b)$ is finite there.

Table I

Specifications of Wings Tested

Wing Number	Planform	Semi-span (inches)	Mid-chord (inches)	Aspect ratio	Airfoil section	Material	Method of manufacture*
1.	elliptic	10.00	2.5	10.20	0015	stainless steel	1
2.	rectangular	4.00	2.0	4.00	0012	brass	2
3.	rectangular	6.00	2.0	6.00	0012	brass	2
4.	rectangular	8.00	2.0	8.00	0012	brass	2
5.	delta	2.55	7.0	1.46	0007	brass	2
6.	delta	4.85	7.0	2.70	0007	brass	2
7.	delta	7.00	7.0	4.00	0007	brass	2
8.	elliptic	3.93	2.5	4.00	0015	brass	2
9.	elliptic	6.37	2.5	7.00	0015	brass	2
10.	elliptic	10.00	2.5	10.20	0015	brass	2
11.	rectangular	4.00	2.0	4.00	flat plate	steel	3
12.	elliptic	3.93	2.5	4.00	flat plate	steel	3
13.	rectangular	2.00	1.0	4.00	0015	brass	1
14.	rectangular	4.00	2.0	4.00	0015	brass	1
15.	rectangular	6.00	3.0	4.00	0015	brass	2

* 1. Machined on special profiler and polished.
2. Rough cut on a milling machine and hand finished.
3. 1/8-inch sheet stock with edges rounded.

Table I - Continued

Specifications of Wings Tested

Wing Number	Planform	Semi-span (inches)	Mid-chord (inches)	Aspect ratio	Airfoil section	Material	Method of manufacture*
16.	rectangular	8.00	4.0	4.00	0015	brass	2
17.	rectangular	6.00	2.0	6.00	0015	brass	1
18.	rectangular	8.00	2.0	8.00	0015	brass	1
19.	rectangular	6.00	3.0	4.00	0015	brass	1

Table II

Sample Raw Data Sheet

TEST NO. 1333 PROJECT 19.4211 ENGR McCormick

DESCRIPTION Tip-Vortex Cavitation -- Wing #8

CONSOLE OPERATOR Lancaster

Long	John	α -Degrees	psia	Temp. °C	Air Content
-10.38	13.10	8.5	34	25.4	8.6
		-9.9			
		-9.3	31.7		
		7.9			
		8.6	30		
		-9.4			
		-9.3	28		
		7.9			
-10.2	12.95	8.0	26		
		-7.7			
		-7.7	24		
		6.8			
		6.2	22		
		-7.6			
		-6.9	20		
		6.3			
		5.7	19	25.7	8.5
		-6.6			
-10.05	12.85	-6.6	18		
		5.9			
		6.4	17		
		-6.1			
		-6.0	16		
		5.9			
		5.1	15		
		-6.0			
		-5.5	14		
		5.0			
		4.4	13		
		-5.5			
		-5.0	12		
		3.9			
-10.15	12.65	3.9	11		8.5
		-4.4			
		-4.4	10		
		3.3			
		2.8	9		
		-3.9			
		-3.9	8		
		2.5			
		2.1	7		
		-3.4			
		1.6	6		
		-3.9			

Table III

Water Vapor Pressure and Kinematic Viscosity as a Function of Temperature

Temperature Degrees C	Water Vapor Pressure psia	$\nu \times 10^5$
10	.17	1.409
11	.18	1.368
12	.20	1.329
13	.21	1.293
14	.23	1.259
15	.24	1.225
16	.26	1.191
17	.28	1.160
18	.30	1.131
19	.31	1.100
20	.34	1.075
21	.36	1.048
22	.38	1.022
23	.41	1.000
24	.43	.978
25	.46	.955
26	.49	.935
27	.52	.915
28	.55	.895
29	.58	.876
30	.62	.860
31	.65	.842
32	.69	.825
33	.73	.808
34	.78	.791
35	.82	.775
36	.87	.760
37	.94	.745
38	.97	.730
39	1.02	.716
40	1.08	.703
41	1.13	.690
42	1.20	.680
43	1.28	.668

Table IV

Summary of Tests

Series I - Considerable difficulty was experienced with the wing positioning mechanism in this series. For this reason the data is felt to be unreliable. This mechanism was redesigned after the failure of the entire apparatus had occurred.

Test Number	Wing Number	Date	Velocity fps	Comments
790	1	10/29/52	Low	Test incomplete
791	1	10/30/52	Varied	Test appears satisfactory
792	1	10/31/52	Varied	Test appears satisfactory
794	1	11/3/52	Varied	Test appears satisfactory
797	1	11/10/52	Varied	Test appears satisfactory
798	1	11/12/52	Varied	Test appears satisfactory
799	1	11/13/52	Varied	Test appears satisfactory
800	1	11/14/52	Varied	Test appears satisfactory
928	2	3/12/53	40	Test incomplete
929	2	3/12/53	40	Angle unsertain
930	3	3/13/53	30	Test appears satisfactory
931	4	3/13/53	30	Test appears satisfactory
932	2	3/14/53	40	Angle unsertain
973	1	4/13/53	30	Test no good
974	1	4/14/53	40	Wing twisted, data no good
975	5	4/15/53	40	Complete failure of apparatus

Table IV - Continued

Summary of Tests

Series II - In this second series of tests, considerable backlash was present in the wing positioning mechanism which made it difficult to determine the wing angle accurately. Also a sealing gasket leaked, allowing an excessive amount of air to enter the tunnel so that although the tests were apparently alright, the data is questionable, particularly in view of the third series of tests.

Test Number	Wing Number	Date	Velocity fps	Comments
1198	2	11/18/53	40	Good test
1199	2	11/19/53	40	Good test
1200	10	11/19/53	30	Considerable amount of air present
1201	5	11/19/53	40	Some uncertainty in wing angle
1202	5	11/20/53	40	Repeat of preceding test
1203	8	11/20/53	40	Good test
1204	9	11/20/53	40	Good test
1205	6	11/20/53	40	No vortex cavitation produced
1206	7	11/20/53	40	No vortex cavitation produced
1207	3	11/21/53	40	Good test
1208	4	11/21/53	40	Good test
1209	1	11/23/53	30	Considerable air present
1210	8	11/23/53	40-20	Good test
1211	9	11/23/53	40-20	Good test
1212	5	11/24/53	40	Good test
1213	2	11/24/53	40	Good test

Table IV - Continued

Summary of Tests

Series III - The potentiometer which measures the wing angle was replaced and the new one attached directly to the wing shaft for this third series of tests. In addition the sealing gasket was redesigned. With these changes, the equipment functioned properly. This third series is therefore the most complete and accurate of the three and is the data from which the experimental data presented in the text is taken.

Test Number	Wing Number	Date	Velocity fps	Comments
1323	2	3/15/54	40	Good test, except at low p
1324	2	3/16/54	40	Good test - complete
1325	11	3/16/54	40	Cavitation not pronounced - pictures taken - incomplete
1326	3	3/17/54	40	Good test
1327	9	3/17/54	40	Test no good
1328	4	3/18/54	40	Test apparently O.K.
1329	10	3/18/54	40	Test apparently O.K.
1330	12	3/19/54	40	Results questionable
1331	9	3/19/54	40	Test no good - angle slipped
1332	9	3/19/54	40	Good test
1333	8	3/20/54	40	Good test
1334	5	3/22/54	40-30	Good test
1335	17	3/22/54	40-30	Cavitation sporadic
1336	18	3/23/54	40-30	Cavitation sporadic
1337	14	3/23/54	40	Test looks O.K.
1338	2	3/23/54	40	Check test

Table IV - Continued

Summary of Tests

Series III - Continued

Test Number	Wing Number	Date	Velocity fps	Comments
1339	2	3/24/54	40	Check test
1340	13	3/26/54	40-30	Good low temperature test
1341	14	3/26/54	40-30	Good low temperature test
1342	15	3/29/54	40-30	Good low temperature test
1343	15	3/29,30,31/54	30	Temperature changed
1344	15	3/31/54	30	Good high temperature test
1345	16	4/1/54	30-40	Good high temperature test
1346	19	4/2/54	30	Good high temperature test
1347	13	4/2/54	40	Good high temperature test
1348	14	4/2/54	35	Good high temperature test

Table V

Parameters for Circulation Distribution

$$\Gamma = \Gamma_0 \sqrt{1 - X^2}\left(1 + a_1 X^2 + a_2 X^4\right)$$

Planform	Aspect Ratio	a_1	a_2
Rectangular	2	.0458	.0117
Rectangular	4	.1815	.0046
Rectangular	6	.2348	.1269
Delta	2.307	-.2381	-.0107
Delta	4	-.2560	-.1073
Elliptic	any	0	0

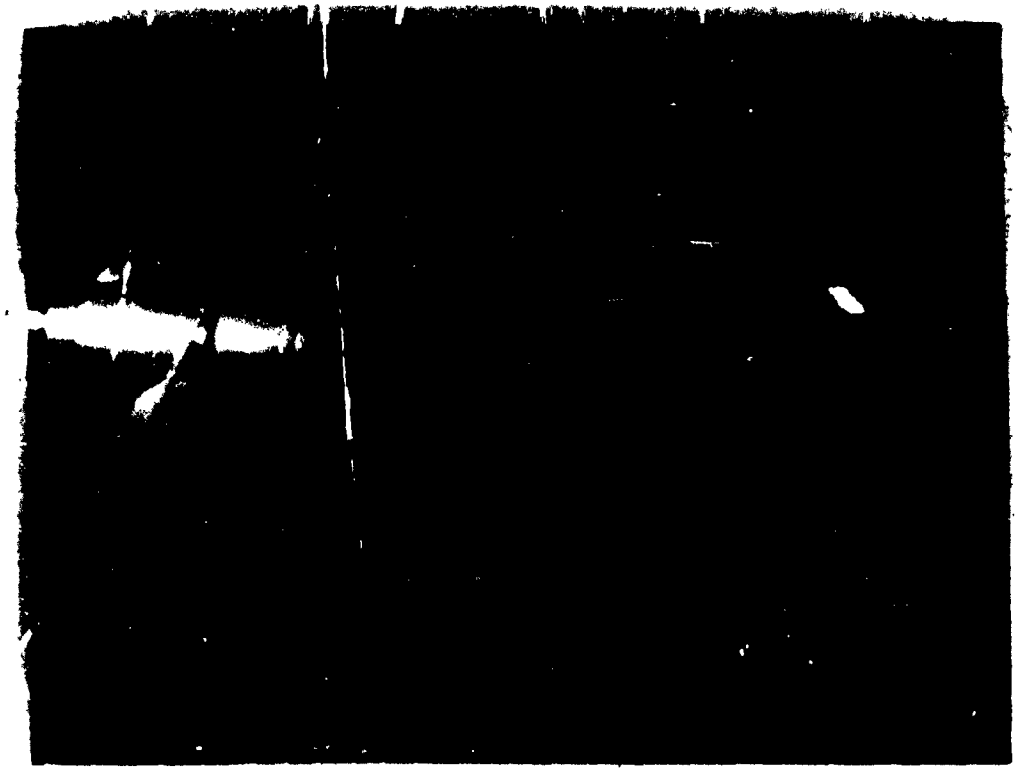

FIGURE 1
Tip Vortex Cavitation from a Marine Propeller

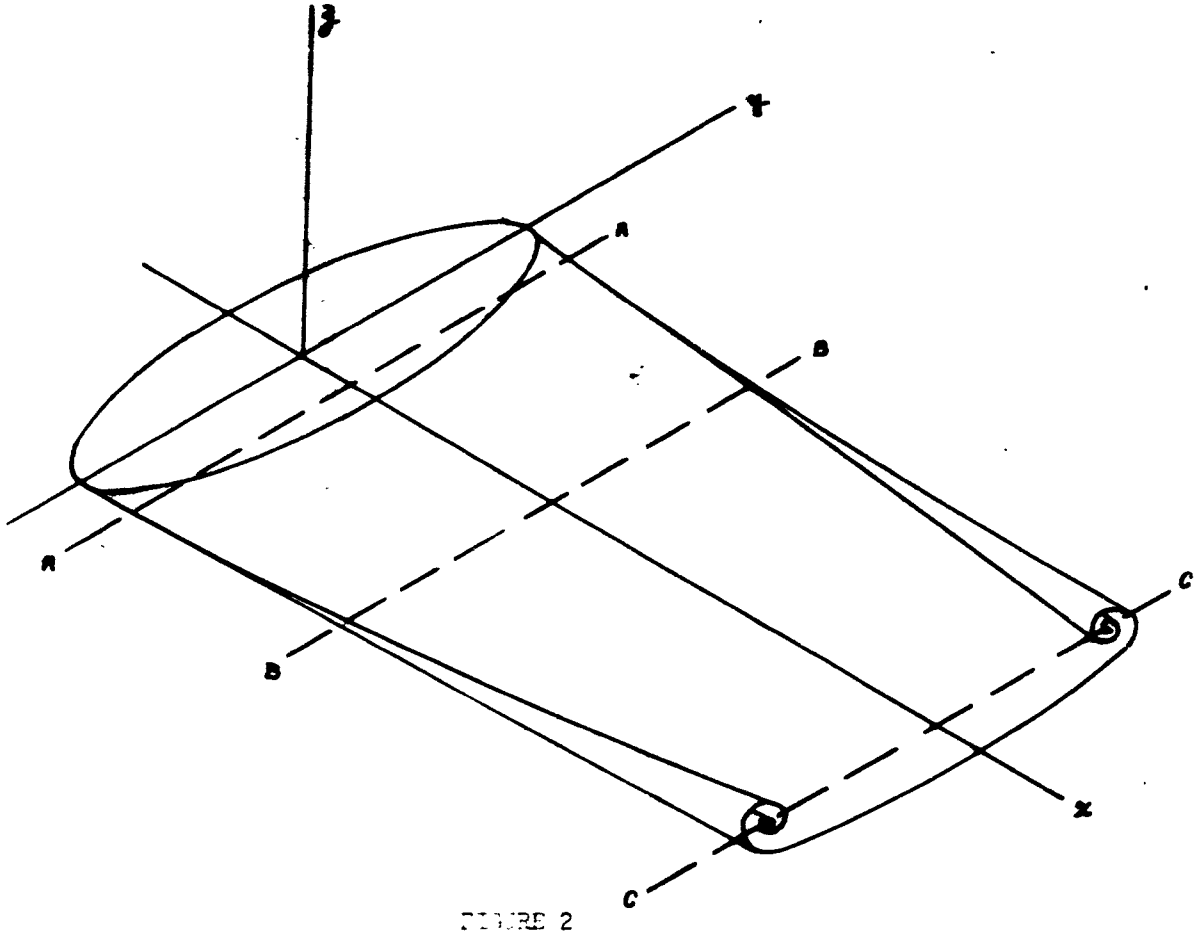

FIGURE 2

A Typical Wing and Associated Trailing Vortex System

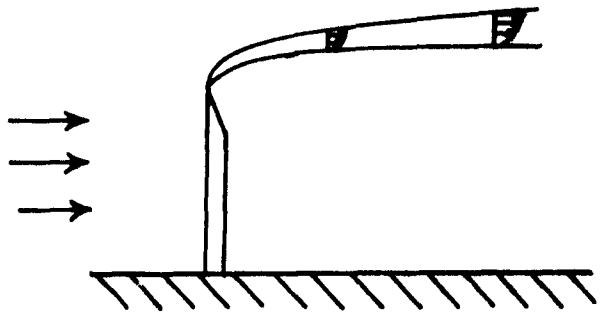

FIGURE 3

The Growth of a Vortex Sheet Behind a Blunt Body

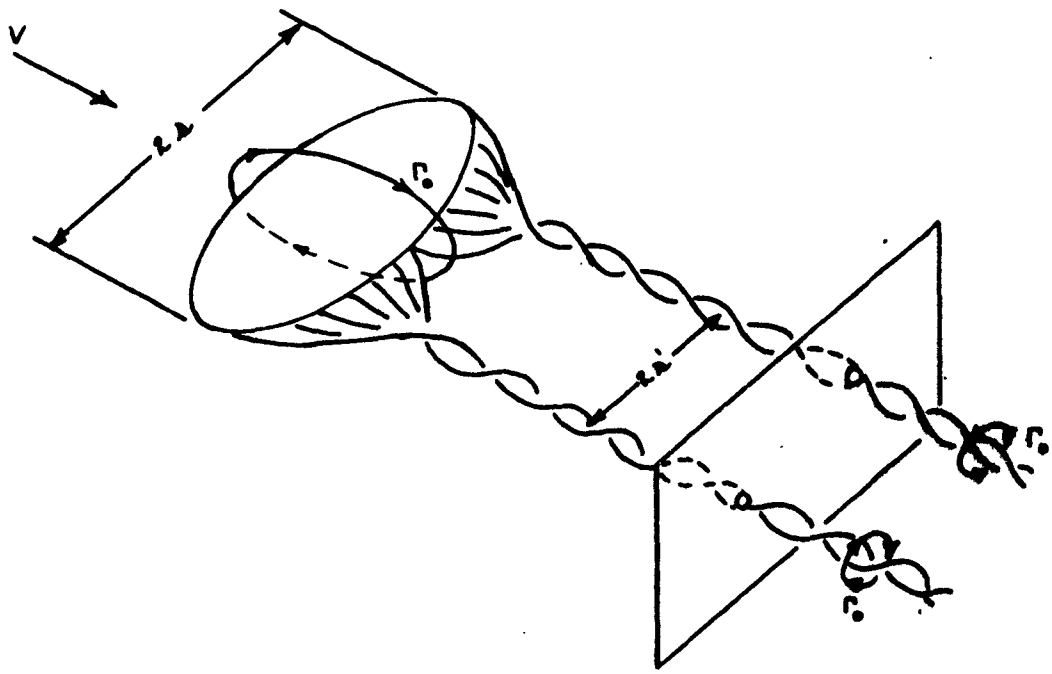

FIGURE 4

Completely Rolled-Up Vortex Sheet

NORWOOD, MASSACHUSETTS

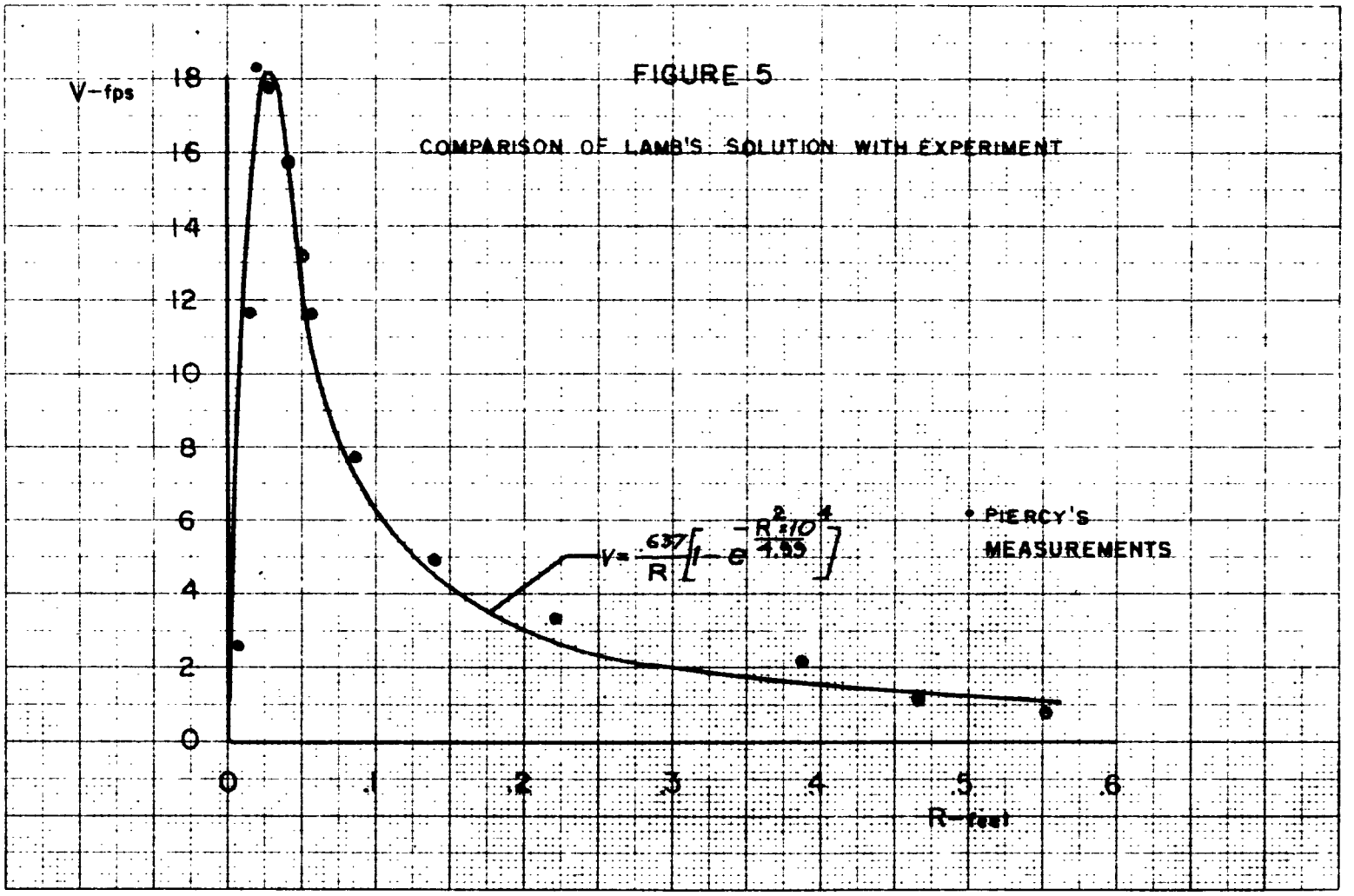

FIGURE 5

COMPARISON OF LAMB'S SOLUTION WITH EXPERIMENT

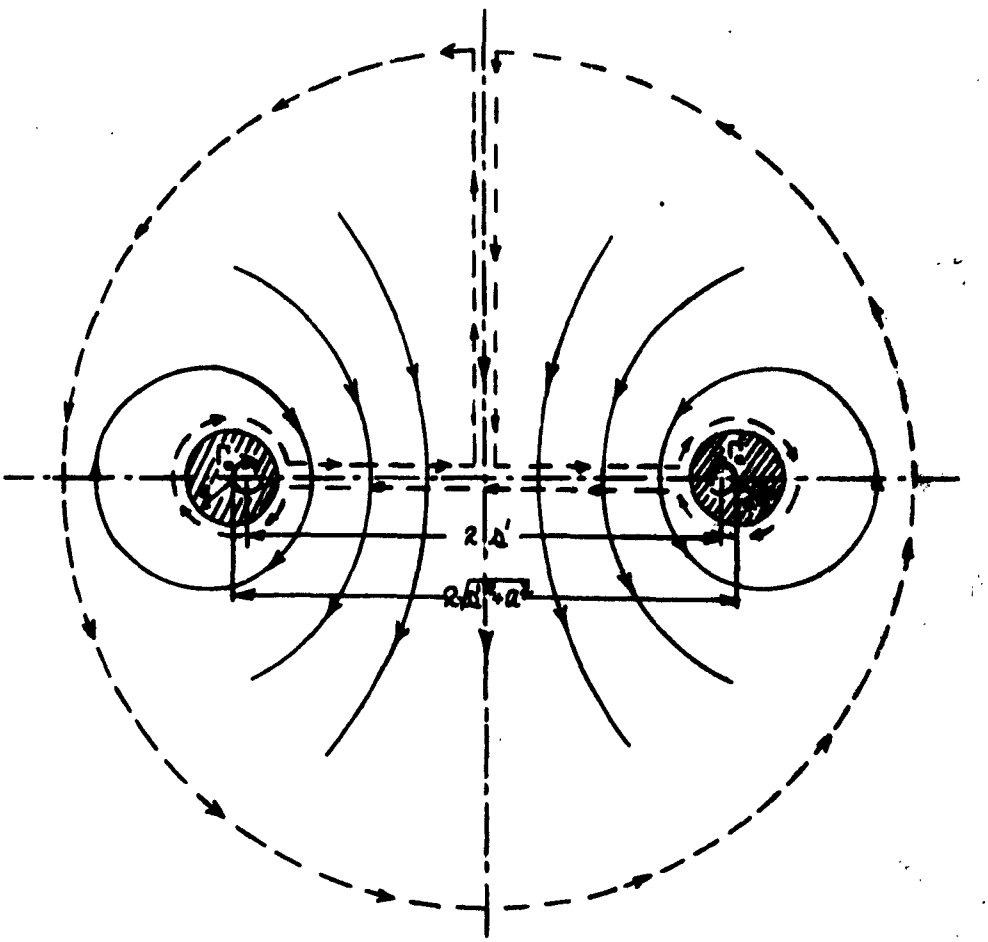

FIGURE 6

Transverse Plane in Ultimate Wake of Completely Rolled-Up Vortex Sheet Including the Path of Integration for Obtaining the Kinetic Energy

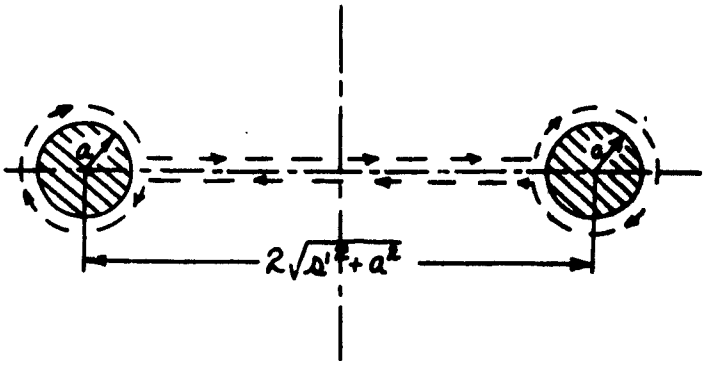

FIGURE 7

Reduced Path of Integration for Obtaining the Kinetic Energy

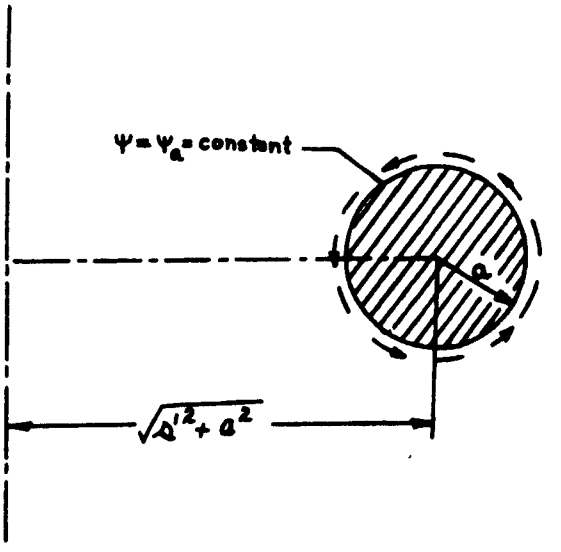

FIGURE 8

Trailing Vortex Core

No. 3 1/2 2 DIVISIONS IN HALF TO THE 3 DIVISIONS
FLEXEX BOOK COMPANY, INC. NORWOOD, MASSACHUSETTS
PRINTED IN U.S.A.

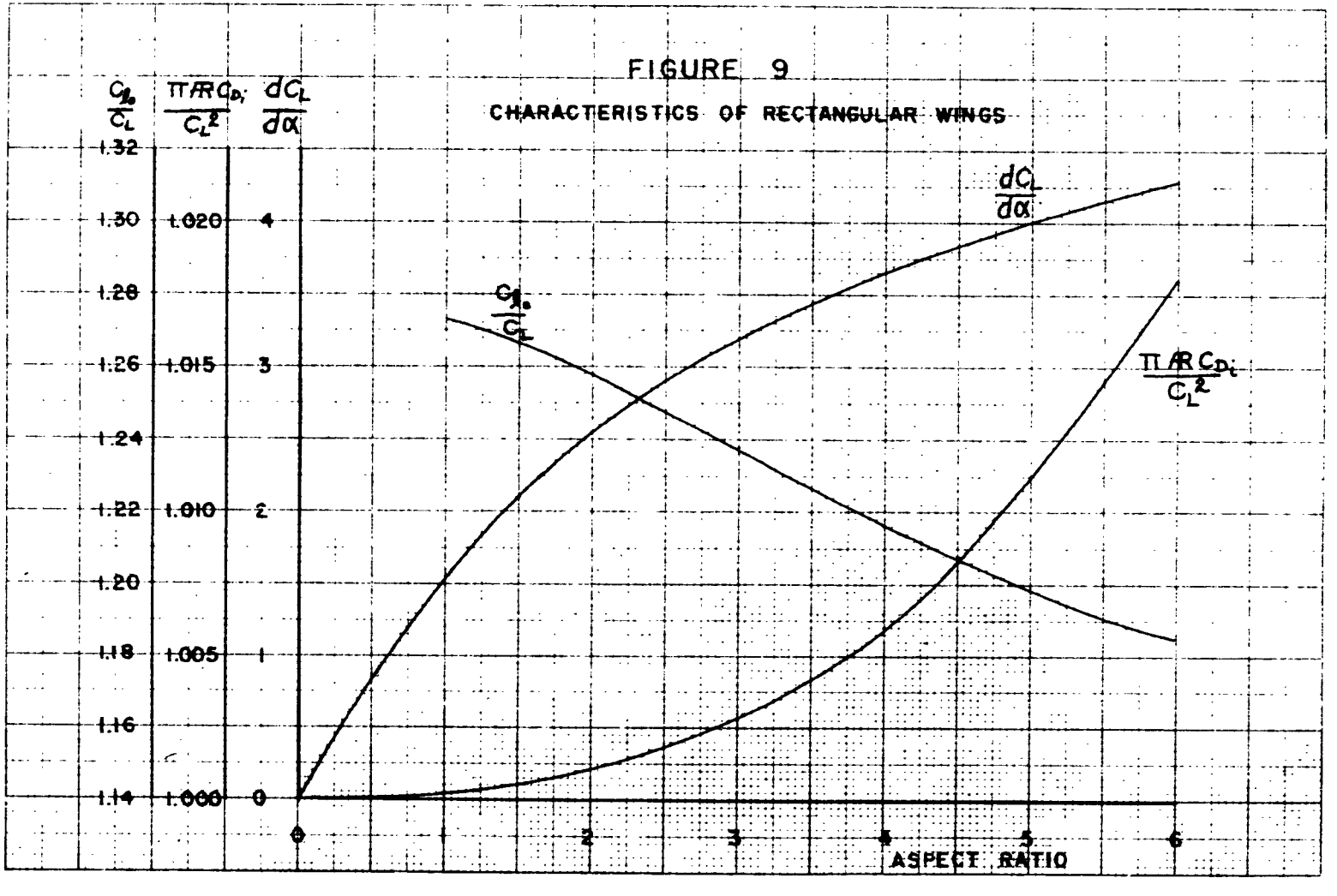

FIGURE 9

CHARACTERISTICS OF RECTANGULAR WINGS

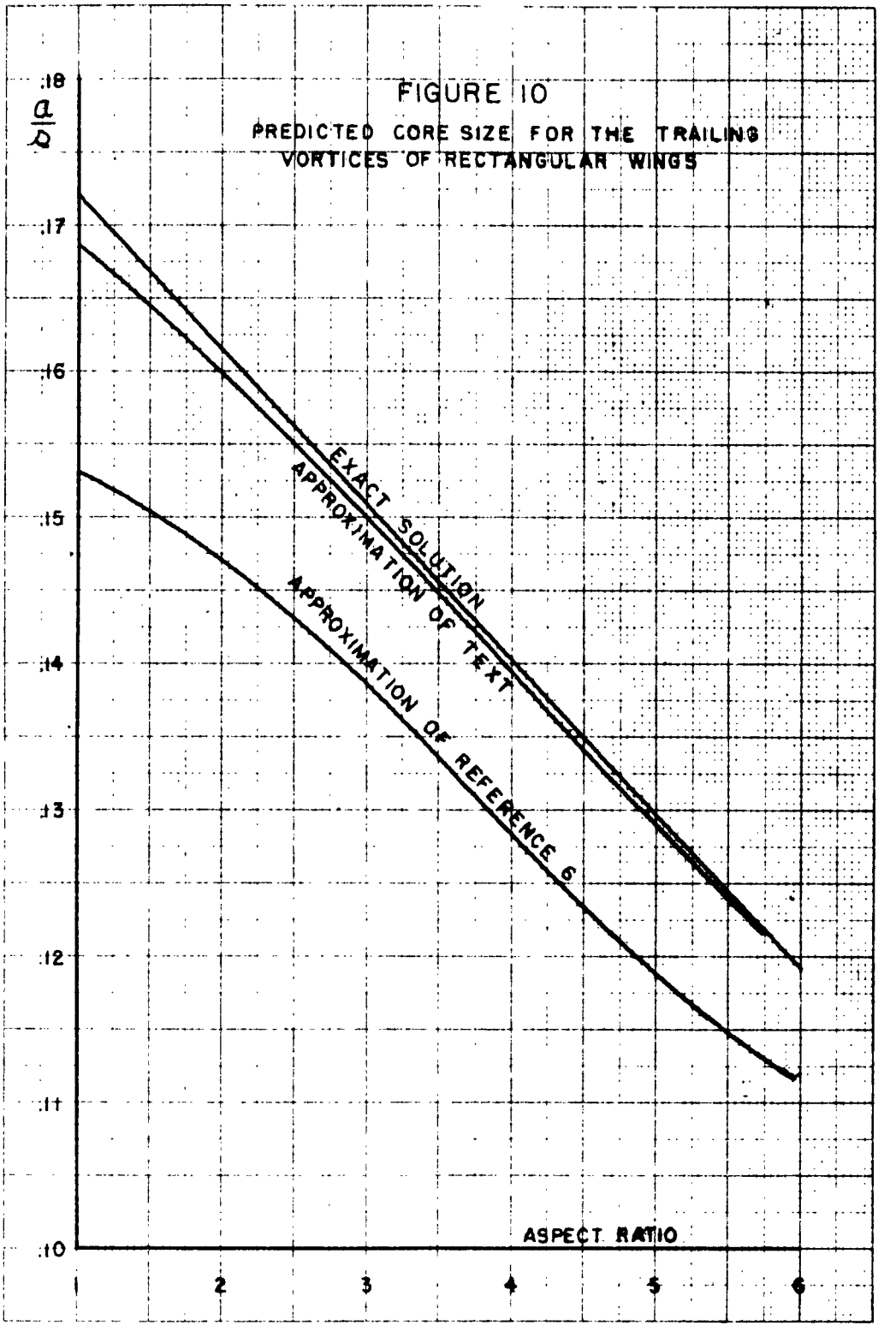
FIGURE 10
PREDICTED CORE SIZE FOR THE TRAILING VORTICES OF RECTANGULAR WINGS
a/b
.18
.17
.16
.15
.14
.13
.12
.11
.10
EXACT SOLUTION
APPROXIMATION OF TEXT
APPROXIMATION OF REFERENCE 6
ASPECT RATIO
1
2
3
4
5
6

NO. 3110 20 DIVISIONS PER INCH BOTH WAYS 120 BY 130 DIVISIONS

CODEX BOOK COMPANY, INC. NORWOOD, MASSACHUSETTS.
PRINTED IN U.S.A.

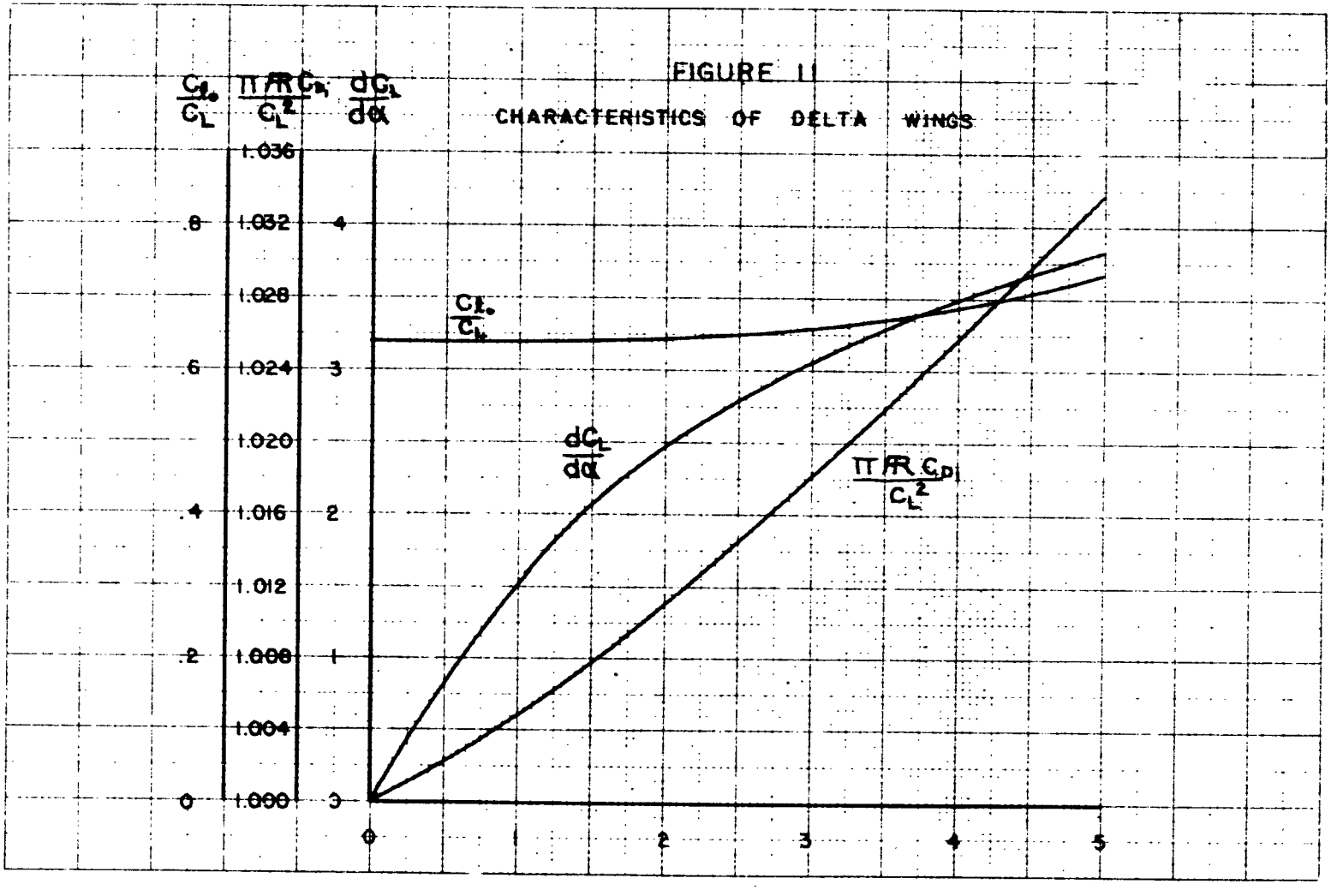

FIGURE 11

CHARACTERISTICS OF DELTA WINGS

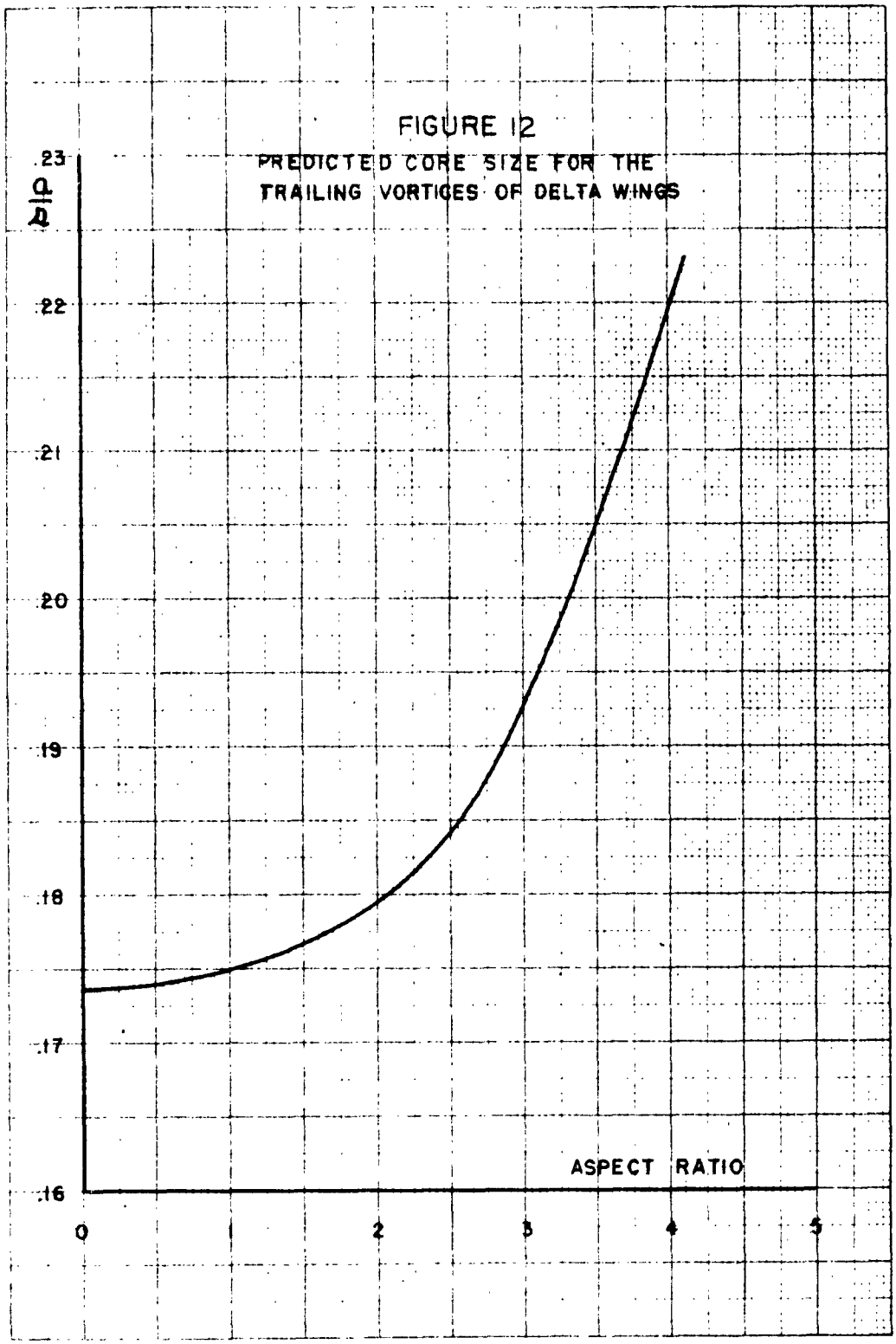
FIGURE 12
PREDICTED CORE SIZE FOR THE
TRAILING VORTICES OF DELTA WINGS
a/b
.23
.22
.21
.20
.19
.18
.17
.16
ASPECT RATIO
0
1
2
3
4
5

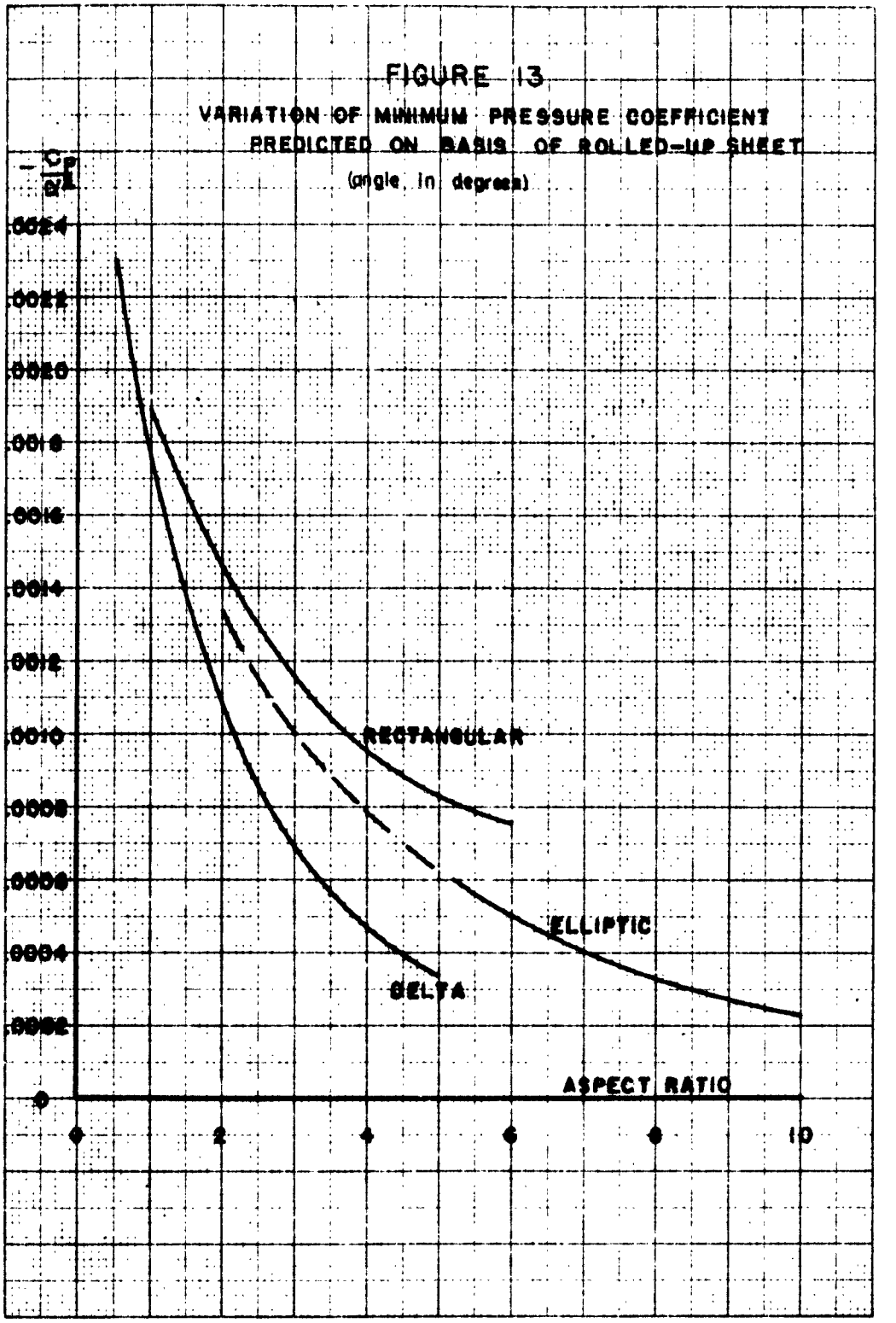

CODEX BOOK COMPANY, INC., NORWOOD, MASSACHUSETTS. PRINTED IN U.S.A.
NO. 3110. 20 DIVISIONS PER INCH BOTH WAYS. 120 BY 1 IN. DIVISIONS

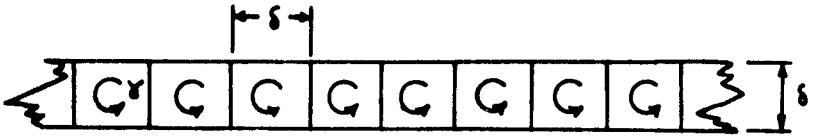

FIGURE 14

Model of a Vortex Sheet

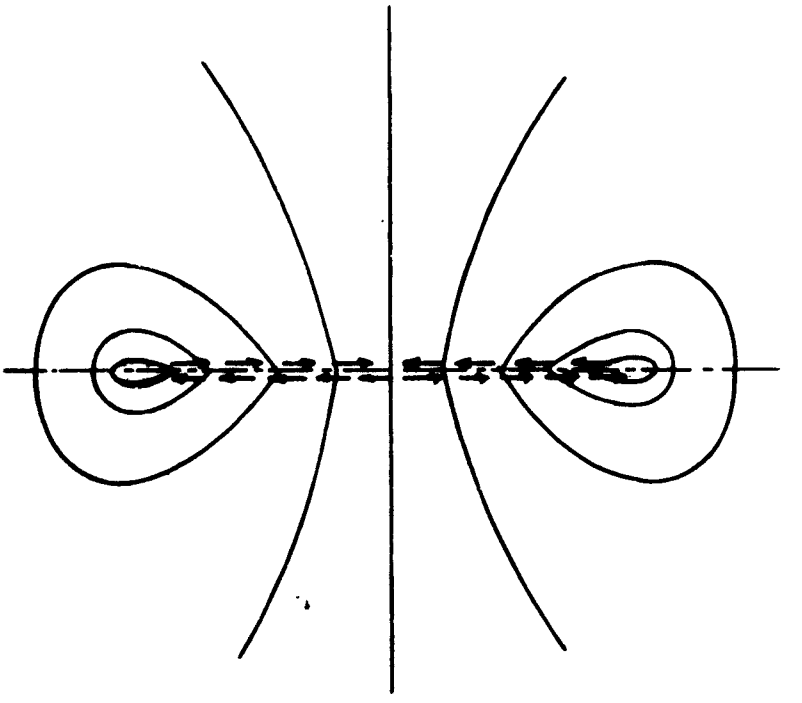

FIGURE 15

Transverse Plane of a Non-Distorted
Vortex Sheet in Irrotational Flow

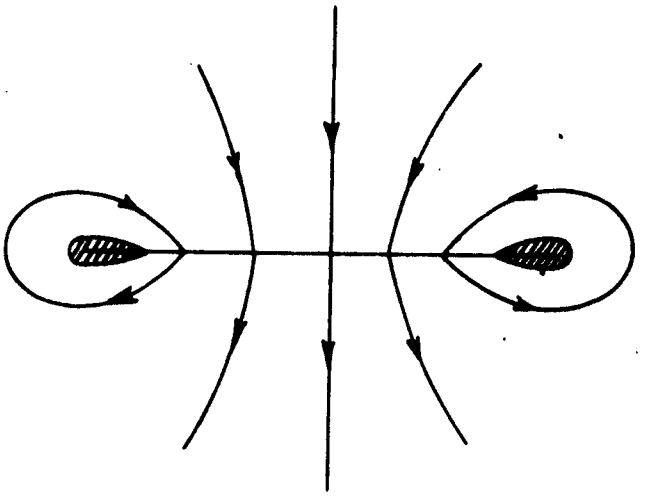

FIGURE 16

Proposed Model of a Non-Distorted Vortex Sheet

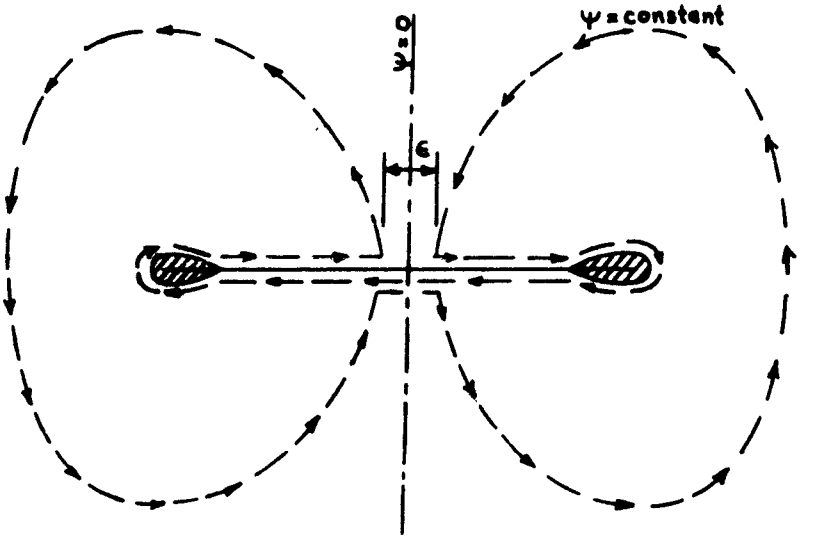

FIGURE 17

Path of Integration for Evaluating the Kinetic Energy
Of the Irrotational Motion for the Model of
The Vortex Sheet

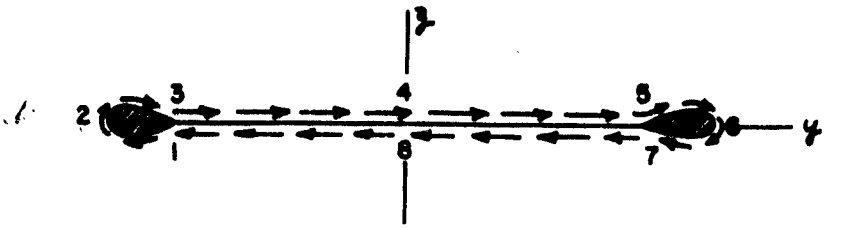

FIGURE 18

Reduced Path of Integration for Evaluating the Kinetic Energy of the Irrotational Motion For the Model of the Vortex Sheet

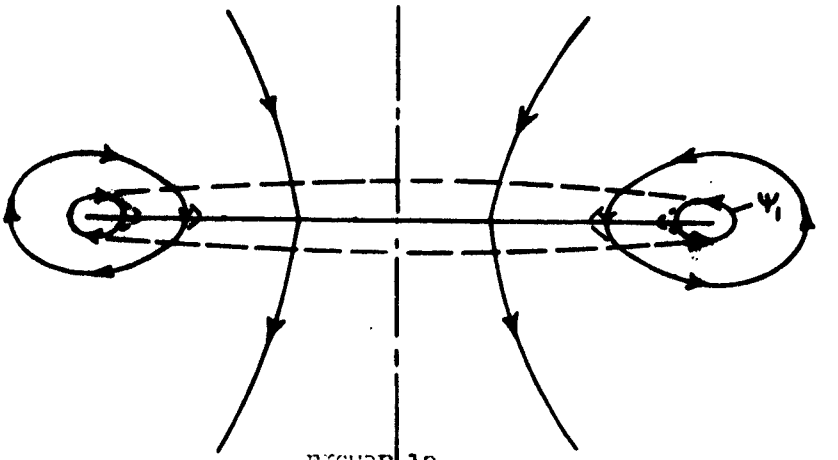

FIGURE 19

Effect of Viscosity on a Trailing Vortex Sheet

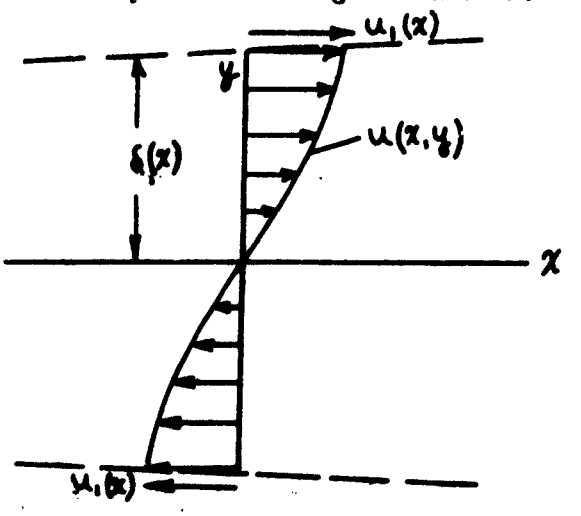

FIGURE 20

The Inner Region of a Vortex Sheet

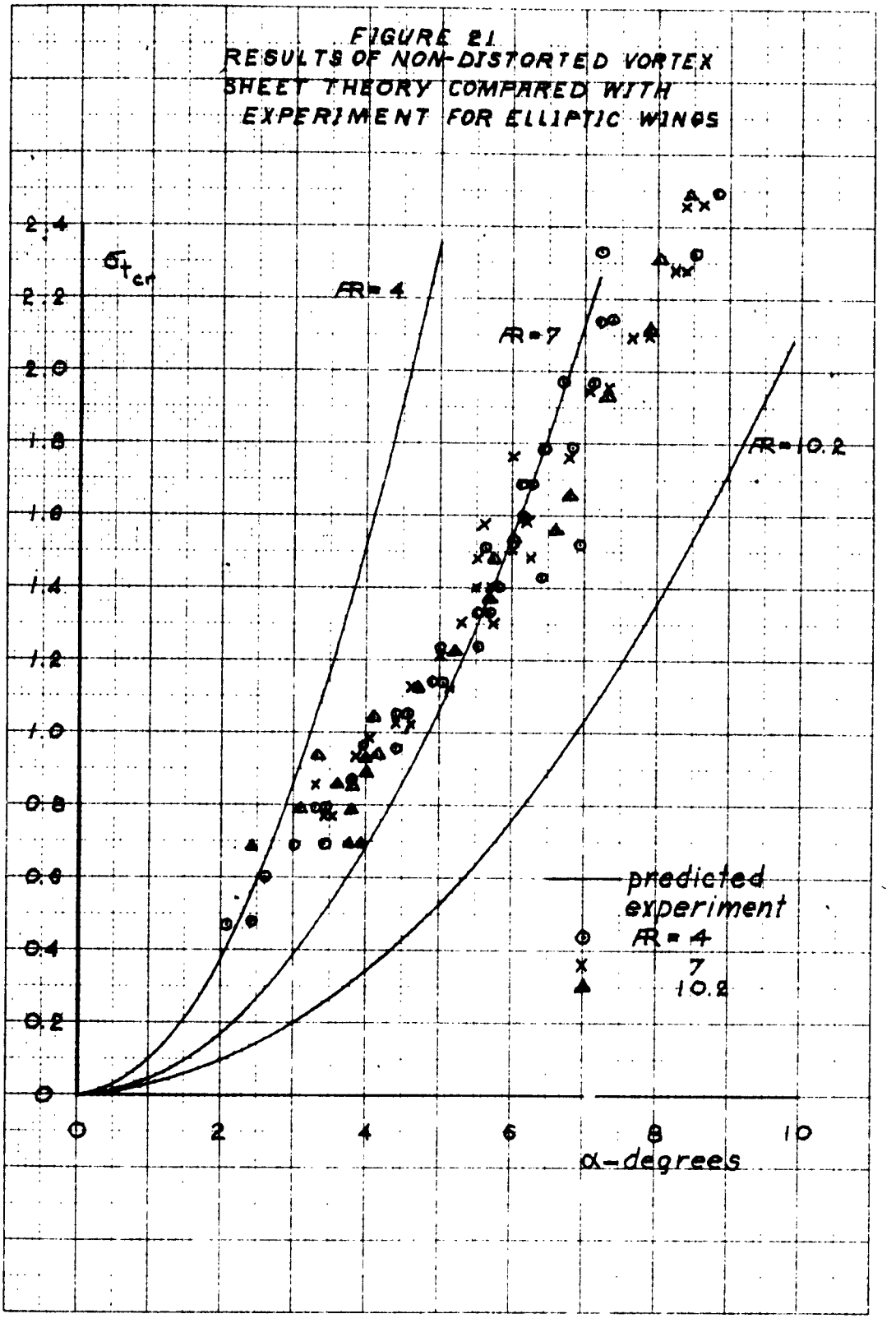

FIGURE 21
RESULTS OF NON-DISTORTED VORTEX SHEET THEORY COMPARED WITH EXPERIMENT FOR ELLIPTIC WINGS

NO. 3110 20 DIVISIONS PER INCH BOTH WAYS 120 BY 180 DIVISIONS.
CODEX BOOK COMPANY INC., NORWOOD, MASSACHUSETTS.
PRINTED IN U.S.A.

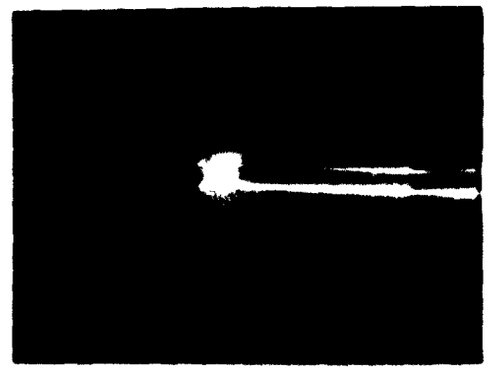

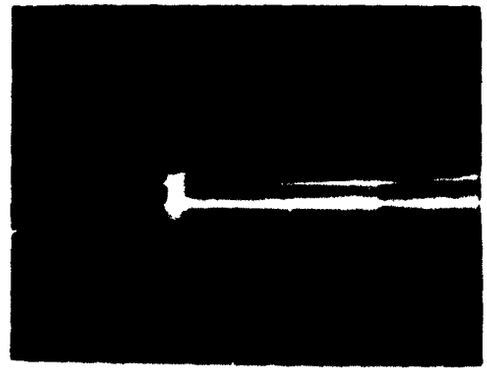

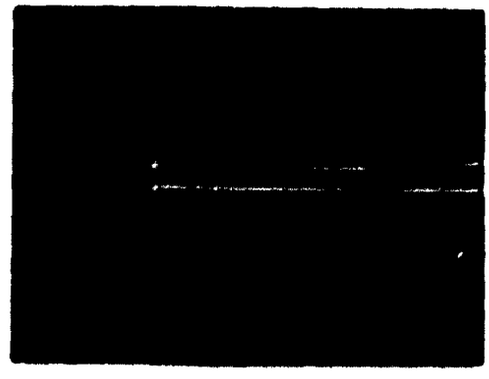

FIGURE 22

Various Stages of Cavitation on a Hemispherical Nose Shape

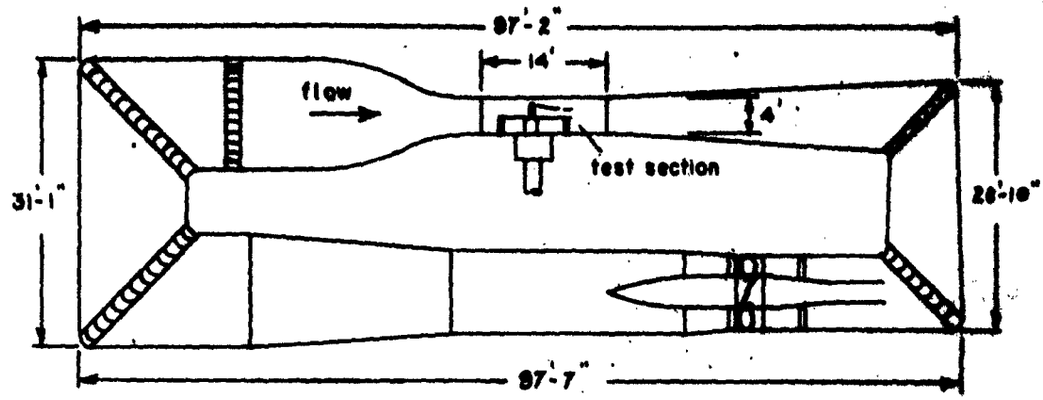

FIGURE 23

Schematic Diagram of the Garfield Thomas Water Tunnel

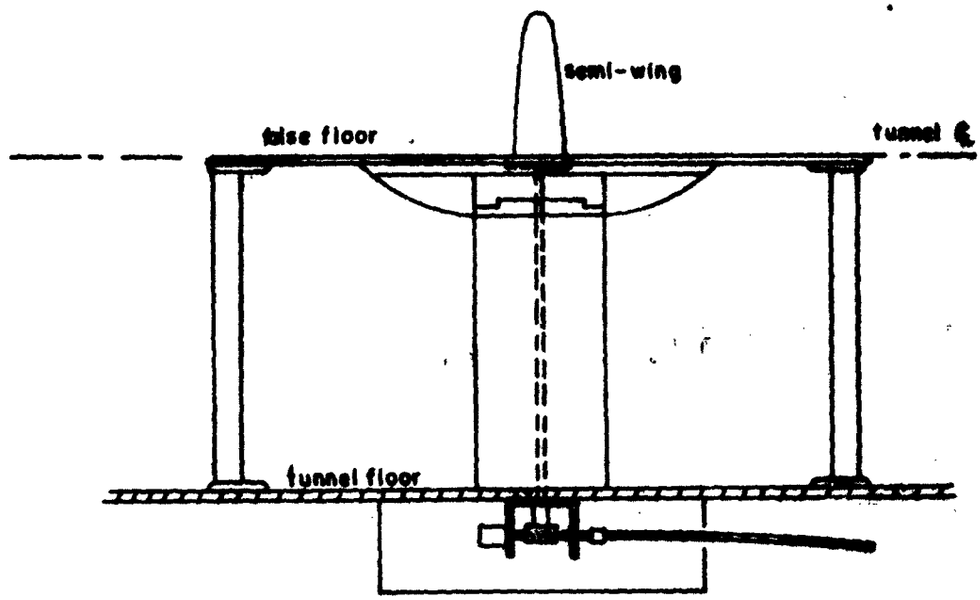

FIGURE 24

Diagram of the Test Equipment

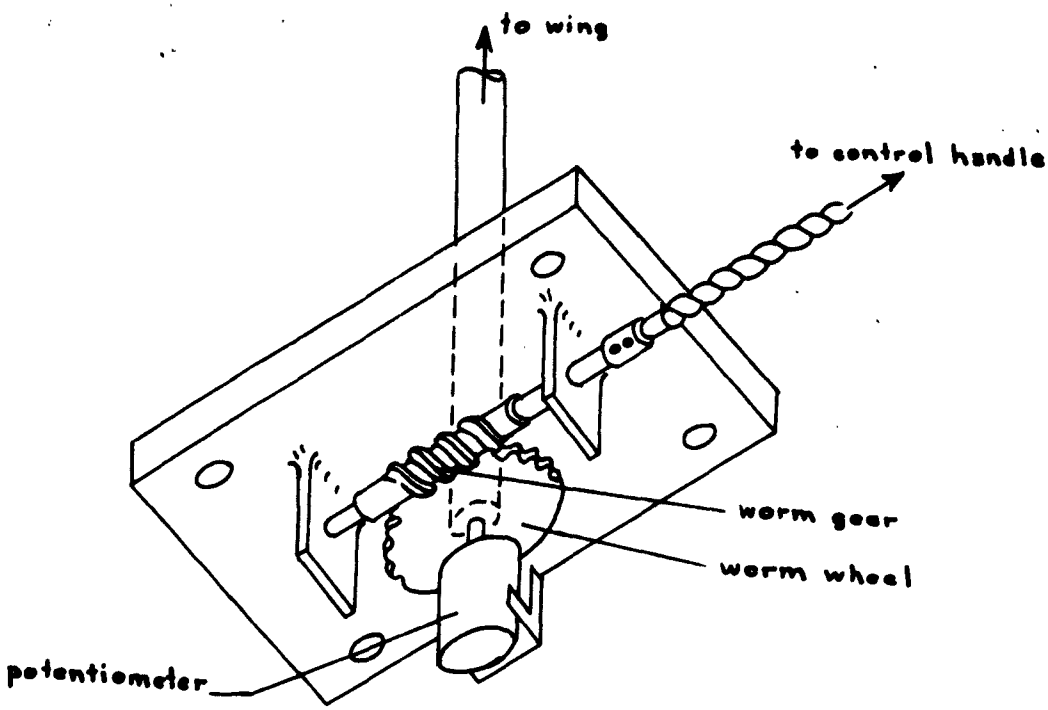

FIGURE 25

Arrangement for Rotating the Wing

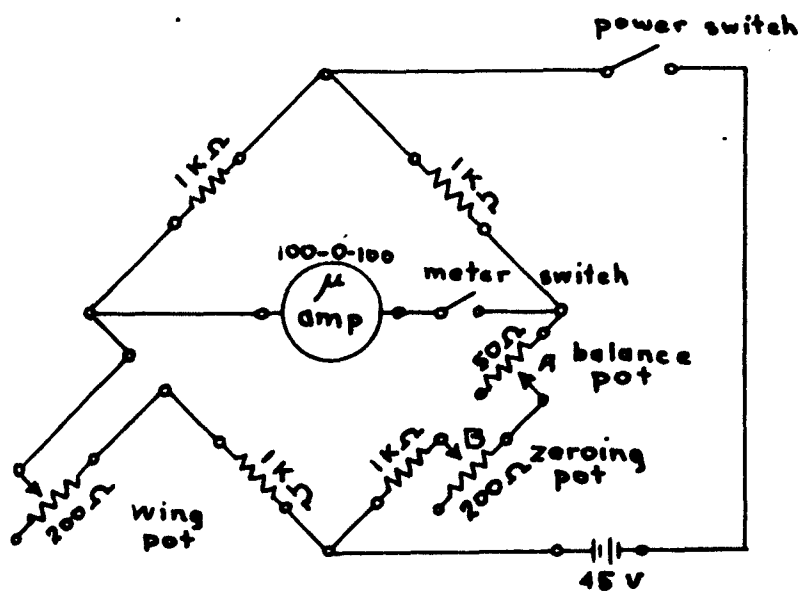

FIGURE 26

Circuit Diagram for Position Indicator

NO. 3110. 20 DIVISIONS PER INCH BOTH WAYS 120 BY 180 DIVISIONS

CODEX BOOK COMPANY, INC., NORWOOD, MASSACHUSETTS.
PRINTED IN U.S.A.

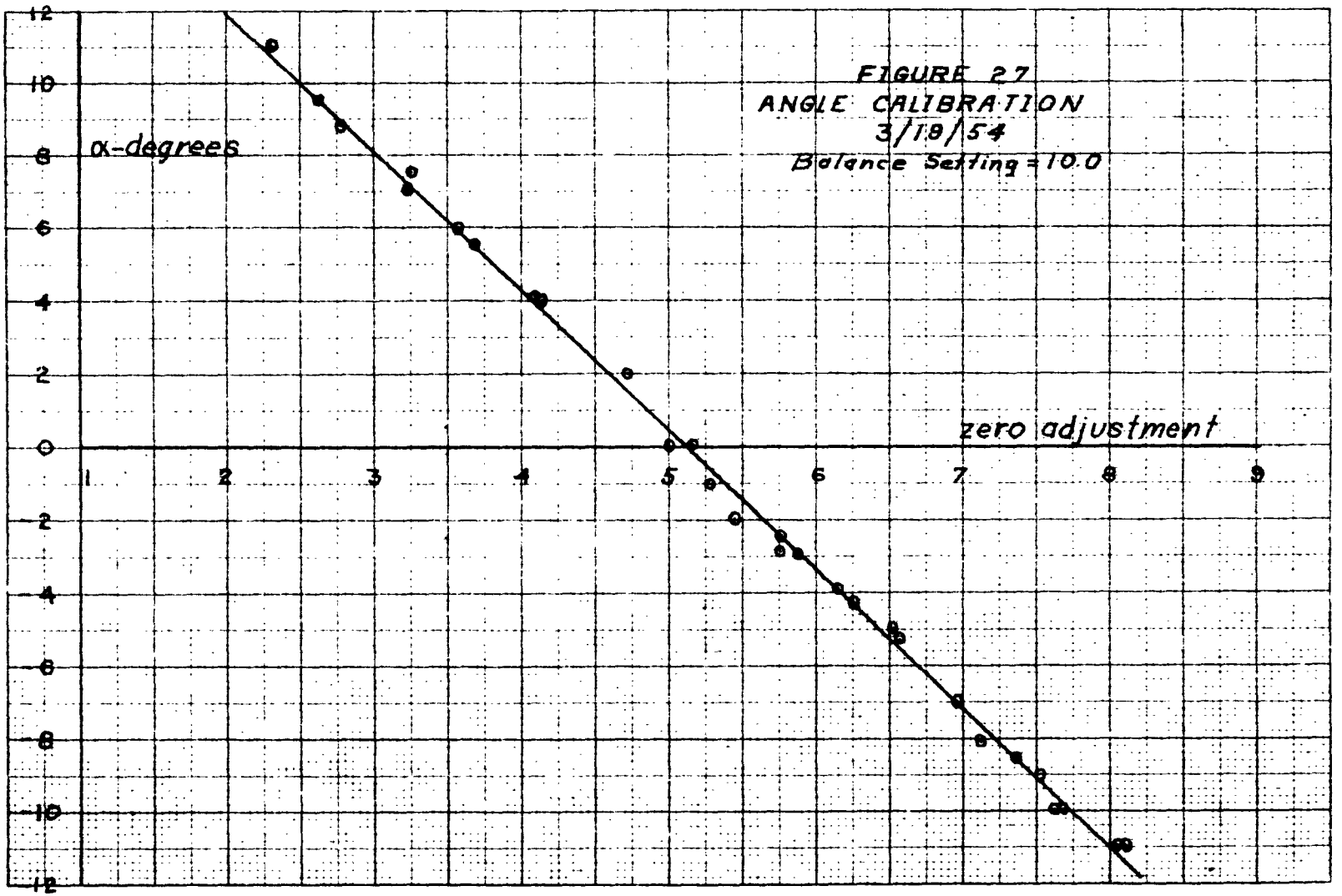

FIGURE 27
ANGLE CALIBRATION
3/19/54
Balance Setting = 10.0

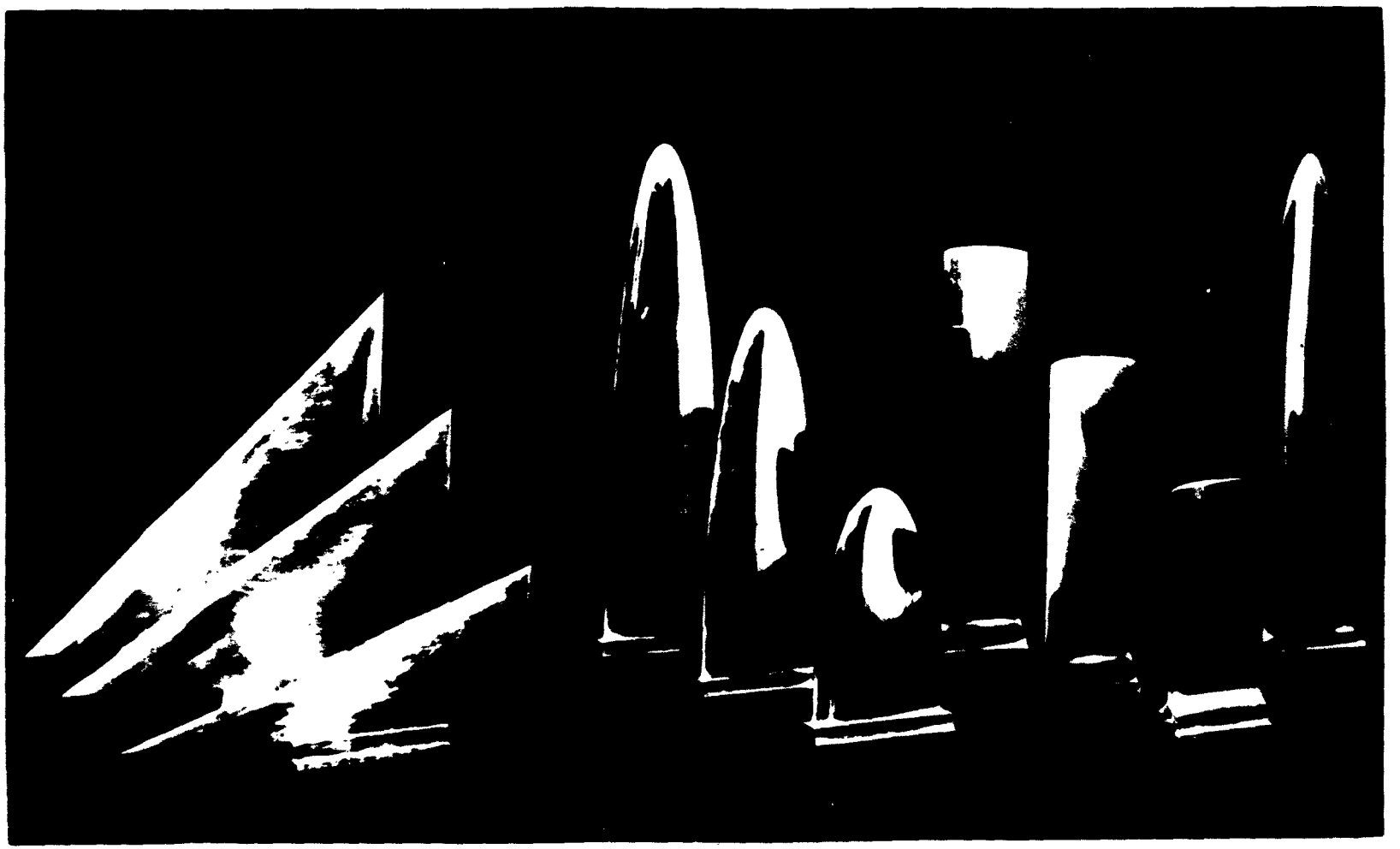

FIGURE 23
Wing Shapes Used in the Experimental Investigation

FIGURE 29
Wing Number 8
V=40 fps, p_o=28.0 psi, α =9.8°

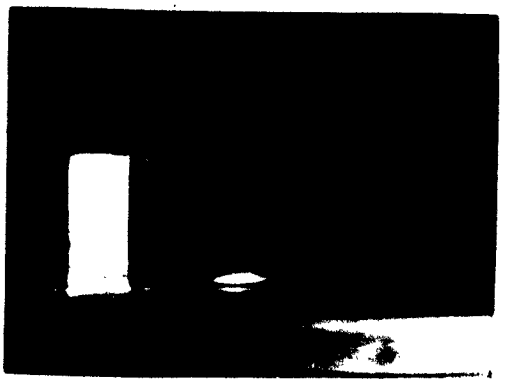

FIGURE 30
Wing Number 2
V=45 fps, p_o=27.5 psi, α =11.9°

FIGURE 31
Wing Number 2
V=45 fps, p_o=30.5 psi, α =11.9°

FIGURE 32
Wing Number 5
V=40 fps, p_o=18.0 psi, α =13.5°

FIGURE 33
Wing Number 5
V=40 fps, p_o=20.0 psi, α =13.5°

FIGURE 34
Wing Number 5
V=40 fps, p_o=26.0 psi, α =13.5°

FIGURE 35
Wing Number 5
V=40 fps, p_o=29.0 psi, α =13.5°

FIGURE 36
Wing Number 6
V=40 fps, p_o= [illegible] psi, α =1[illegible].3°

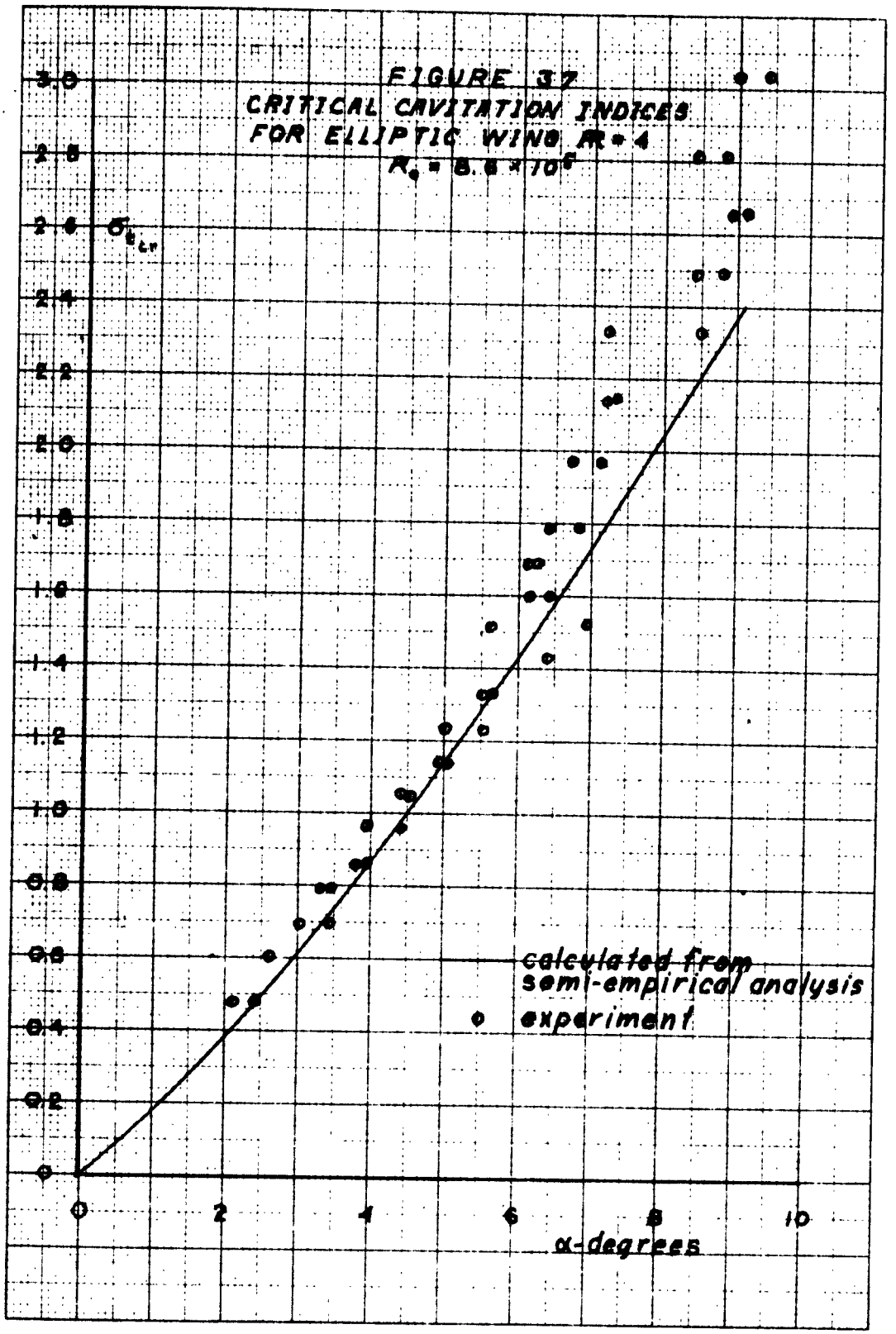

NO. 3110. 20 DIVISIONS PER INCH BOTH WAYS. 120 BY 180 DIVISIONS.
CODEX BOOK COMPANY, INC., NORWOOD, MASSACHUSETTS.
PRINTED IN U.S.A.

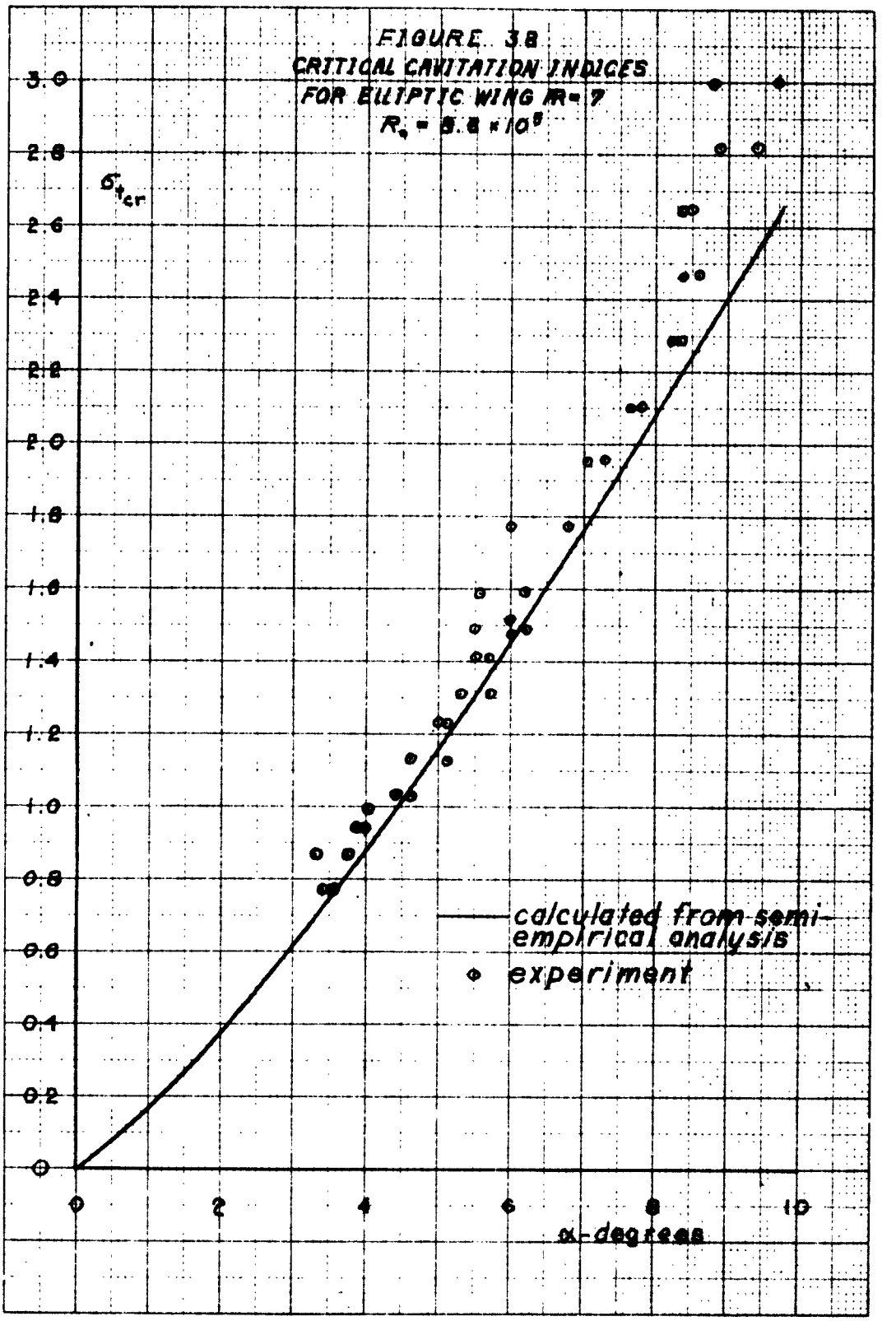

NO 3110 20 DIVISIONS PER INCH BOTH WAYS 120 BY 190 DIVISIONS
CODEX BOOK COMPANY INC. NORWOOD, MASSACHUSETTS
PRINTED IN U.S.A.

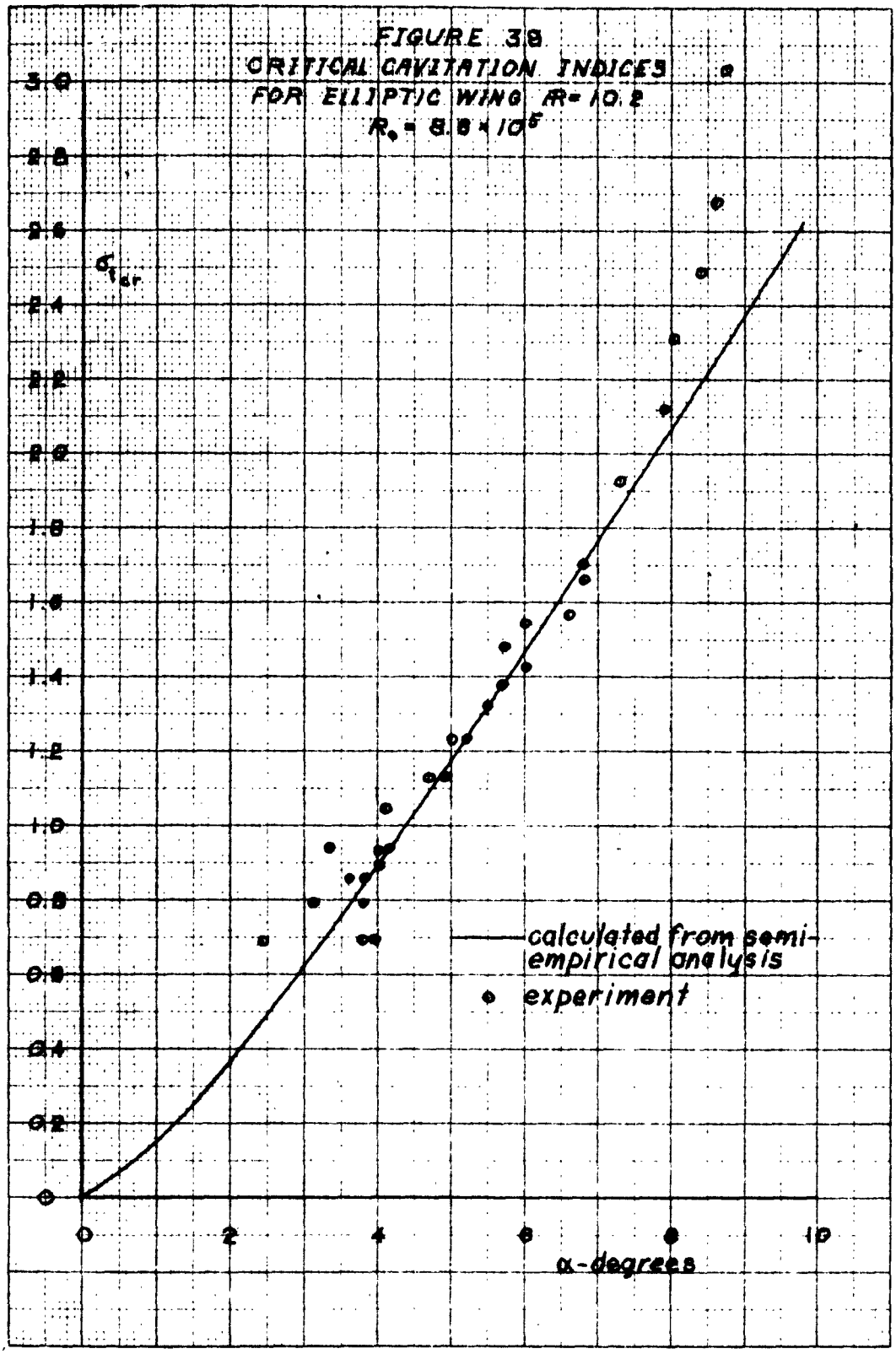

NO. 3110. 20 DIVISIONS PER INCH BOTH WAYS. 120 BY 180 DIVISIONS.
CODEX BOOK COMPANY, INC., NORWOOD, MASSACHUSETTS.
PRINTED IN U.S.A.

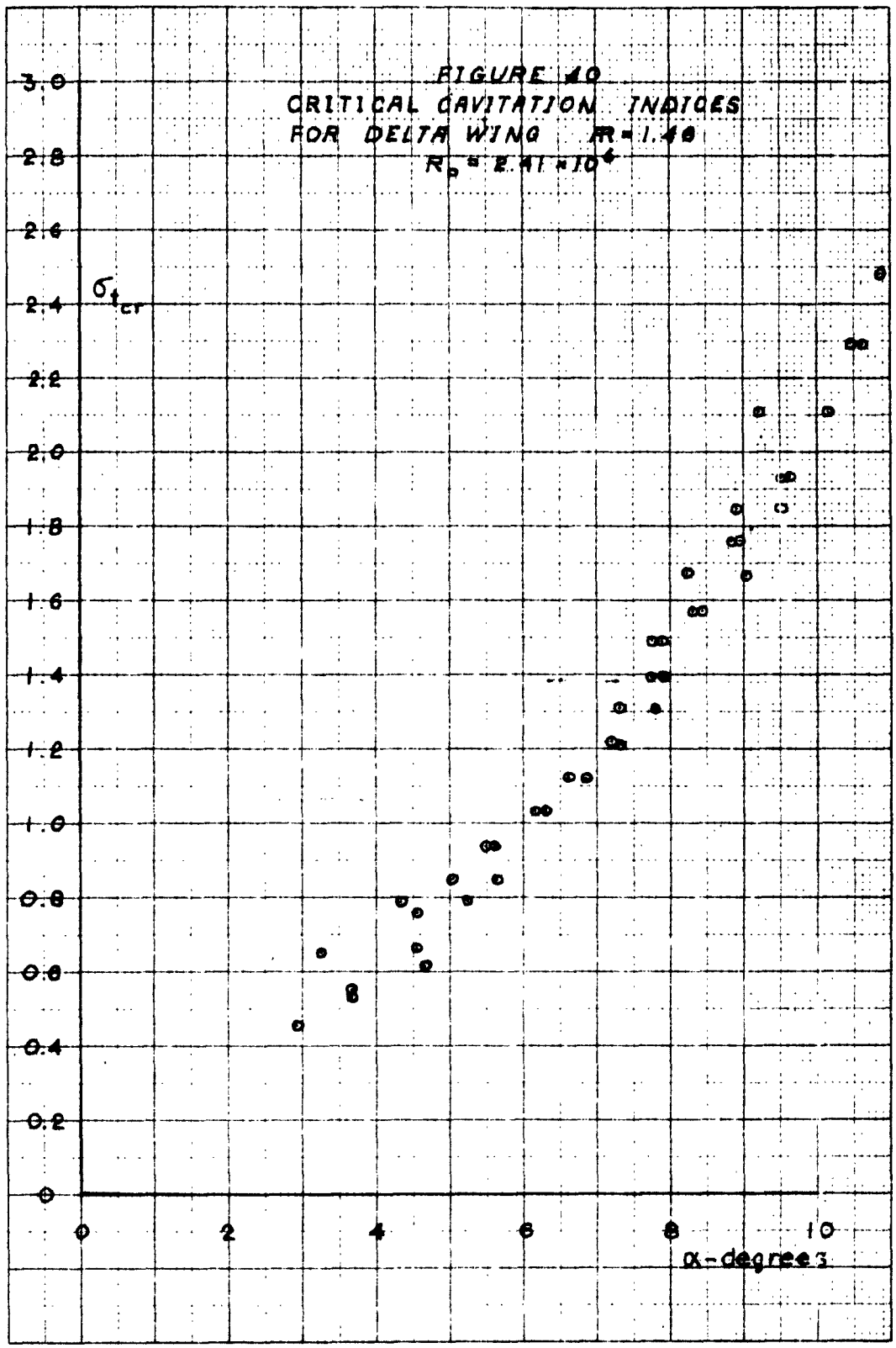

NO. 3110 20 DIVISIONS PER INCH BOTH WAYS 12" BY 180 DIVISIONS
CODEX BOOK COMPANY, INC., NORWOOD, MASSACHUSETTS.
PRINTED IN U.S.A.

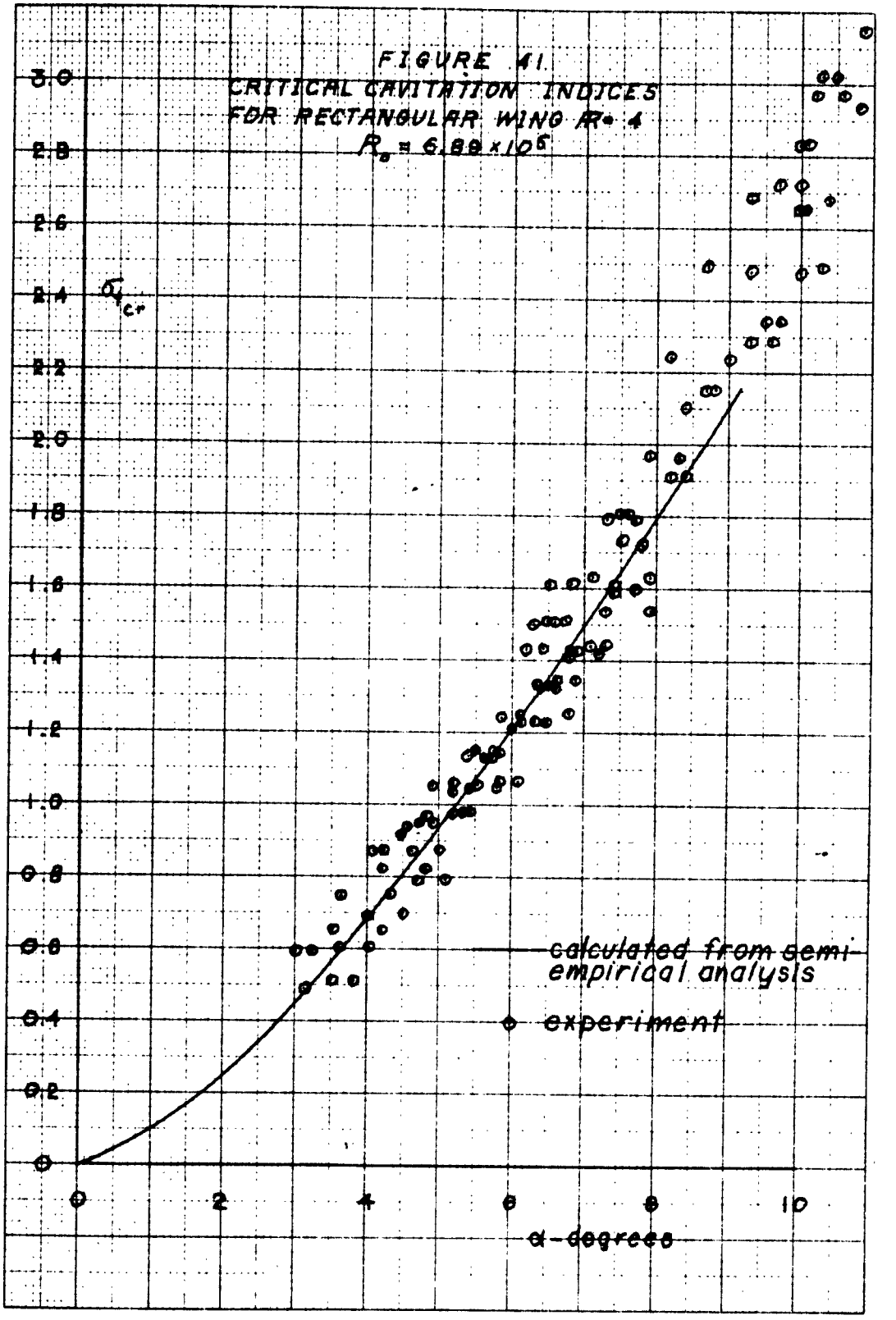

NO. 3110. 50 DIVISIONS PER INCH BOTH WAYS. 120 BY 180 DIVISIONS.
CODEX BOOK COMPANY, INC., NORWOOD, MASSACHUSETTS.
PRINTED IN U.S.A.

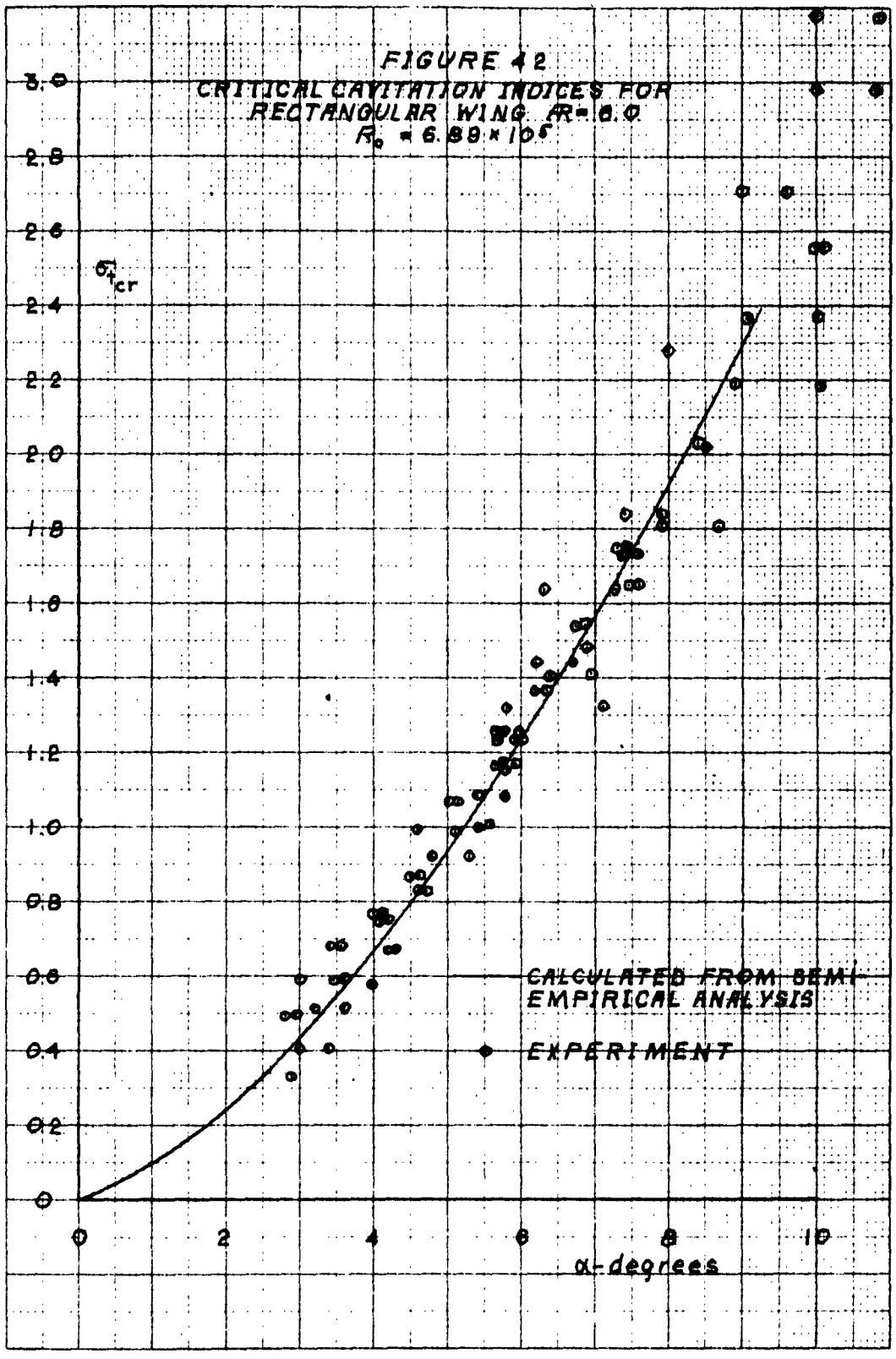

NO 3110 20 DIVISIONS PER INCH BOTH WAYS 120 BY 180 DIVISIONS
CODEX BOOK COMPANY, INC., NORWOOD, MASSACHUSETTS.
PRINTED IN U.S.A.

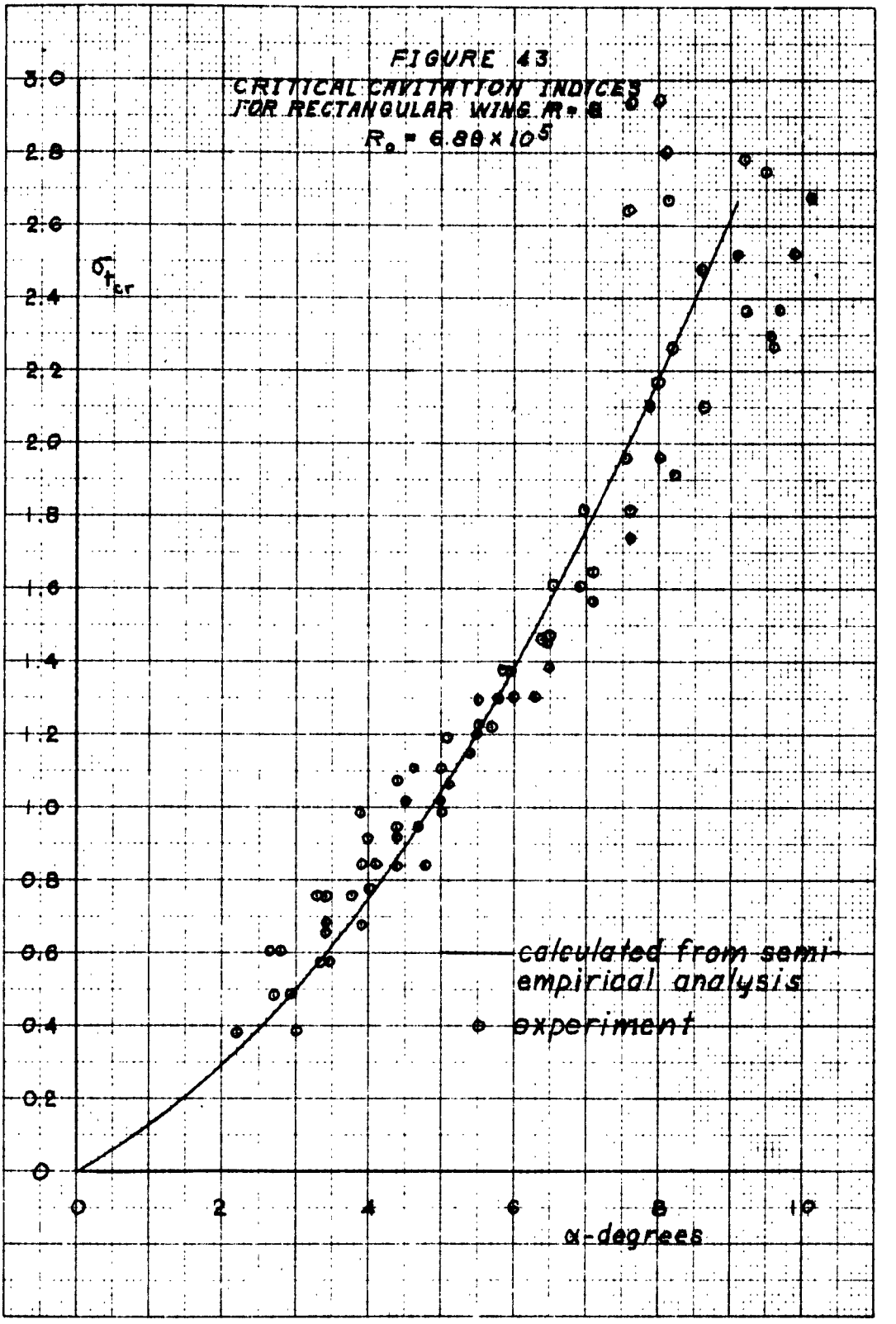

NO. 3110 20 DIVISIONS PER INCH BOTH WAYS 120 BY 180 DIVISIONS
CODEX BOOK COMPANY, INC., NORWOOD, MASSACHUSETTS.
PRINTED IN U.S.A.

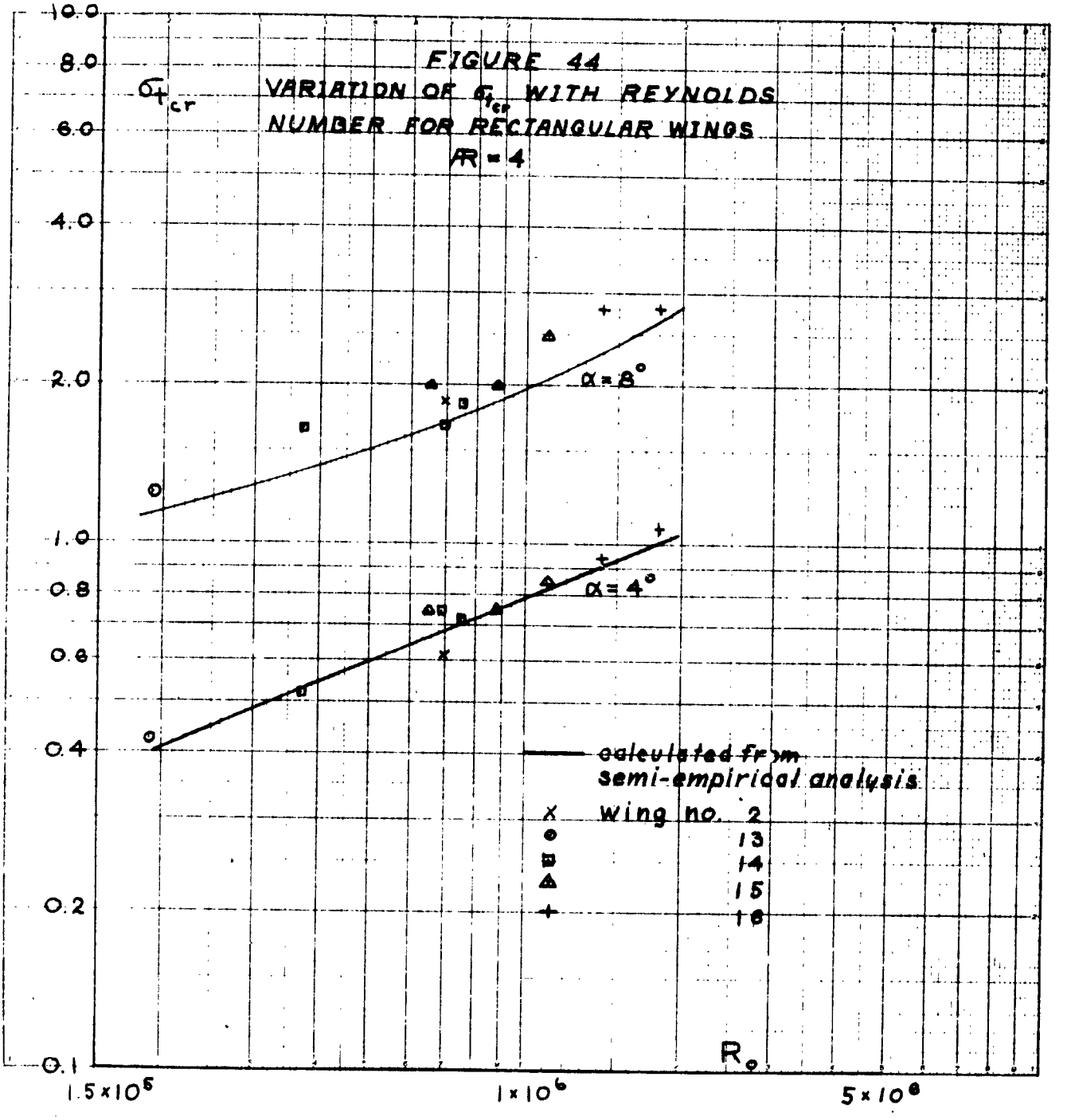
FIGURE 44
VARIATION OF $\sigma_{t_{cr}}$ WITH REYNOLDS NUMBER FOR RECTANGULAR WINGS
AR = 4
$\sigma_{t_{cr}}$
10.0
8.0
6.0
4.0
2.0
1.0
0.8
0.6
0.4
0.2
0.1
$\alpha = 8°$
$\alpha = 4°$
calculated from semi-empirical analysis
wing no. 2
13
14
15
16
R_o
1.5×10^5
1×10^6
5×10^6

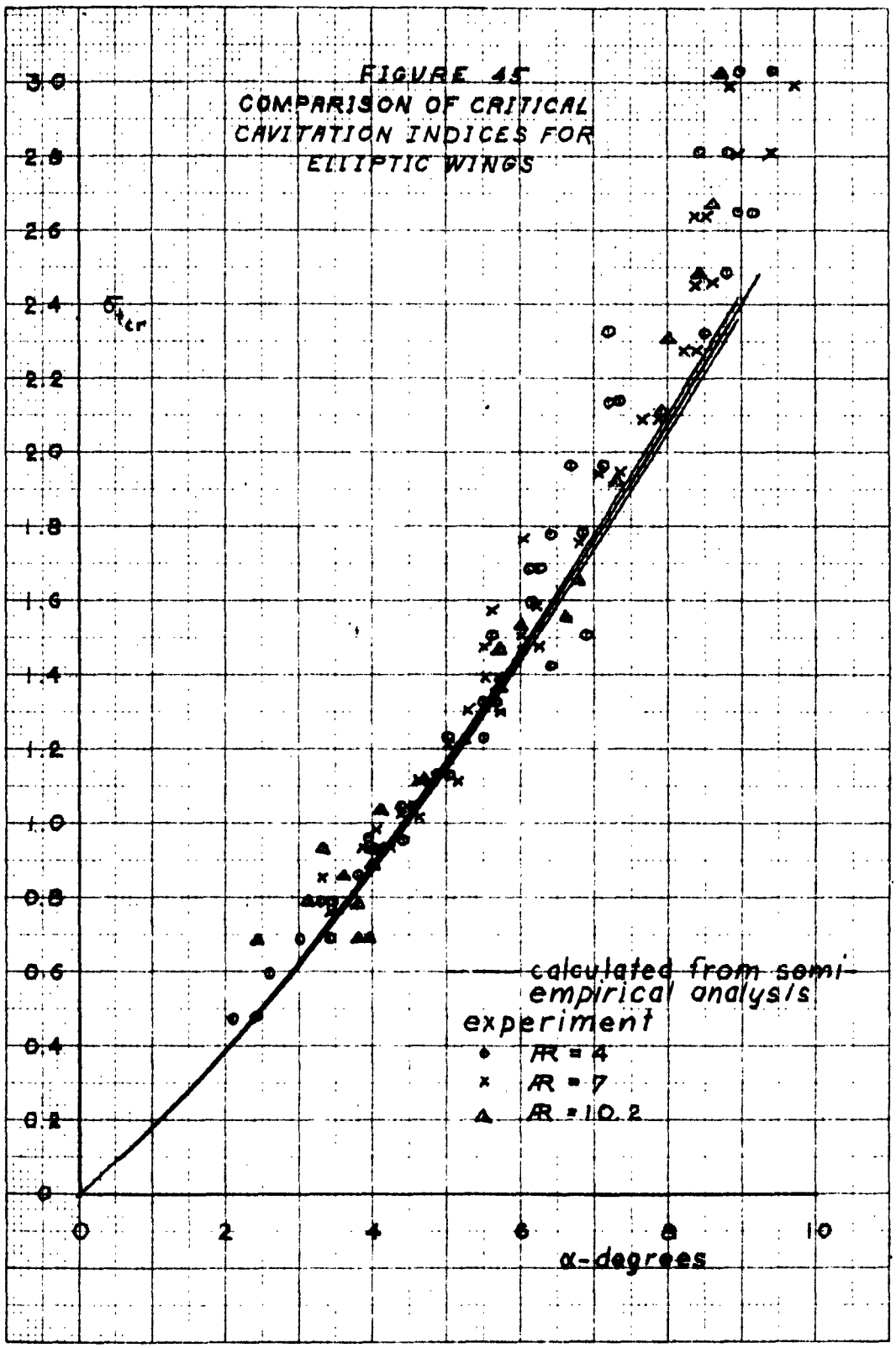

NO. 3110. 20 DIVISIONS PER INCH BOTH WAYS 120 BY 180 DIVISIONS
CODEX BOOK COMPANY, INC., NORWOOD, MASSACHUSETTS.
PRINTED IN U.S.A.

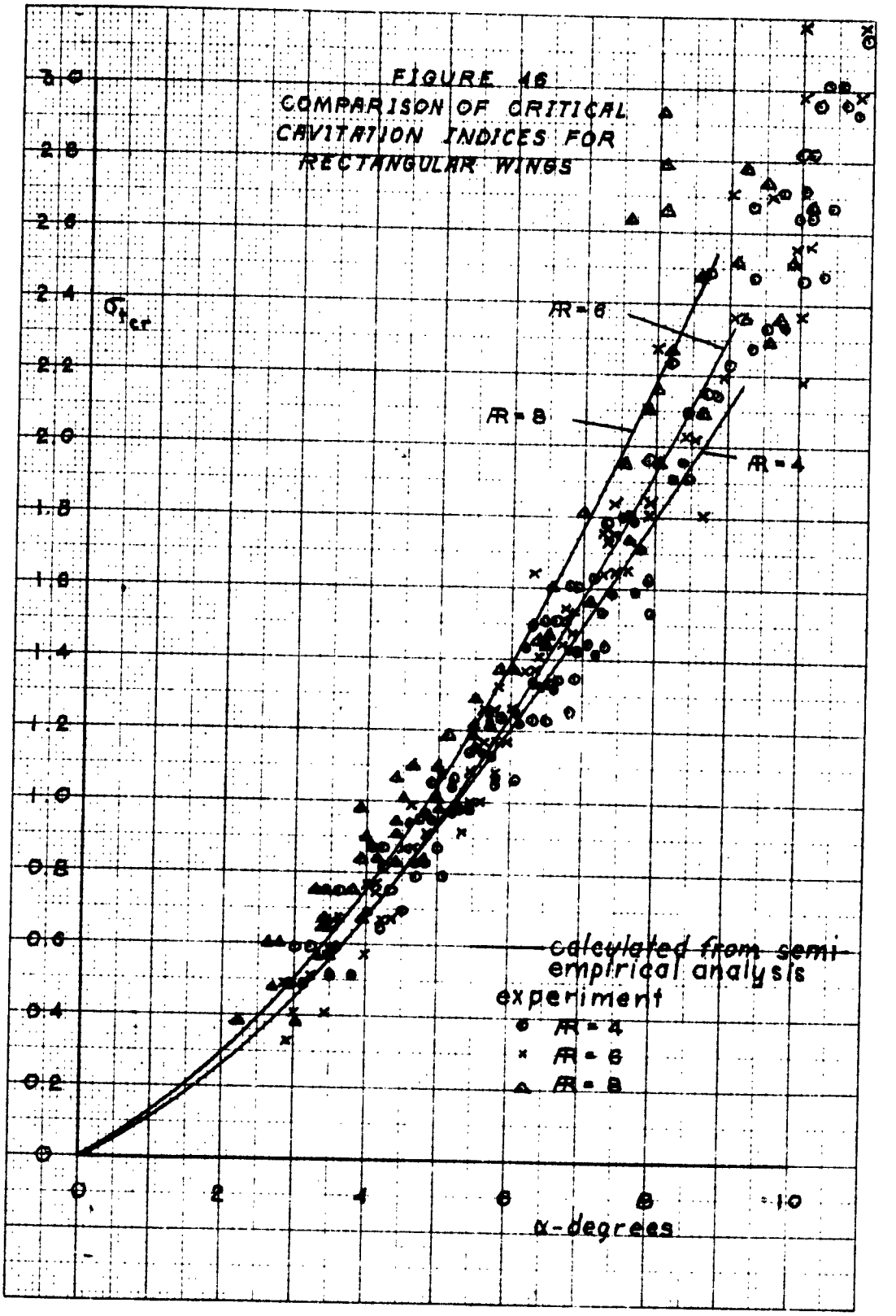

NO. 3110. 20 DIVISIONS PER INCH BOTH WAYS 120 BY 180 DIVISIONS
CODEX BOOK COMPANY, INC., NORWOOD, MASSACHUSETTS.
PRINTED IN U.S.A.

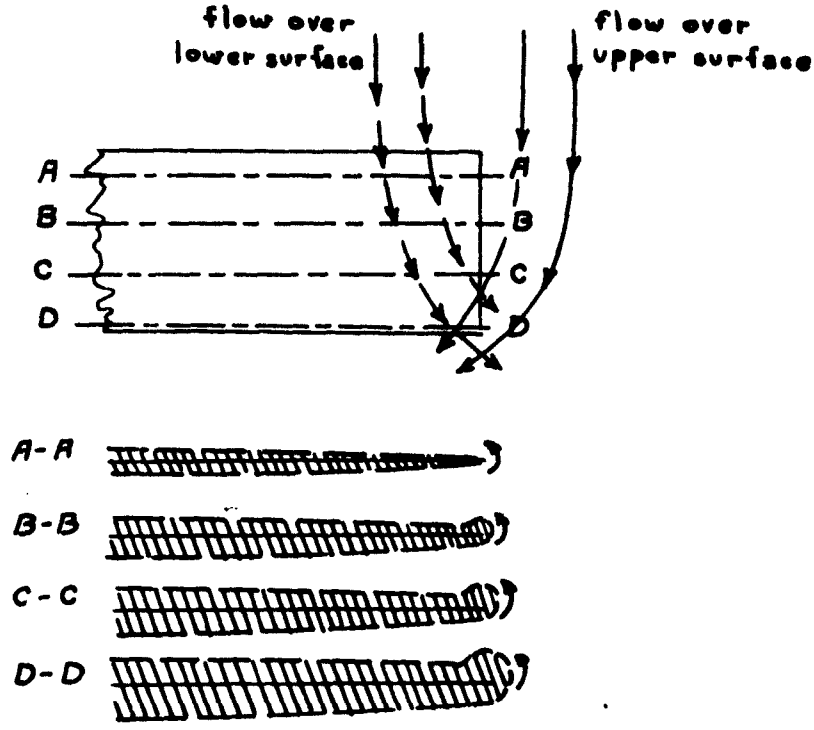

FIGURE 47

Flow Directions on the Upper and Lower Surfaces of a Rectangular Wing

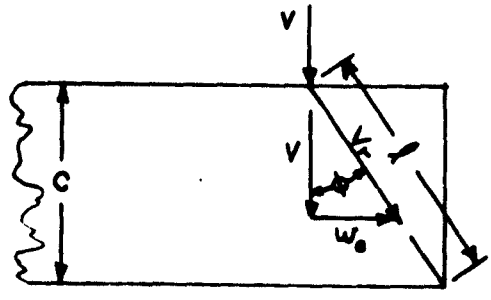

FIGURE 48

Geometry of the Flow on the Lower Surface of a Rectangular Wing

NO. 3110 20 DIVISIONS PER INCH BOTH WAYS 120 BY 180 DIVISIONS

CODEX BOOK COMPANY, INC., NORWOOD, MASSACHUSETTS.
PRINTED IN U.S.A.

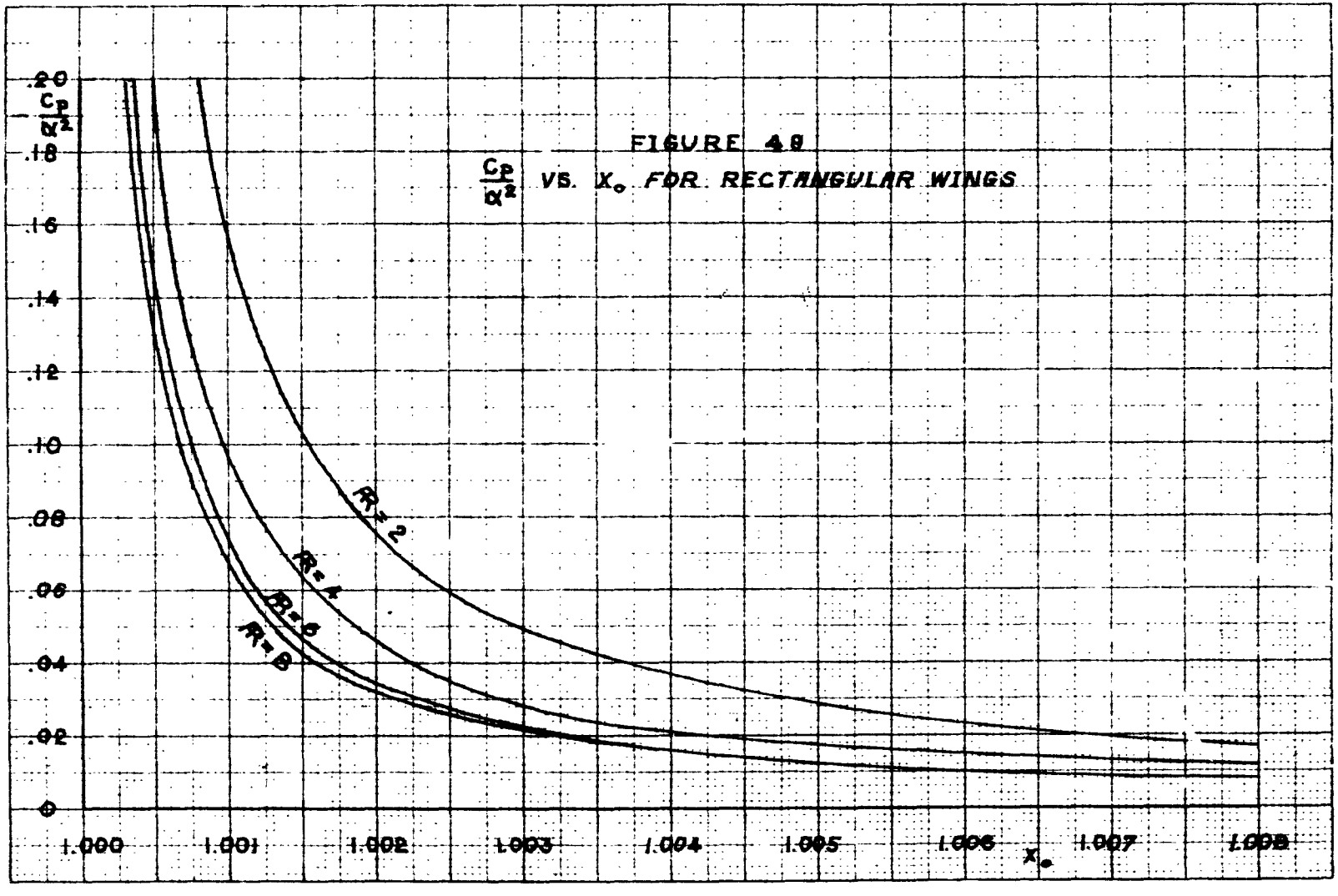

NO. 3158. LOGARITHMIC: 1 BY 1-1, 5 7½-INCH CYCLES.

CODEX BOOK COMPANY, INC., NORWOOD, MASSACHUSETTS.
PRINTED IN U.S.A.

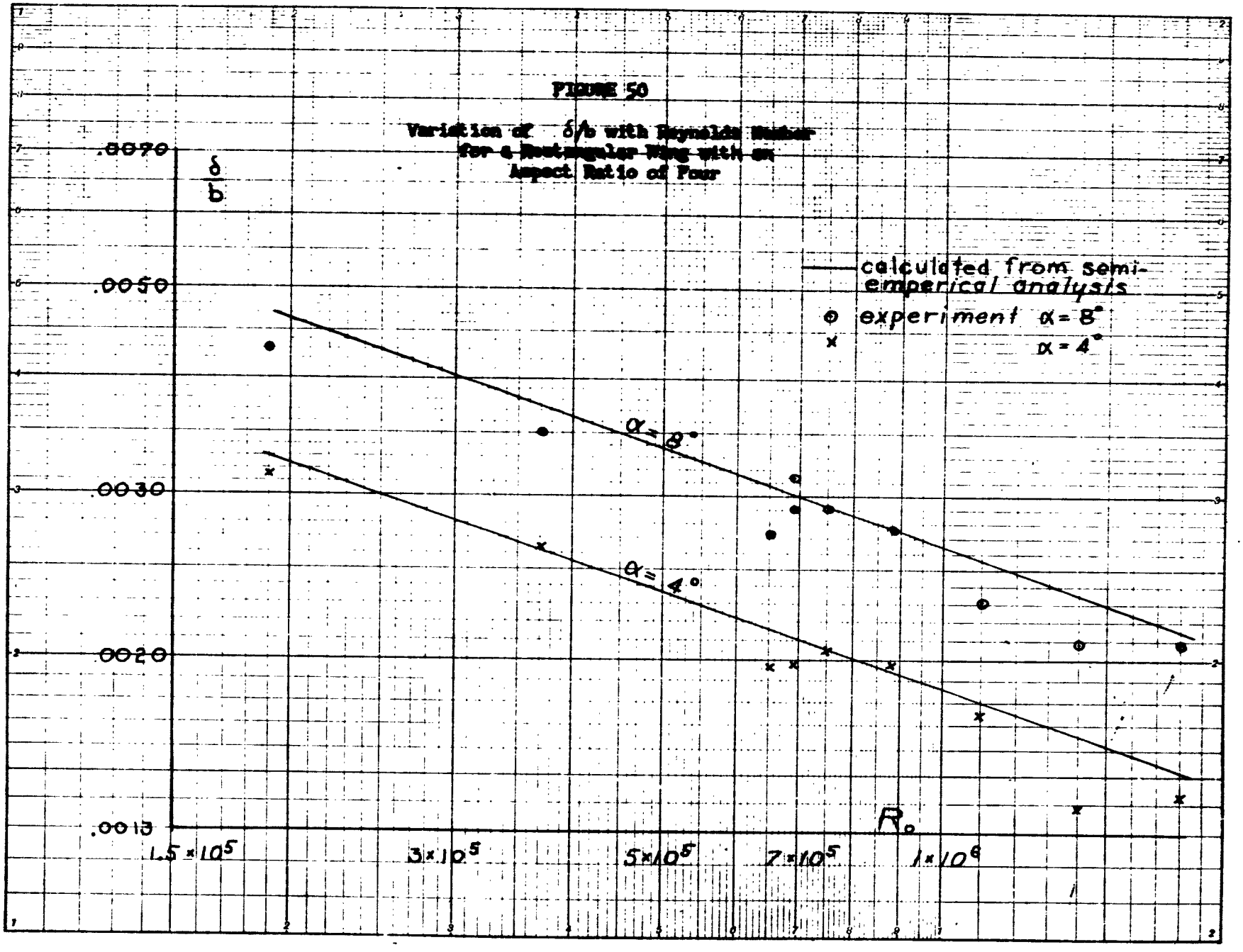

FIGURE 50

Variation of δ/b with Reynolds Number for a Rectangular Wing with an Aspect Ratio of Four

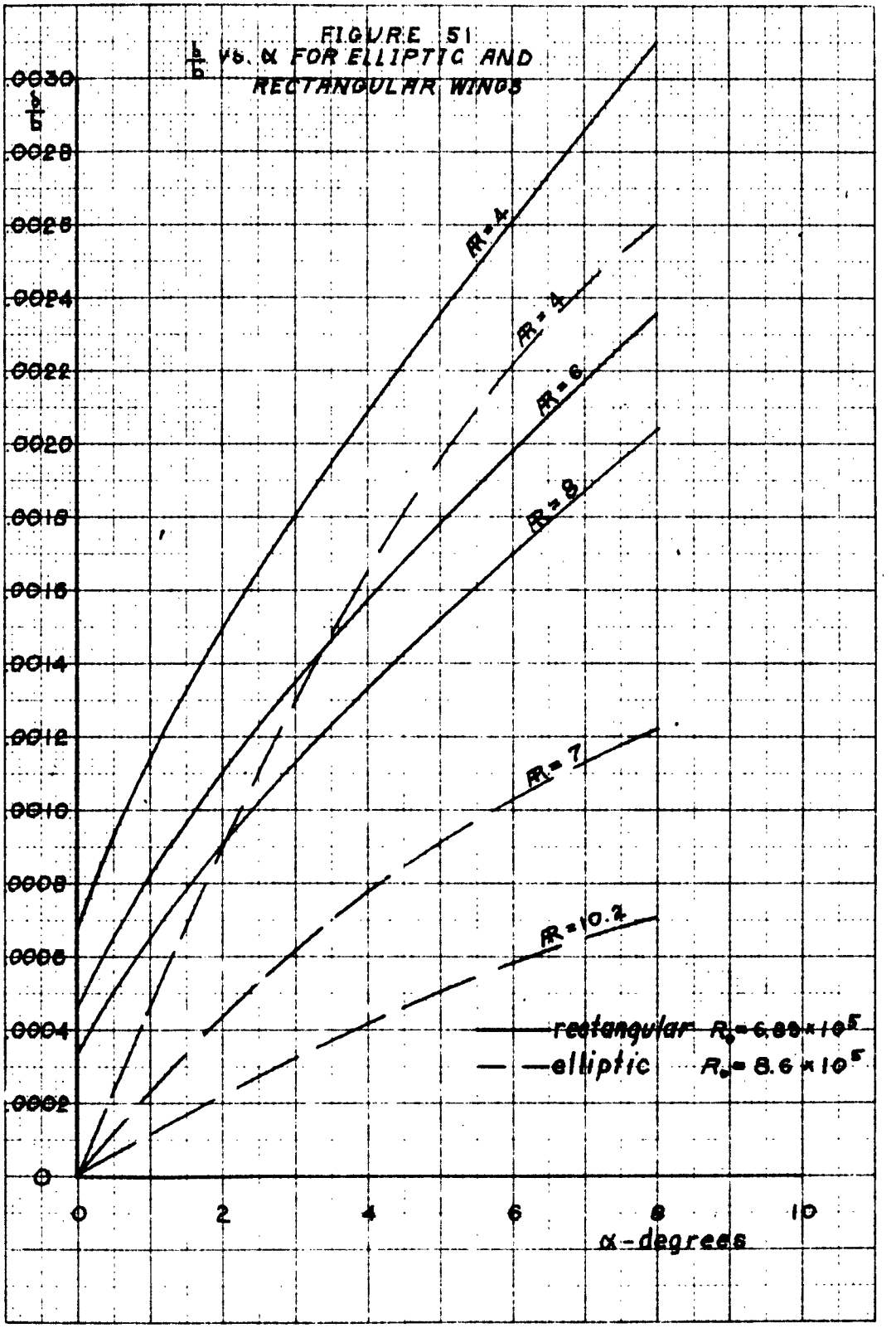

NO. 3110. 20 DIVISIONS PER INCH BOTH WAYS 120 BY 180 DIVISIONS
CODEX BOOK COMPANY, INC., NORWOOD, MASSACHUSETTS.
PRINTED IN U.S.A.

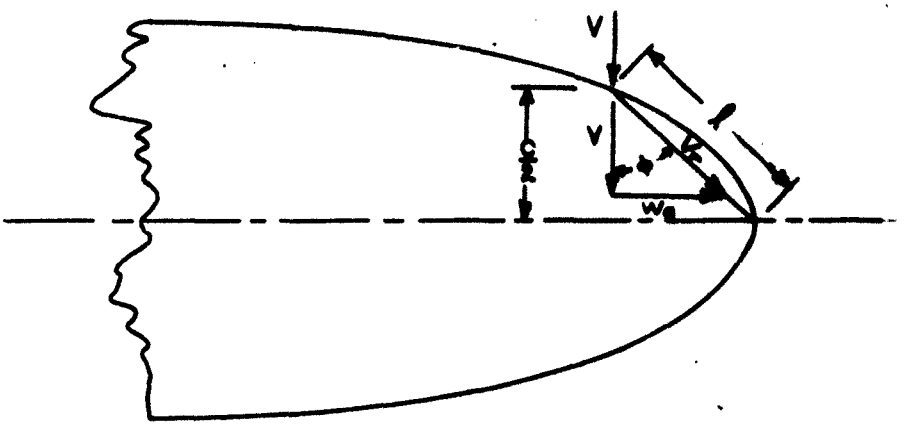

FIGURE 52

Geometry of the Flow Over the Lower Surface of an Elliptic Wing

NO. 3110. 20 DIVISIONS PER INCH BOTH WAYS. 120 BY 150 DIVISIONS

CODEX BOOK COMPANY, INC., NORWOOD, MASSACHUSETTS.
PRINTED IN U.S.A.

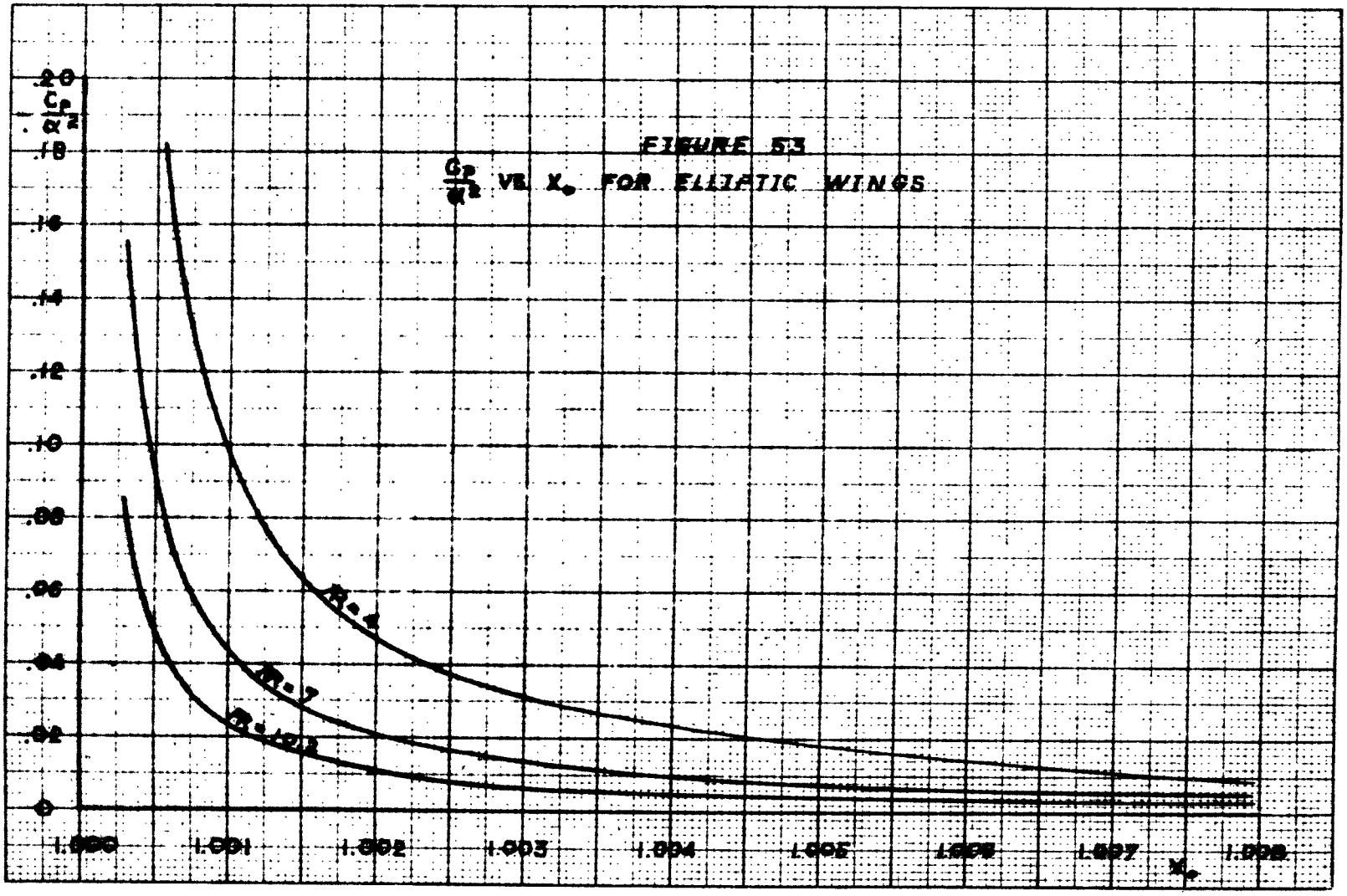

FIGURE 53

$\frac{C_p}{\alpha^2}$ VS. X_∞ FOR ELLIPTIC WINGS